5-2021

Investigating a novel function for phosphoserine aminotransferase 1 (PSAT1) in epidermal growth factor receptor (EGFR)-mediated lung tumorigenesis.

Rumeysa Biyik-Sit
University of Louisville

Follow this and additional works at: https://ir.library.louisville.edu/etd

Part of the Biochemistry Commons, Cancer Biology Commons, and the Molecular Biology Commons

INVESTIGATING A NOVEL FUNCTION FOR PHOSPHOSERINE AMINOTRANSFERASE 1

(PSAT1) IN EPIDERMAL GROWTH FACTOR RECEPTOR (EGFR)-MEDIATED LUNG

TUMORIGENESIS

By

Rumeysa Biyik-Sit
B.S. Bilkent University 2007
M.S. Bilkent University 2009
M.S. The Ohio State University 2012
M.S. University of Louisville 2017

A Dissertation
Submitted to the Faculty of the
School of Medicine at the University of Louisville
In Partial Fulfillment of the Requirements for the Degree of

Doctor of Philosophy in
Biochemistry and Molecular Genetics

Department of Biochemistry and Molecular Genetics
University of Louisville
Louisville, Kentucky

May 2021

INVESTIGATING A NOVEL FUNCTION FOR PHOSPHOSERINE AMINOTRANSFERASE 1

(PSAT1) IN EPIDERMAL GROWTH FACTOR RECEPTOR (EGFR)-MEDIATED LUNG

TUMORIGENESIS

By

Rumeysa Biyik-Sit
B.S. Bilkent University 2007
M.S. Bilkent University 2009
M.S. The Ohio State University 2012
M.S. University of Louisville 2017

A Dissertation Approved on

March 18, 2021

by the Following Dissertation Committee:

_____

Brian Clem, Ph.D.

_____

Carolyn Klinge, Ph.D.

_____

Barbara Clark, Ph.D.

_____

Levi Beverly, Ph.D.

_____

Jason Chesney, M.D., Ph.D.

DEDICATION

This dissertation is dedicated to my parents Mr. Habib Biyik and Mrs. Guluzar Biyik,

my sister Mrs. Fatma Biyik-Sari, and my husband Mr. Atilla Sit, who have supported me

throughout my educational career.

ACKNOWLEDGEMENTS

ABSTRACT

INVESTIGATING A NOVEL FUNCTION FOR PHOSPHOSERINE AMINOTRANSFERASE 1

(PSAT1) IN EPIDERMAL GROWTH FACTOR RECEPTOR (EGFR)-MEDIATED LUNG

TUMORIGENESIS

Rumeysa Biyik-Sit

March 18, 2021

Phosphoserine aminotransferase 1 (PSAT1) catalyzes the second enzymatic step within the serine synthetic pathway (SSP) and its expression is elevated in numerous human cancers, including non-small cell lung cancer (NSCLC). Epidermal growth factor receptor (EGFR) mutant NSCLC is characterized by activating mutations within its tyrosine kinase domain and accounts for 17% of lung adenocarcinomas. Although elevated SSP activity has been observed in EGFR-mutant lung cancer cells, the involvement of PSAT1 in EGFR-mediated oncogenesis is still unclear.

Here, we explore a putative non-canonical function for PSAT1 using biochemical approaches to elucidate unknown interacting proteins and genomic RNA-seq profiling to identify cellular processes impacted by PSAT1. We further determined the cellular phenotypes affected by PSAT1 loss, which were verified by experimental rescue studies, including metabolite supplementation and restoration of protein expression/localization.

Initially, we identified PKM2 as a novel PSAT1 associating protein. Although PSAT1 selectively induced the pyruvate kinase (PK) activity of recombinant PKM2, its loss in NSCLC cells did not alter cellular PK activity or expression of PKM2. However, fractionation studies revealed that PSAT1 localized to the nucleus and was required for EGFR-mediated nuclear PKM2 translocation. Phenotypically, PSAT1 loss led to a defect in EGFR-activated cell motility, which was partially restored by a nuclear expression of an acetyl-mimetic PKM2 mutant, but not wild-type

PKM2 or metabolite supplementation. To get insight into cellular mechanisms downstream of PSAT1 activity, we conducted RNA-seq profiling. Consistent with the reported function of PSAT1, E2F targets and nucleotide metabolism genes were decreased upon PSAT1 silencing. Accordingly, the anchorage-independent growth was impacted by PSAT1 silencing and rescued by metabolite supplementation, but not by nuclear PKM2 expression. The correlation between decreased expression of actin-related genes and F-actin formation upon PSAT1 silencing suggested a role for PSAT1 in actin cytoskeleton rearrangements. Furthermore, identified PSAT1-associated gene signatures were predictive towards survival outcomes in EGFR-mutant NSCLC. Together, our data suggest multiple roles for PSAT1 in promoting EGFR-mutant NSCLC involving not only canonical SSP activity but also a non-canonical nuclear function through mediating protein localization. These findings have laid the foundation for future studies to fully define PSAT1's response under EGFR-activation.

TABLE OF CONTENTS

LIST OF TABLES

LIST OF FIGURES

CHAPTER 1

INTRODUCTION

Tumor cells require metabolic reprogramming to fulfill the high energy demand and macromolecule synthesis necessary for tumor growth. This also allows for cell survival under unfavorable conditions, including nutrient deprivation and hypoxia, which are commonly found in tumors (5, 6). Aerobic glycolysis, also known as the Warburg effect, is classically defined as glycolytic metabolism to lactate even in the presence of oxygen (9). This was the earliest demonstration of altered metabolism in cancer made by Otto Warburg in the 1920's. Within this phenomenon, tumor cells consume high amounts of glucose that allows for not only glycolytic ATP production but also the production of the required biosynthetic precursors, such as nucleotides, that stem from glycolytic metabolites. Although the importance of glucose metabolism has been appreciated for some time, elucidation of changes within other metabolic pathways is an intense area of study and a target for developing new anti-cancer drugs.

Recently, changes in serine metabolism have been a focus of extensive work due to its role in the biosynthesis of many biological molecules, including nucleic acid synthesis, lipid synthesis, and other amino acids (15, 16). In certain tumor cells, depletion of intracellular serine through culture media manipulation leads to decreased cell proliferation, which can be rescued by the addition of downstream metabolites (17, 18).   However, limiting extracellular serine may not impact some types of tumors as they exhibit activated *de novo* serine biosynthesis (19). For example, inhibition of the serine biosynthetic pathway by small-molecule antagonists suppresses tumor cell proliferation even under serine proficient media, suggesting that activation of the serine biosynthetic pathway may go beyond the requirement for general serine production for tumor progression (20).

1

In this introduction, we will discuss the contribution of serine metabolism to biosynthetic pathways, cellular mechanisms leading to activation of serine biosynthesis, the cellular consequences of pathway activation, and the importance of glycolytic enzyme function that impinges on serine biosynthesis. Specifically, we will discuss the connection between glycolysis and serine synthesis in non-small cell lung cancer (NSCLC) and review the reports investigating the requirement of serine synthesis pathway (SSP) genes in lung cancer. As a substantial portion of existing literature examines these metabolic changes in different subtypes of NSCLC, we will provide a brief introduction about epidermal growth factor receptor (EGFR)-mutant lung cancer, which comprises a significant percentage of NSCLC adenocarcinoma. Since phosphoserine aminotransferase (PSAT1) catalyzes the second step in serine biosynthesis and is the focus of this study, we will also review current reports related to its tumorigenic function. Lastly, we will highlight recent reports implicating non-canonical functions for metabolic enzymes; specifically, those within glycolytic, tricarboxylic acid (TCA) cycle, and serine synthetic pathways, all culminating with the specific aims used to test the overall hypothesis of this work.

Serine metabolism in cancer

Serine as a central donor for macromolecule synthesis

Serine functions as a central donor for many anabolic reactions that promote tumor growth and survival (15, 28) (Fig. 1). Beyond the requirement for protein synthesis, cells can utilize serine for the synthesis of other amino acids such as glycine and cysteine, which can then be used for the production of glutathione for the maintenance of cellular redox homeostasis. Serine also contributes to cell membrane formation via incorporation into sphingosine and phosphatidylserine.

In tumors, serine also impacts RNA/DNA synthesis through providing one-carbon units to the folate cycle. 5,10-methylenetetrahydrofolate (CH2-THF), which is synthesized from tetrahydrofolic acid (THF) methylation from the conversion of serine to glycine, contributes to thymidine and purine synthesis (16, 28). Under serine starvation, cells convert glycine into serine at the expense of one-carbon metabolism, which leads to inhibition of purine synthesis. This underscores the importance of serine for cell proliferation. In addition to glutathione biosynthesis, serine also promotes redox balance via nicotinamide adenine dinucleotide (NADH) synthesis within the folate cycle (28).

Serine further contributes to S-adenyl-methionine (SAM) production within the methionine cycle via its functional interaction with the folate cycle. Although the contribution of serine to homocysteine's re-methylation to methionine is controversial, serine is required for the *de novo* biosynthesis of ATP. This is utilized for the adenylation of methionine, thereby highlighting a putative requirement for SAM production (38). Furthermore, global decreases in DNA and histone methylation upon serine depletion implicate cellular serine in maintaining the epigenetic landscape of cells (38, 39).
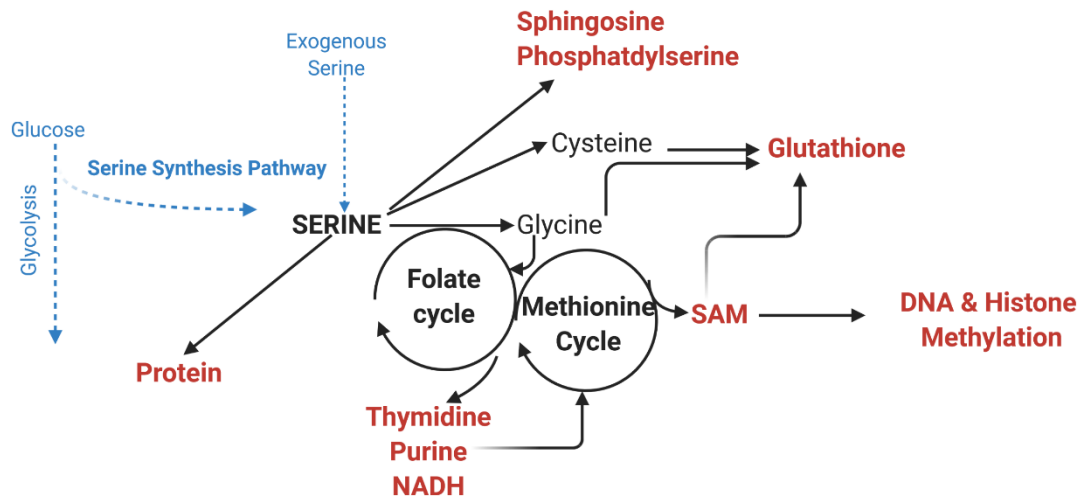
Figure 1. Serine contributes to many aspects of biomolecule synthesis.

Contribution of serine biosynthesis to tumor progression

Serine is a non-essential amino acid that can be synthesized from the glycolytic intermediate, 3-phosphoglycerate (3-PG) (Fig. 2). Phosphoglycerate dehydrogenase (PHGDH) is the rate-limiting enzyme that catalyzes the first reaction of 3-PG and NAD^+ to 3-phosphohydroxypyruvate (3-PHP) and NADH. PSAT1 then transfers the amino group from glutamate to 3-PHP to generate phosphoserine and α-ketoglutarate (α-KG). The final reaction in the SSP pathway is the production of serine through dephosphorylation of phosphoserine by phosphoserine phosphatase (PSPH) (28). Although serine is one of the most abundant amino acids in the serum, many tumor types exhibit elevated serine biosynthetic activity. The importance of serine in cellular biosynthesis and the elevated expression of the biosynthetic enzymes prompted researchers to investigate a potential role for the SSP in tumorigenesis (15).

PHGDH amplification, frequently observed in melanoma and triple-negative breast cancer (TNBC), accounts for the increased serine biosynthesis observed in these tumors (19, 40). While this provides a growth advantage under serine-limiting conditions, it also makes them vulnerable to PHGDH inhibitors (41). Stratification of NSCLC based on PHGDH expression found that increased PHGDH correlates with elevation of downstream SSP genes and activity, supporting the correlation between high PHGDH expression and serine biosynthesis (42). In addition, upregulation of PHGDH and PSAT1 expression correlates with poor patient outcomes in various tumor types, including NSCLC, colon, and estrogen receptor (ER) negative breast cancer (40, 43, 44).

It is obvious that activation of serine biosynthesis can provide a growth advantage to tumor cells when serine is limiting. Yet, as serine is abundant in the serum, it is unclear why tumors exhibit high SSP expression when they can readily obtain serine from the extracellular environment (15). Inhibition of PHGDH activity via depletion or small-molecule inhibitors diminishes cell proliferation *in vitro* and tumor growth *in vivo* (20, 45). Since NSCLC cells with high SSP activity produce more RNA/DNA precursors, suppression of PHGDH leads to DNA damage, which can be partially rescued by nucleoside addition (42). Another mechanistic study found a reduction in extracellular ^{13}C-labeled serine into AMP and dTMP in PHGDH inhibited cells (20). They found that inhibition of
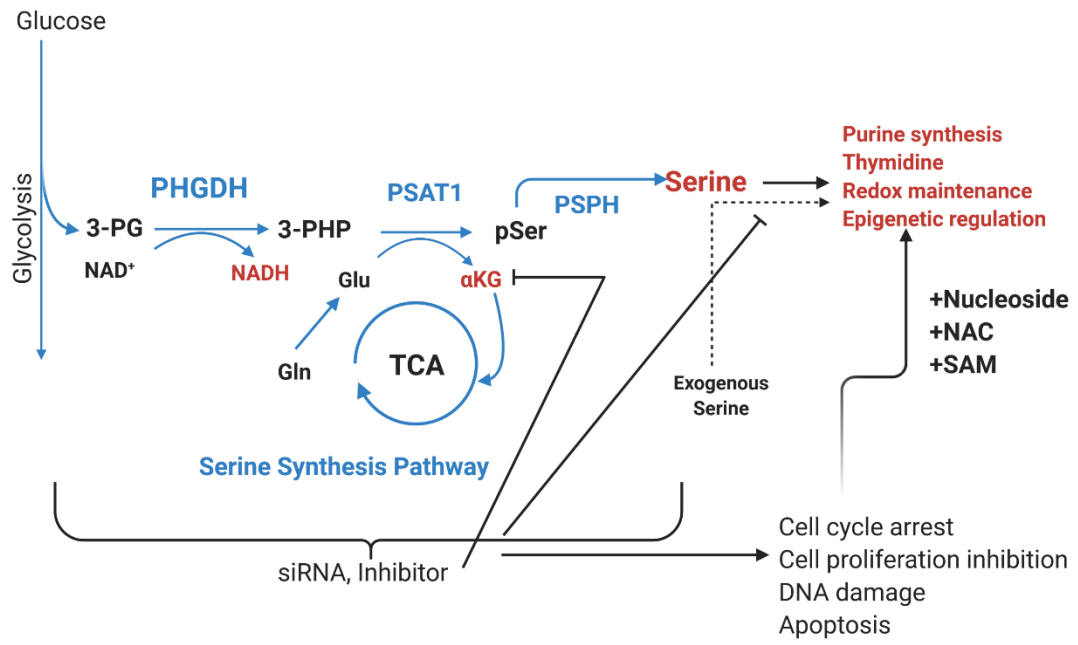
Figure 2. The schematic illustration of serine synthesis pathway (SSP) and contribution to tumor metabolism. Pathway inhibition via siRNA gene targeting or inhibitor impacts downstream metabolite production even in the presence of exogenous serine. Supplementing SSP downstream metabolites can, in some cases, mitigate the siRNA/inhibitor affect.

serine synthesis leads to active cytosolic serine hydroxymethyl transferase 1 (SHMT1), which "wastes" the one-carbon unit in order to regenerate serine from glycine at the expense of nucleotide synthesis. Yet, depletion of SHMT1 restores the nucleotide production in SSP inhibited cells. This strongly suggests that serine biosynthesis is necessary to promote the forward reaction in serine-glycine one-carbon metabolism via suppressing SHMT1 activity.

Active serine synthesis has also been reported to be required for other pro-tumorigenic processes. Serine production is necessary to maintain the epigenetic landscape in a Kras-activated pancreatic cancer mouse model with loss of Lkb1 functions (46). Loss of Psat1-mediated SAM production impacts DNA methylation, which is rescued by SAM addition. Further, elevated PHGDH expression in EGFR-mutant NSCLC cells participates in erlotinib-resistance (47). While either siRNA or pharmacological inhibition sensitizes resistant cells to erlotinib treatment via inducing DNA damage, supplementation of the reactive oxygen species (ROS) scavenger, N-acetyl-cysteine (NAC), is protective and indicates that serine biosynthesis may contribute to drug resistance through redox balancing. Lastly, in addition to impacting downstream serine-derived metabolites, SSP suppression also negatively impacts intermediary metabolism in tumors. As PSAT1 catalyzes the conversion of glutamate to α-KG, it is an active player in glutamine anaplerosis in providing a key TCA cycle intermediate. In TNBC cells, the SSP was found to contribute 50% of glutamine-derived α-KG (40). In short, serine biosynthesis has been found to be crucial for efficient biosynthetic reactions, glutamine anaplerosis, and tumor growth.

Regulators of SSP transcription

Increased gene expression of serine biosynthetic enzymes primarily accounts for the activation of serine biosynthesis in tumors. Transcriptional regulation of SSP genes has been observed under various conditions but is primarily induced by two main causes: oncogenic activation and nutrient/oxidation stress (Fig. 3).
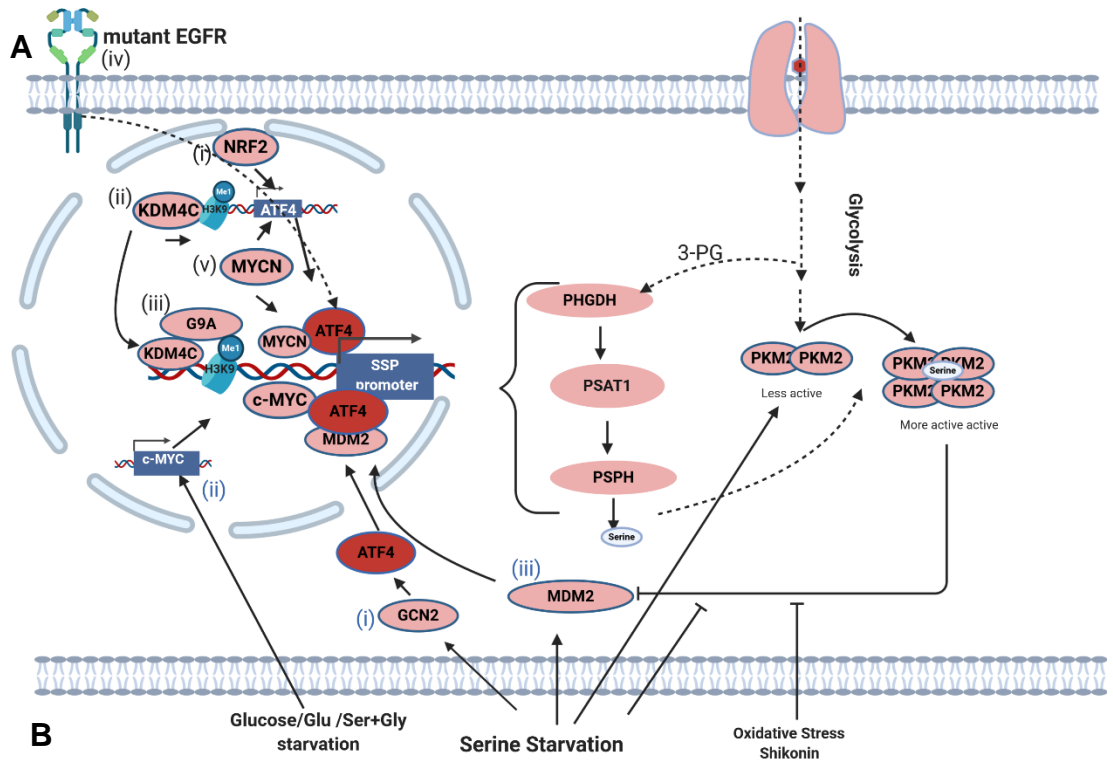
Figure 3. Transcriptional regulation of SSP genes in cancer. A) Oncogenic activation: (i) NRF2-ATF4; (ii) KDM4C-ATF4; (iii) G9A; (iv) EGFR mutant-ATF4; (v) MYCN-ATF4. **B)** Stress-induced activation: (i) Serine starvation-GCN2-ATF4; (ii) nutrient stress (Glucose/Glutamine/Serine-Glycine starvation)-c-MYC; (iii) Serine starvation/oxidative stress/ inhibition of PKM2-MDM2-ATF4

The analysis of serine biosynthesis activity using ^{13}C-labeled glucose metabolomics coupled to transcriptomic analysis of a large panel of NSCLC tumors found that the transcription factor nuclear factor erythroid-2-related factor 2 (NRF2) is an upstream regulator of SSP gene expression (45). Silencing of NRF2 leads to down-regulation of SSP genes through decreased activating transcription factor 4 (ATF4), as ATF4 restoration in NRF2 depleted cells rescues SSP expression in NSCLC cells (Fig. 3A(i)). Lysine-specific demethylase 4C (KDM4C) functions as a histone demethylase via removing methyl groups from the tri/di-methylated histone H3 lysine 9 (H3K9me3/2). Separately, the euchromatic histone-lysine N-methyltransferase 2 (EHMT2/G9A) acts as monomethylase and accounts for the mono-methylation of H3K9. Both KDM4C and G9A action results in the generation of a known epigenetic activation mark, H3K9me1, which leads to transcriptional induction. KDM4C-mediated H3K9me1 at the *ATF4* proximal promoter induces *ATF4* transcription (48). Subsequently, an ATF4-KDM4C interaction promotes SSP expression (Fig. 3A(ii)). Another report demonstrated that G9A facilitates SSP gene expression via mono-methylation of H3K9 at the promoter sites (Fig. 3A(iii)) (49). Although it remains unknown whether KDM4C and G9A act together to promote SSP expression, the mechanism is not mutually exclusive.

Investigation of the role of receptor tyrosine kinases in metabolic reprogramming has found that activating mutations in EGFR lead to increased glucose-derived serine biosynthesis (Fig. 3A(iv)) (50). Bioinformatic analysis suggests both c-Myc and ATF4 as candidate transcription factors responsible for EGFR-activated SSP transcription. However, siRNA loss of function studies found activation of SSP expression was due to ATF4 and not c-MYC. Another study compared the transcriptomic profiles of *MYCN* amplified neuroblastoma cells and non-amplified cells and demonstrated elevated expression of SSP genes in *MYCN* amplified cells (51). Further functional studies revealed that *MYCN* actually induces ATF4 expression via binding to the promoter region, and subsequently, MYCN and ATF4 stimulate SSP transcription (Fig. 3A(v)). Taken together, these reports demonstrate that SSP enzymes in cancer cells are elevated through various oncogenic pathways, but induction of ATF4 expression seems a pre-requisite to promote SSP expression.

In addition to oncogenic activation, limited nutrient availability and oxidative stress are able to induce SSP expression in order to mediate the cellular stress response (Fig. 3B). Serine starvation induces general control nonderepressible 2 (GCN2)-mediated translation of ATF4, which as described above leads to ATF4-dependent SSP transcription (Fig. 3B(i)) (52). Simultaneously, decreased pyruvate kinase activity in pyruvate kinase M2 (PKM2)-expressing cells results in accumulation of the glycolytic intermediate 3-phosphoglycerate for serine biosynthesis. Also, the mouse double minute 2 homolog (MDM2) can localize to the SSP promoter under oxidative stress, serine starvation, or PKM2 inhibition to facilitate SSP expression (Fig. 3B(ii)) (53). However, MDM2 mediated SSP transcription still requires ATF4 transactivation. Nutrient deprivation such as glucose, glutamine, or serine/glycine triggers c-MYC transcription in hepatocellular carcinoma (HCC) cells (Fig. 3B(iii)) (54). c-MYC can promote SSP transcription via binding to their proximal promoters to adapt the cells to the stress conditions, while the involvement of ATF4 in this scenario is unclear. Together, these findings indicate the relevance of oncogenic drivers and stress responses to coordinately activate SSP transcription and serine biosynthesis in various tumors.

Functional cross-talk between glycolysis and serine biosynthesis

As described above, oncogenic activation or nutrient-limitations can induce SSP gene expression. However, serine biosynthesis not only depends on the expression of SSP genes but also on the availability of substrate, mainly glycolytic derived 3-phosphoglycerate. Therefore, alteration in glycolytic flux can substantially influence activity through the SSP.

In maximizing high glucose uptake, tumor cells promote the accumulation of glycolytic intermediates for anabolic processes through reducing glycolytic flux through pyruvate (55). Specifically, tumor glycolytic flux can be regulated by pyruvate kinases that catalyze the final and irreversible step in glycolysis: ATP and pyruvate production from phosphoenolpyruvate (PEP) via phosphate transfer to ADP. Mammals have four different kinds of pyruvate kinases. While *PKL* and *PKR* are transcribed from the same gene, they are driven from different promoters and expressed in liver and red blood cells, respectively. PKM1 and PKM2 are transcribed from the *PKM* gene and arise via alternative splicing of exons 9 and 10, which leads to differential expression in

tissues. While other pyruvate kinases form constitutively active tetrameric enzymes, PKM2 can be found in either a highly active tetrameric or low active dimeric state. Tumor cells predominantly express PKM2, as low active dimeric PKM2 allows for the accumulation of glycolytic intermediates. In addition, tumor cells have developed a variety of mechanisms to disrupt tetramer formation and preserve the low active PKM2 dimer, including allosteric regulation by metabolites, post-translational modifications, and protein:protein interactions (56).

Mechanistically, PKM2 functions as a key node between glycolysis and serine biosynthesis. As serine is an allosteric activator of PKM2, serine binding to PKM2 induces tetramer formation and consequently increases pyruvate kinase activity to promote glycolytic flux to lactate (57). Conversely, serine starvation reduces the pyruvate kinase activity in PKM2 expressing cells to divert the glycolytic flux into serine biosynthesis through 3-phosphoglycerate availability. When the intracellular serine level is restored, glycolytic flux is re-established by elevated activity of PKM2. Therefore, PKM2 acts as a sensor for intracellular serine levels. To explore the relationship between PKM isoforms and serine, Ye *et al.* generated ectopic PKM1 or PKM2 expressing cells in endogenous PKM2 depleted H1299 cells (52). While the proliferation rate of PKM1 expressing cells is comparable to PKM2 expressing cells in serine replete conditions, PKM2 expressing cells displays better survival ability than PKM1 expressing cells under serine depleted conditions. This supports the concept that PKM2 links the glycolytic pathway to serine metabolism. Further, receptor tyrosine kinase activity contributes to serine biosynthesis via blocking tetramer formation by phosphorylating PKM2 at Tyr105 (58). However, induction of tetramer formation of PKM2 by CARM1 methylation impacts serine biosynthesis in MEF cells, further highlighting the link between serine biosynthesis and PKM2 oligomeric status (59).

Given the reported pro-tumorigenic effects of diminished activity of dimeric PKM2, different PKM2 activators have been developed as anti-cancer therapeutics. These small molecules induce tetramer formation and block the phospho-tyrosine protein interaction induced dimer formation (60, 61). Interestingly, although these activators induced tetramer formation of PKM2 in tumor cells, no significant cell proliferation difference was observed between activator-treated and untreated cells

under standard cell culture conditions *in vitro* (62). However, PKM2 activators blocked cell proliferation when serine is depleted from the media. Mechanistic studies demonstrated that PKM2 activators induce an acute increase in pyruvate kinase activity that led to a reduction in intracellular glucose-derived biomolecules, including serine. This, in turn, induced expression of SSP genes and serine transporters, SLC1A4 and SLC1A5, to restore the intracellular serine level (60, 61). As serine biosynthetic activity is limited by lack of substrate production (low 3-PG levels due to high PKM2 activity), tumor cells become dependent on exogenous serine to survive, thereby explaining why the anti-tumorigenic actions of PKM2 activators require serine-limited conditions *in vitro*. In short, the metabolic link between PKM2-regulated glycolysis and serine metabolism is mutual as serine biosynthesis needs low active PKM2 while serine itself can act as an allosteric activator of PKM2.

Phosphoserine aminotransferase 1

Since PHGDH is the rate-limiting enzyme in the SSP, there is considerable literature describing its tumorigenic activities. Yet, the contribution of other SSP enzymes, including PSAT1, is just now being investigated, which is the focus of this dissertation. As stated above, PSAT1 is the second enzyme within the serine synthesis pathway that catalyzes the amino transfer from glutamate to synthesize phosphoserine. Neu–Laxova syndrome (NLS) is a rare autosomal recessive serine deficiency disorder with a broad range of manifestations. Several mutations in PSAT1 have been discovered in NLS patients (63). Computational modeling of PSAT1 with patient-derived mutations has found that while the A99V mutation is related to protein instability, S179L affects the cofactor binding sites (64). Sirr *et al.* has conducted yeast complementation assays to explore the functions of patient-derived PSAT1 mutations in SER1 (yeast ortholog of PSAT1) knockout yeast and categorize the mutations based on survival effects (65). Consistent with computational modeling, expression of S179L-PSAT1 mutant fails to rescue the growth of SER1 knockout yeast cells under serine-deprived media, demonstrating the importance of PSAT1 function in serine biosynthesis.

PSAT1 correlates with clinical outcomes

Upregulation of PSAT1 expression has been discovered in a variety of tumor types in comparison with normal tissue (1, 43, 66-72). Furthermore, higher PSAT1 correlates with metastasis, advanced tumor stage, and poorer overall survival in ovarian cancer, triple-negative breast cancer, ER-negative breast cancer, nasopharyngeal carcinoma, and esophageal squamous cell carcinoma (ESCC) (43, 67, 69, 73). These clinical data strongly suggest a role for PSAT1 in tumor progression. As colorectal cancer (CRC) patients with chemoresistance and breast cancer patients with tamoxifen resistance display higher PSAT1 expression than patients with chemosensitive lesions, elevated PSAT1 expression can serve as a prognostic marker for chemotherapy (66, 74-76).

Regulation of PSAT1 expression in tumorigenesis

Coordinated regulation of SSP gene expression was detailed in earlier sections within this introduction. Apart from these, other reported mechanisms directly regulate PSAT1 expression (Fig. 4).

Elevated Psat1 expression has been observed in genetic models used in cancer research. In mouse models for *Kras* mutant lung cancer, deletion of neurofibromin 1 (*Nf1*) leads to upregulation of Psat1 expression (68). Further analysis has found that hyperactivation of focal adhesion kinase 1 (Fak1) upon *Nf1* deletion accounts for the upregulation of Psat1, which was validated by Fak1 activator treatment of *Nf1* wild-type cells. These findings were also recapitulated with *NF1* mutant and wild-type human patient-derived xenograft (PDX) cells. In the *Kras* mutant pancreatic cancer model, deletion of liver kinase b1 (*Lkb1*) tumor suppressor gene was found to increase Psat1 expression through AMPK/mTOR pathway activation (46).

Apart from these oncogene-driven cancer models, PSAT1 expression can also be regulated epigenetically. Up-regulation of PSAT1 expression in CRC cells is mediated by G9A histone H3K9 methyltransferase (77). Increased monomethylation of histone H3K9 in the PSAT1 promoter region activates PSAT1 transcription. G9A-mediated PSAT1 expression contributes to several oncogenic processes, including cell migration, invasion, and cell proliferation. An investigation
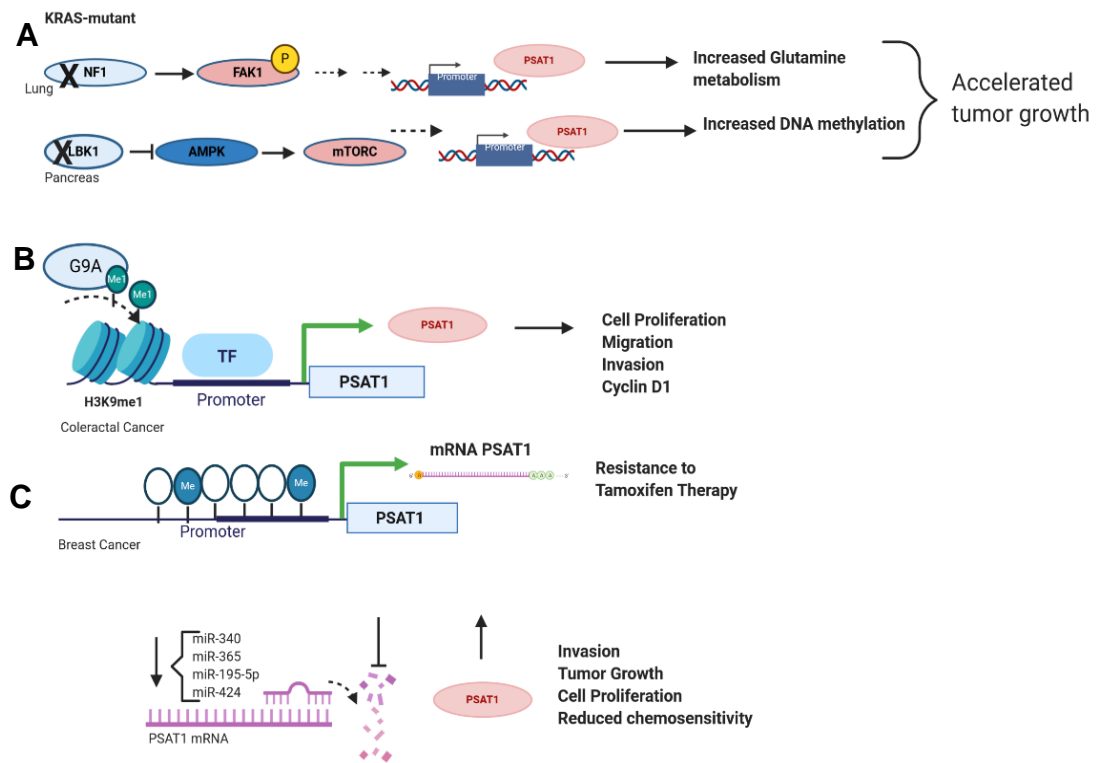
Figure 4. Regulation of PSAT1 expression in cancer. A) Genetic drivers that induce PSAT1 expression. **B)** Epigenetic regulation of PSAT1. **C)** miRNA-mediated regulation of PSAT1.

conducted with ER-positive breast cancer patients found that the PSAT1 promoter is hypermethylated and correlates with low PSAT1 expression, thereby implying the involvement of epigenetic mechanisms on PSAT1 expression in ER-positive breast cancer (75). Survival analysis demonstrated that both PSAT1 promoter hypermethylation and low mRNA expression are associated with better outcomes after tamoxifen treatment.

MicroRNAs can participate in tumorigenesis via regulating mRNA translation and can be oncogenic or tumor suppressive depending on their target proteins and expression ratio between tumor and normal tissue. Down-regulated miRNAs in tumor tissue are expected to function as tumor suppressers and miRNA-mediated PSAT1 expression has been reported in some cancers. Mir-340 and miR-365 are two low expressed miRNAs in ESCC that may regulate PSAT1 and their expression negatively correlate with *PSAT1* in tumor tissue (77, 78). Ectopic expression of these miRNAs in ESCC cells decreases cell proliferation, invasion, and colony formation *in vitro* and tumor growth *in vivo,* as well as PSAT1 expression. Restoration of PSAT1 expression in miRNA overexpressed cells mitigates their tumor suppressive functions. miR-195-5p has been identified as a tumor suppressor miRNA in ovarian cancer due to loss of expression in tumor tissue and restoration of chemosensitivity to cisplatin upon overexpression (79). PSAT1 has been found as a direct target of miR-195-5p. While PSAT1 silencing recapitulates the miR-195-5p overexpression mediated phenotype, increased PSAT1 reverts it, suggesting that loss of miR-195-9p contributes to elevated expression of PSAT1 in ovarian cancer. PSAT1 in CRC cells is not only subjected to epigenetic regulation by G9A histone H3K9 methyltransferase but also loss of miR-424 (80, 81). A negative correlation between miR-424 expression and PSAT1 expression has been shown in CRC tissue. While miR424 expression leads to growth inhibition and apoptosis induction, overexpression of PSAT1 impacts the miR424-mediated anti-tumorigenic phenotype.

PSAT1 metabolic function in tumorigenesis

Several studies have reported an oncogenic function of PSAT1, but few provide direct evidence for its metabolic function through a rescued phenotype by metabolite supplementation.

According to gene expression analysis from the TCGA database, high levels of *PSAT1* correlates with the proliferation rates of many types of tumors (82). As *Lkb1* loss in the *Kras* mutant pancreatic cancer mouse model induces Psat1 expression, Psat1 depletion affects the cell proliferation and anchorage-independent growth in these cells but not in *Lkb1* wild-type cells (46). Rescue studies with down-stream metabolite supplementation reveal that Psat1 is crucial in supplying SAM for cell proliferation but not to maintain nucleoside pools or redox homeostasis.

Suppression of PSAT1 in ovarian cancer cells induces apoptosis and cell cycle arrest and impairs clonogenic growth (73). Consistent with these findings, silencing leads to reduction in cyclin D1 and CDK4 expression and increased in BAX and cleaved caspase3 levels. Further analysis of PSAT1 mediated-metabolic pathways has shown decreased reduced glutathione (GSH)/ oxidized glutathione (GSSG) ratio and increased ROS levels under PSAT1 silencing, which is restored via GSH supplementation.

As mentioned above, loss of *Nf1* tumor suppressor in *Kras* mutant lung cancer mouse model increases the Psat1 expression (68). While inhibition of Psat1 activity with transaminase inhibitor severely affects cell proliferation, preincubation of the cells with α-KG abolishes the effect of inhibitor treatment, suggesting an anaplerotic requirement of Psat1 expression in these cells.

The oncogenic role of PSAT1 via mediating glycogen synthase kinase 3 beta (GSK3β) pathway

Despite the presence of several reports showing the oncogenic function of PSAT1, the involvement of PSAT1 in downstream signaling pathways requires further investigation. According to previous studies, PSAT1 is linked to a GSK3β-dependent pathway. Increased phosphorylation of GSK3β at Ser9 upon elevation of PSAT1 has been found in many tumor cell types even though the downstream effector may be context-dependent. In general, phosphorylation of GSK3β at Ser9 inhibits its serine/threonine kinase activity and phosphorylation-dependent proteasomal degradation of target proteins (83, 84). Figure 5 summarizes the PSAT1-GSK3β pathway in tumorigenesis.
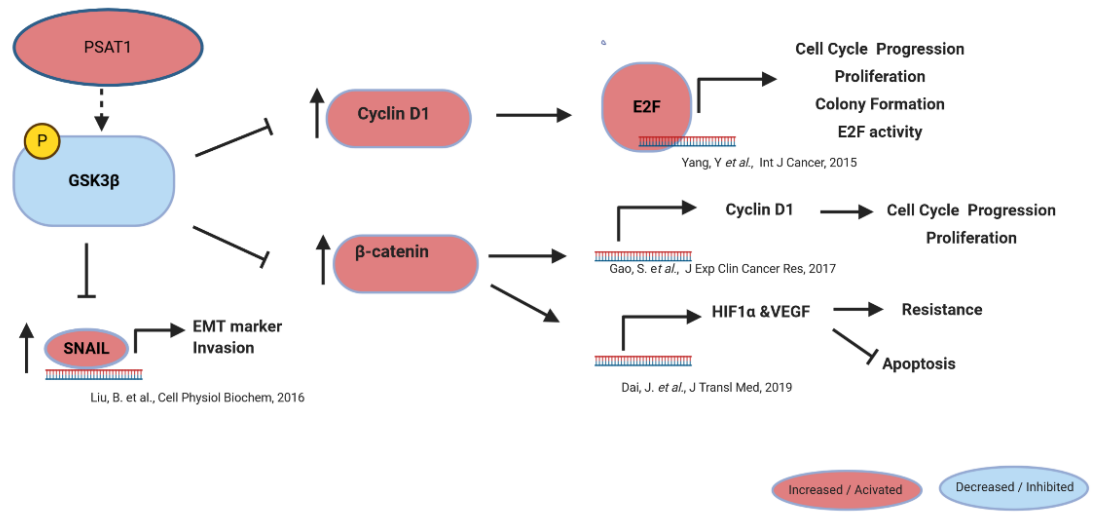
Figure 5. The oncogenic function of PSAT1 mediated by GSKβ pathway.

Yang *et al.* found that cyclin D1 expression at the protein level decreases in PSAT1 silenced NSCLC cells and increases upon overexpression, which is independent of transcriptional regulation (1). Further analysis shows that high PSAT1 leads to increased phosphorylation of GSK3β at Ser9 and inhibits GSK3β-dependent cyclin D1 phosphorylation at T286. Decreased phosphorylation protects cyclin D1 from proteasomal degradation, resulting in the accumulation of cyclin D1, which increases cell cycle progression via enhancing E2F activity.

The role of PSAT1 in ER-negative breast cancer cells has been investigated via both silencing and ectopic expression (43). PSAT1 mediates cell proliferation, cell cycle progression, and colony formation *in vitro* and tumor growth *in vivo.* A mechanistic study revealed that high PSAT1 expression correlates with the inhibitory phosphorylation level of GSK3β (Ser9). Inhibition of GSK3β activity leads to accumulation and nuclear localization of β-catenin in breast cancer cells and subsequently increases expression of cyclin D1. Therefore, PSAT1 is involved in ER-negative breast cancer proliferation and cell cycle progression, in part, via regulation of the GSK3β/β-catenin/cyclin D1 pathway.

Dai *et al.* also demonstrated the connection between PSAT1 and GSK3β/β-catenin pathway in ovarian cancer (79). Restoration of low expressed miR-195-5p in ovarian cancer reduces phosphorylated GSK3β levels and β-catenin. As PSAT1 has been found as a direct target of miR-195-5p, overexpression of PSAT1 in miR-195-5P expressing cells reconstitutes phosphorylated GSK3β and β-catenin expression. Reduced sensitivity to cisplatin treatment upon PSAT1 overexpression or β-catenin agonist treatment indicates that this PSAT1/GSK3β/β-catenin pathway is involved in chemoresistance in ovarian cancer.

Liu *et al.* examined the role of PSAT1 function in ESCC cells via loss and gain of function studies (69). Modulation of PSAT1 expression in ESCC alters cell proliferation and invasion *in vitro* and tumor growth *in vivo.* PSAT1 expression correlates with inhibitory phosphorylation of GSK3β and downstream SNAIL-mediated expression of E-cadherin and vimentin. Consistent with this finding, observation from PSAT1 targeting miRNAs, miRNA-340 and miR-365, suggest that PSAT1 has an oncogenic function in ESCC cells via regulating the GSK3β/SNAIL pathway (69, 77, 78).

Integrative transcriptomic and proteomic analyses of samples derived from both primary and PDX lung tumors have been performed in attempts to discover genes with prognostic value (85). Increased PSAT1 has been observed in both primary and PDX NSCLC tumors, and it is upregulated in NSCLC tumor-initiating cells and induces cellular transformation of 3T3 cells (86). Together, these suggest PSAT1's involvement in lung tumorigenesis.

Within the serine-one carbon metabolic pathway, Yang *et al.* found that PSAT1 is the most upregulated enzyme in NSCLC tumors (1). Immunohistochemistry (IHC) staining of lung cancer tissue validates the upregulation of PSAT1 in NSCLC and its association with poorer patient outcomes. E2F has been identified as a potential downstream regulator of PSAT1, which is evident from reporter assays with decreased E2F transactivation upon PSAT1 silencing in lung cancer cells. Consistent with this, suppression of PSAT1 impairs cell proliferation and cell cycle progression and correlates with hypo-phosphorylated retinoblastoma (RB) protein. Further examination shows that PSAT1 leads to the accumulation of cyclin D1 in NSCLC cells through inhibiting GSK3β-induced phosphorylation and degradation. Therefore, they conclude that PSAT1 can mediate cell cycle progression, cell proliferation, and colony formation *in vitro* and tumor growth *in vivo* through regulating the GSK3β /cyclin D1/RB/E2F pathway in NSCLC cells.

Chan *et al.* investigated the role of PSAT1 in lung adenocarcinoma metastasis (2). Evaluation of publicly available datasets demonstrated that high expression of PSAT1 expression is associated with poorer overall and disease-free survival of patients with lung adenocarcinoma. Highly metastatic CL1-5 cells have increased PSAT1, while depletion of PSAT1 impacts this invasion capacity both *in vitro* and *in vivo* (2, 87). The involvement of PSAT1's metabolic activity in cell invasion has been tested via altering glucose, glutamine, and serine. After observing unaffected cell invasion upon metabolic manipulations, they concluded that PSAT1 mediated cell invasion is independent of its metabolic function. PSAT1-mediated genome-wide gene expression profiling suggested that PSAT1 participates in lung cancer metastasis by suppressing STAT1/IRF1/IFIH1 pathway.

EGFR mutant lung cancer

In this work, we investigated a role for PSAT1 under EGFR activation. Activating mutations within EGFR are found in a substantial percentage of NSCLC and were used as the model system for these studies. For this, the following section briefly introduces the function of EGFR mutations in lung tumorigenesis.

EGFR mutations in NSCLC

Lung cancer is the leading cause of cancer-related deaths in the US with an overall five-year survival rate of 19% (88). NSCLC accounts for 84% of lung cancer cases with another 13% of cases classified as small cell carcinoma. Surgery is the primary treatment option for NSCLC patients diagnosed at early stage, but more than 55% of new cases are diagnosed at advanced stages with distant metastasis (89).

Smoking is a major risk factor for developing lung cancer and is responsible for 80% of lung cancer deaths in the US (88). However, approximately 20% of lung cancer cases are observed in never-smokers. Adenocarcinoma is the most common histologic sub-type of NSCLC and 60% of the cases are related to oncogenic-driver mutations. Among these, activation mutations within the EGFR tyrosine kinase region constitute 17% of genetic alterations in adenocarcinoma and are significantly found in never smokers (90).

EGFR belongs to the ErbB family of tyrosine kinase receptors, which is genetically localized to chromosome 7p12 (91). It is comprised of an N-terminal extracellular ligand-binding domain, single-span transmembrane domain, intracellular tyrosine kinase domain, and regulatory C-terminal region (92). Epidermal growth factor (EGF), transforming growth factor α (TGFα), and amphiregulin (AREG) are all ligands that bind to and induce receptor dimerization, resulting in tyrosine kinase activation. Subsequently, several tyrosine residues at the C-terminal region are transphosphorylated and function as docking sites for proteins involved in the activation of downstream pathways such as PI3K/AKT/mTOR, RAS/MAPK, and the JAK/STAT (92-95).

Activation of EGFR signaling promotes several tumorigenic processes, including cell proliferation, survival, migration, angiogenesis, and metastasis (91, 92).

The observation of dysregulated EGFR signaling in multiple tumor types led to the development of targeted therapies (92, 96, 97). Inhibition of ligand binding by monoclonal EGFR antibody or blocking tyrosine kinase activity by small-molecule antagonists are two distinct approaches to suppress EGFR signaling. Although monoclonal antibody treatment improves patient outcomes within colorectal and laryngeal cancers, the effect on lung cancer is controversial (98). Gefitinib and erlotinib are first-generation EGFR tyrosine kinase inhibitors (TKI). Gefitinib was initially developed as a tyrosine kinase inhibitor in 2003. It was initially administered to unselected lung cancer patients, with only 10% of them demonstrating any response to therapy (92). Stratification of the gefitinib-treated patients found that a subgroup of NSCLC patients with adenocarcinoma histology and never-smoking status from East Asian females are associated with the higher response rate to treatment. Further investigation within this group led to the discovery of mutations in the EGFR tyrosine kinase region that predicts gefitinib response (91, 92, 94). The discovery of mutated EGFR and the presence of small-molecule inhibitors have provided the opportunity to explore EGFR signaling, particularly as it relates to the metabolic enzyme functions highlighted in this dissertation.

Metabolic alterations are driven by mutant EGFR

Makinoshima *et al.* examined glycolytic metabolism in EGFR mutant lung cancer via EGFR-TKI treatment (99). Inhibition of EGFR signaling decreases glycolytic activity as demonstrated by lower lactate production, glucose consumption, and glucose-derived extracellular acidification rate (ECAR). Consistent with these results, hexokinase II (HK II) and glucose transporter 3 (GLUT3) expression are down-regulated in response to treatment. Metabolite analysis has found that the pentose phosphate pathway (PPP) and redox metabolism are also affected. Furthermore, EGFR signaling may contribute to pyrimidine biosynthesis via phosphorylating and activating CAD (carbamoyl-phosphate synthetase 2, aspartate transcarbamylase and dihydroorotase). In another study, De Rosa *et al.* also found that TKIs

reduce lactate production, HK II expression, and phosphorylation of PKM2 at Y105 (100). Yet, they also observed increased oxygen consumption, expression of mitochondrial complexes, and ATP production that indicated increased oxidative phosphorylation, suggesting that activating mutations in EGFR impacts not only glycolysis but also oxidative phosphorylation. EGFR-mediated glycolysis was further confirmed via EGFR knockdown, which decreased many of the genes involved in glycolysis (101). Glycolysis is crucial to sustain TCA cycle intermediates in EGFR mutant cells and both glucose starvation and inhibition of mitochondrial activity induce apoptosis. Mechanistic studies found that inhibition of mitochondrial ATP production induces autophagy-mediated degradation of EGFR protein. Taken together, glycolytic activity is not only driven by EGFR oncogenic activity but is also required for EGFR stability in EGFR mutant lung cancer.

The role of receptor tyrosine kinases (RTKs) in lung cancer metabolic reprogramming has been investigated via gain of function studies (50). Metabolic tracing experiments with ^{13}C-labeled glucose, glutamine, and palmitate were done in BAF3 isogenic cells stably transfected with mutant forms of RTKs including EGFR, FGFR, RET, and MET. Among these, mutant EGFR yielded higher glucose-derived serine biosynthesis and inhibition of serine biosynthesis impairs cell proliferation. These findings were further corroborated with EGFR mutant cell lines using PHGDH inhibitor treatment, indicating that activation mutation in EGFR promotes serine biosynthesis. Further upregulation of PHGDH has been shown in erlotinib resistance cells and inhibition of activity via either inhibitor or silencing induces the sensitivity (47). Another study supports this via ectopic expression of PSAT1 in EGFR mutant HCC827 NSCLC cells, which induces resistance to EGFR-TKI treatment (70). Thus, these reports imply that while EGFR mutation activates serine biosynthesis, it is further enhanced under TKI resistance.

The relationship between glutamine metabolism and EGFR mutation has been demonstrated using glutaminase (GLS) inhibition (102). In a xenograft tumor model, suppression of GLS activity does not affect tumor growth but enhances the anti-tumor activity of erlotinib. Molecular analysis has found that glycolysis and glutaminolysis are inhibited by combination

therapy, which negatively impacts the cellular energetic status and subsequently results in AMPK-mediated cell death.

Monounsaturated fatty acid (MUFA) synthesis is associated with the activation of lipid metabolism in tumorigenesis. Investigation of molecular mechanism in lung cancer has found that stearoyl-CoA desaturase 1 (SCD1), which plays a role in MUFA synthesis, interacts with EGFR in EGFR mutant cells (103). This interaction contributes to SCD1 protein stability via EGFR-mediated phosphorylation at Y55 and promotes lipid synthesis for tumor growth.

In short, mutant oncogenic activation of EGFR signaling modulates a variety of enzymes within metabolic pathways. These changes may not only involve manipulation of their canonical activities but also putative alternative functions, all of which may allow for the development of EGFR-TKI resistance.

Metabolic enzymes with non-canonical functions in tumorigenesis

The observation of metabolic reprogramming in tumor cells prompted researchers to examine specific enzyme function under varying conditions, including oncogenic activation, nutrient limitation, and hypoxia. This has provided significant insight into their involvement in tumorigenesis (104). In some cases, supplementation of downstream metabolites failed to rescue a loss of function phenotype, whereas restoration of a catalytically inactive enzyme rescued the cellular phenotype under specific conditions. This implied that certain metabolic enzymes possess a novel tumorigenic function beyond their role in metabolic pathways (105-107). To date, non-canonical functions have been discovered for multiple metabolic enzymes, particularly those involved in the glycolytic and TCA cycle pathways (104).

In many cases, non-canonical functions of enzymes are induced by post-translational modification, relocalization into a different cellular compartment, and /or interaction with non-metabolic proteins. In other cases, elevated expression of the enzyme is sufficient to display non-canonical functions (108).

Non-canonical functions can be categorized into two groups based on the requirement of catalytic activity. In the catalytic-dependent pathway, metabolic enzymes follow one of two routes to exert their non-canonical functions. Either they expand their substrate specificity from small metabolites to protein targets, resulting in protein modifications, or translocating to a different cellular compartment where their metabolic products are utilized as co-factors or substrates for posttranslational modifications (104, 108). In the catalytic-independent pathway, they can modify associating protein function via their physical interaction (104).

Catalytic-dependent non-canonical functions

i) Proteins, not metabolites, serve as substrates for metabolic enzymes

Various metabolic enzymes with kinase activity can exhibit protein kinase function using proteins as a substrate instead of their defined metabolites (108, 109). PKM2 has been the most-studied metabolic enzyme with protein kinase activity that influences several tumorigenic processes. One distinction is that it transfers the phosphate from PEP to protein targets instead of ATP. Mitogenic and growth factor stimulation, particularly EGF, leads to nuclear localization of PKM2 by post-translational modifications (110). Nuclear PKM2 can phosphorylate STAT3 at Tyr705 and Histone H3 at Thr11 that subsequently induces the expression of genes involved in cell proliferation, migration, and the Warburg effect (111, 112). Restoration of a catalytically inactive mutant of PKM2 in endogenous PKM2 depleted cells fails to restore the phosphorylation level of Histone H3 and the phenotype even though it can translocate into the nucleus (111, 113). Similarly, nuclear localization mutant forms of PKM2 decrease protein phosphorylation even though they have intact catalytic activity (110, 114). In the mitotic process, PKM2 participates in different steps, including phosphorylating Bub3 in chromosome segregation and phosphorylating MLC2 in cytokinesis (115, 116). In addition, the protein kinase activity of PKM2 contributes to cell survival in response to oxidative-stress induced apoptosis (117). PKM2 can translocate into the mitochondria upon oxidative stress and phosphorylate BCL2. Phosphorylated BCL2 is resistant to proteasomal degradation and promotes cell survival. These are just a few examples of the non-

canonical oncogenic functions of PKM2, whose roles can also be extended to tumor cell secretion, migration, and DNA damage response (108).

Phosphoglycerate kinase 1 (PGK1) is another ATP generating enzyme within the glycolytic pathway that utilizes the intermediate 1,3-diphosphoglycerate (108). Like PKM2, PGK1 also displays protein kinase activity, but unlike PKM2, it uses ATP as a phosphate source. Hypoxic activation of ERK signaling, EGFR stimulation, expression of mutant KRAS and BRAF induce PGK1 phosphorylation at S203 and mitochondrial localization (118). Mitochondrial PGK1 activates pyruvate dehydrogenase kinase isozyme 1 (PDHK1) through phosphorylation at T388. Phosphorylated PDHK1 subsequently inhibits the activity of pyruvate dehydrogenase complex (PDC), resulting in decreased pyruvate oxidation in mitochondria and increased pyruvate conversion to lactate in the cytosol. This suggests that PGK1 not only contributes to glycolytic flux through its canonical activity but also by inhibiting the usage of pyruvate by the mitochondria. Separately, glutamine starvation and hypoxia lead to mTOR-dependent phosphorylation of ARD1, which results in binding to PGK1 and acetylation at K388 in glioblastoma (GBM) cells (119). Acetylated PGK1 initiates autophagosome formation via phosphorylating Beclin1 at S30. The correlation between acetylated PGK1 and Beclin1 phosphorylation has been supported by GBM human tumor data and is associated with poor patient outcomes.

ii) Metabolites serve as substrates or cofactors for other enzymes

In some cases, nuclear-localized metabolic enzymes supply metabolic products that allow for global changes in histone modifications (108, 120). For example, acetyl-CoA for histone acetylation can be generated by nuclear ATP-citrate lyase (ACLY) using citrate or nuclear PDC using pyruvate (121, 122). While oncogenic signaling promotes nuclear localization of ACLY by AKT-dependent phosphorylation, serum and EGF stimulation can trigger the nuclear localization of PDC.

Tumor cells can also utilize metabolic enzymes to regulate gene expression within a specific locus by their translocation into the nucleus and complex formation with specific chromatin-modifying enzymes (108, 123). As further detailed below, metabolic enzymes within protein

complexes provide substrates for the chromatin-modifying enzymes and contribute to the regulation of gene expression.

Sivanand *et al.* demonstrated that induction of DNA damage by ionizing radiation (IR) leads to phosphorylation of ACLY at S455 (124). This is required for histone acetylation near double-strand breaks (DSB) and recruitment of BRCA1 for homologous recombination (HR) repair. Furthermore, reconstitution of neither inactive mutant ACLY nor nuclear export signal (NES) tagged ACLY in ACLY depleted cells are able to promote HR-dependent DBS repair, implicating the importance of nuclear-localized active ACLY function. Fumarate hydratase (FH) is an enzyme within the TCA cycle that catalyzes the reversible conversion of fumarate to malate (108). However, a recent study reported a novel nuclear function for FH in IR-induced DSB repair (125). After nuclear localization of FH in response to IR treatment, DNA-PK phosphorylates FH at T236 that promotes its interaction with histone H2A.Z at the DSB site. Fumarate production by DSB localized FH inhibits the histone demethylase activity of KDM2B. This results in enhanced dimethylated H3K36 at DSB sites, which is required for non-homologous end-joining (NHEJ) DNA repair complex recruitment. While the addition of high levels of fumarate restores NHEJ-mediated DNA repair in FH depleted cells, the expression of an inactive mutant does not. Thus, these studies implicate the importance of a locally produced metabolite in DNA damage repair.

Under glucose limitation, tumor cells can activate autophagy to survive. As nuclear acetyl-CoA levels are impacted due to limited substrates for ACLY and PDC activity, activation of autophagy-related gene expression still requires histone acetylation. Li *et al.* found that glucose deprivation triggers AMPK-mediated phosphorylation of acetyl-CoA synthetase 2 (ACSS2) at S659, which leads to nuclear localization (126). Nuclear ACSS2 interacts with transcription factor EB (TFEB) and forms a transcription complex to initiate lysosomal and autophagy gene expression via binding to their promoter regions. ACSS2 within this complex locally produces acetyl-CoA for histone acetylation.

Alpha-ketoglutarate dehydrogenase (α-KGDH) is another well-known TCA cycle enzyme that produces succinyl-CoA from α-KG and acetyl-CoA and has also been observed in the nucleus (127). Nuclear α-KGDH interacts with lysine acetyltransferase 2A (KAT2A) and leads to

succinylation of histone H3K79 near the promoter region. Inhibition of nuclear localization of α-KGDH or disruption of the succinyl-CoA binding site of KAT2A (Y645A) suppresses gene expression, cell proliferation, and tumor growth, thereby showing the importance of nuclear α-KGDH produced succinyl-CoA in tumorigenesis.

Proteomic analysis of MafK associating partners found nuclear localization of methionine adenosyl transferase IIα (MatIIα), suggesting a mechanism for local SAM production (128). Mat IIA within the MafK-associated complex leads to gene repression of the heme oxygenase-1 gene (*Ho-1*). Further, MatIIα forms a complex with chromatin-modifying proteins such as Swi/Snf and NuRD and provides SAM for histone methylation.

In short, the relocalization of metabolic enzymes into a different cellular compartment can be exploited by tumor cells for the epigenetic regulation of gene expression and DNA-damage repair, resulting in cell survival and tumor growth.

Catalytic-independent non-canonical functions

Metabolic enzymes can also exert non-canonical functions via interacting with non-metabolic proteins, relocalization into a different cellular compartment, or both in a catalytic independent manner (104). In this scenario, reconstituted expression of catalytically inactive mutant forms restores the phenotype in endogenous protein depleted conditions, while inhibition of metabolic activity by inhibitor treatment does not significantly affect the phenotype.

Dimeric PKM2 can bind to the phosphorylated-tyrosine residue of proteins (129). Changing the amino acid residue from K433 to 433E by site-directed mutagenesis leads to loss of this ability. In EGFR mutant lung cancer cells, the interaction between PKM2 and mutant EGFR sustains EGFR signaling by inhibition of proteasomal degradation of EGFR (130). While catalytically inactive PKM2 still contributes to EGFR stability, the half-life of mutant EGFR is reduced upon either PKM2 activator treatment or mutant PKM2 (K433E) expression. In GBM cells, nuclear PKM2 binding to HuR blocks HuR-dependent p27 translation via retaining HuR in the nucleus (131). Depletion of PKM2 leads to cell cycle arrest due to HuR-mediated p27 translation while reconstituted wild-type and catalytically inactive mutant PKM2, but not the K433E mutant,

can restore cell cycle progression. Phosphoglycerate mutase 1 (PGAM1) is another glycolytic enzyme with an identified non-canonical function, which is independent of its catalytic activity (107). While investigating a novel function for PGAM1, alpha-smooth muscle actin (ACTA2) was identified as a PGAM1 interacting protein. PGAM1 plays a key role in F-actin formation and cell migration via interacting with ACTA2 and inhibition of metabolic activity by either mutation or inhibitor treatment does not affect this interaction and cell motility.

Contrary to oncogenic roles for non-canonical functions of metabolic enzymes, nuclear malate dehydrogenase 1 (MDH1) and nuclear fructose-1,6-bisphosphatase 1 (FBP1) exhibit tumor suppressor functions (106, 132). Glucose starvation induces nuclear localization of MDH1. Nuclear MDH1 interacts with p53 that results in decreased proteasomal degradation and induction of gene expression via acting as a co-activator for p53 (106). Transactivation of p53 target genes, including BAX, triggers apoptosis. Glucose deprivation-induced apoptosis has not been observed in MDH1-silenced, p53 proficient cells or MDH1 overexpressed p53-deficient cells. However, reconstituted catalytically inactive MDH1 expression in p53 proficient cells exhibits increased apoptosis, confirming that nuclear MDH1-p53 interaction mediates apoptosis in glucose-limited conditions in a metabolic independent manner. Loss of FBP1 has been found to play a role in clear cell renal carcinoma (ccRCC) tumorigenesis and is associated with poor prognosis (132). Nuclear FBP1 inhibits hypoxia-inducible factor (HIF) target gene expression via interacting with the inhibitory domain of HIF1α and HIF2α in VHL tumor suppressor deficient cells. While expression of catalytically inactive mutant FBP1 still abolishes HIF-dependent gene expression and cell proliferation under normoxia, expression of NES-tagged FBP1 cannot recapitulate the phenotype of wild-type FBP1 activity, indicating that the nuclear, catalytic-independent function blocks HIF transactivation.

Non-canonical function of genes involved in the serine synthesis pathway

As mentioned above, many reports have defined the non-canonical functions of glycolytic and TCA cycle enzymes in tumorigenesis. Although we speculate that SSP enzymes may also possess non-canonical functions, few reports have identified novel functions for the SSP proteins.

PHGDH has been found as a potential prognostic marker for GBM (133). Silencing of PHGDH inhibits cell proliferation, migration, and invasion. Further study has shown that PHGDH contributes to these oncogenic processes via increasing protein stability of FOXM1 by physical interaction that promotes the expression of genes involved in cell migration and invasion. Another study found that PHGDH interacts with the translation initiation factors, eIF4A1 and eIF4E, in pancreatic adenocarcinoma and involves the translation initiation process via increasing complex stability, especially under nutrient-stress conditions (134). Pharmacological inhibition of PHGDH activity does not alter the interaction with this initiation complex and translation of mRNAs, including E-cadherin and ZO-1, but the suppression of PHGDH expression abolishes complex formation and affects translation initiation of the relevant mRNAs. Separate from these non-canonical functions, PHGDH can produce the oncometabolite D-2-hydroxyglutarate (D-2-HG) from α-KG (135). D-2-HG acts to competitively inhibit α-KG-dependent dioxygenases, which results in reduced histone and DNA demethylation. Therefore, it will be intriguing to investigate whether PHGDH-produced 2-HG can alter the epigenetic landscape of tumor cells.

PSPH is the final enzyme within the serine biosynthetic pathway and produces serine via removing phosphate from phosphoserine. A recent study has reported that PSPH also dephosphorylates serine phosphorylated peptides, implicating a potential protein phosphatase activity *in vitro* (105). Insulin Receptor Substrate 1 (IRS1) has been found as a protein substrate for PSPH phosphatase activity due to its interaction with PSPH and the reduction of S794 phosphorylation level upon PSPH overexpression in NSCLC cells. Removal of inhibitory phosphate from IRS-1 (S794) initiates the activation of the AKT1-mTORC pathway and cell migration and invasion. Yet, the restoration of inactive mutant PSPH expression in PSPH silenced cells fails to dephosphorylate IRS-1 at S794 and rescue the cell migration defect, supporting a non-canonical function of PSPH.

On the other hand, the oncogenic function of PSAT1 has been implicated in many types of cancer via loss and gain of functions, but a mechanistic study demonstrating a non-canonical function of PSAT1 has yet been reported. For example, elevated expression of PSAT1 has been

implicated in GSK3β mediated pathway in several cancer types but whether PSAT1's canonical or non-canonical function is crucial in the regulation of this pathway is yet to be determined (1, 43, 69, 79). The involvement of PSAT1 in epigenetic gene regulation has been shown in mouse embryonic stem cell maintenance via supplying α-KG for dioxygenases leading to histone and DNA demethylation, but then again, it is unknown whether PSAT1 displays such function for tumor cells or if the compartmental specific expression is required (136).

As described above, non-canonical functions of metabolic enzymes have been observed under specific conditions and each enzyme is regulated separately in order to exert its novel function. This is highlighted by EGFR-mediated nuclear functions of PKM2 and PDC and indicates that EGFR signaling does not only promote metabolic reprogramming but also induces non-canonical activities of target proteins (113, 122). Unraveling the non-canonical functions of enzymes is experimentally challenging, but it is necessary to develop new cancer therapies.

We postulate that PSAT1 exhibits a non-canonical function in EGFR-mediated lung tumor progression. This hypothesis was tested in multiple aims that utilized biochemical approaches to identify new PSAT1 associating proteins (Aim1) and the impact of PSAT1 loss on an interacting protein's function and localization (Aim1). Aim 2 intended to define a cellular phenotype due to PSAT1 silencing in NSCLC and undertake rescue studies to evaluate a role for a novel interacting protein. Lastly, gene expression profiling was performed to characterize downstream genomic changes and prognostic relevance of a PSAT1 associated gene signature in EGFR-mutant NSCLC (Aim 3).

CHAPTER 2

NUCLEAR PYRUVATE KINASE M2 (PKM2) CONTRIBUTES TO PHOSPHOSERINE AMINOTRANSFERASE 1 (PSAT1)-MEDIATED CELL MIGRATION IN EGFR-ACTIVATED LUNG CANCER CELLS

Introduction

The impact of metabolic reprogramming has been well accepted in cancer pathogenesis (6, 137). Mainly, the contribution of the Warburg effect and glutamine addiction has been extensively investigated in the growth and survival of multiple tumor types (138-140). More recently, several reports have described additional functions for glycolytic enzymes in tumor progression beyond their metabolic activities (141). For example, PKM2 can be translocated into the nucleus in response to a variety of oncogenic signals and regulate gene expression, particularly through direct interaction with transcription factors or by transcription factor phosphorylation by inherent PKM2 protein kinase activity (110, 111, 113, 114, 142). Through an interaction with ACTA2, phosphoglycerate mutase 1 (PGAM1) mediates actin filament assembly and increases cell migration and invasion in breast cancer (107). Although pro-tumorigenic functions of glycolytic enzymes are well-established, the requirement for serine synthesis enzymes has only recently been described (1, 15, 45, 105, 133).

De novo cellular production of serine may contribute to tumor growth by providing precursors for macromolecular production and one-carbon metabolism (15). Accordingly, multiple cancers exhibit increased expression of SSP enzymes (44, 71, 105, 133). For example, elevated PSAT1, which catalyzes the second step in converting 3-phosphohydroxypyruvate to phosphoserine, is associated with poorer clinical outcomes (1, 43, 67, 69, 70, 72, 74, 143, 144). Depending on tumor type, several reports have implicated PSAT1 in the proliferation, migration, invasion, and chemo-resistance of malignant cells (1, 43, 46, 69, 71, 74, 79, 143). Yet, the

31

complete mechanism by which the serine biosynthetic pathway facilitates metabolic or cellula changes necessary for tumor growth is still not fully understood (15). As observed with certain glycolytic proteins, studies have also described non-canonical activities of SSP enzymes. Phosphoglycerate dehydrogenase (PHGDH) contributes to glioma progression through direct interaction and stabilization of FOXM1(133). Separately, phosphoserine phosphatase (PSPH) can promote tumorigenesis through direct IRS1 dephosphorylation (105). While multiple studies indicate a pro-tumorigenic role for PSAT1, alternative functions for this SSP enzyme have yet to be fully described.

We now report a novel direct interaction between PSAT1 and PKM2. While the loss of PSAT1 does not alter cellular PKM2 expression or activity, it disrupts PKM2 nuclear translocation in response to EGFR-activation in lung cancer cells. In addition, PSAT1 silencing decreases migration in these cell types, while PSAT1 restoration or overexpression promotes cell motility and PKM2 nuclear localization. PSAT1 also undergoes nuclear translocation upon EGFR-activation, but it is still unclear whether disruption of the PSAT1:PKM2 association alters nuclear compartmentalization. Yet, re-expression of a nuclear localization signal (NLS) tagged PKM2 acetyl-mimetic (K433Q) mutant partially restores cell migration in PSAT1 suppressed cells. Taken together, our findings suggest that PSAT1-promoted nuclear PKM2 translocation contributes, in part, to cell migration under EGFR-activation in lung cancer.

Materials and Methods

Reagents and antibodies

Erlotinib was purchased from (Selleckchem, OSI-744). Human recombinant proteins PKM2 (SAE0021), PKM1 (SRP0415), and EGF (E9644), anti-β-actin (A2228) antibody, PSAT1 shRNA (TRCN0000291729), and control shRNA (SHC202) were purchased from Sigma-Aldrich. Antibodies against PKM2 (4053), PKM1 (7067), OCT1(8157), a-Tubulin (3873), DYKDDDDK-Tag (2368), and rabbit IgG (2729) were obtained from Cell Signaling Technology. Anti-PSAT1 (10501-1-AP) antibody was purchased from Proteintech Group Inc. The PSAT1 Double Nickase CRISPR Plasmid system (sc-403001-NIC) was purchased from Santa Cruz Biotechnology.

GST-Pulldown and Mass Spectrometry

PSAT1 cDNA was subcloned into the pGEX4T-1 plasmid (Amersham) to generate pGEX-GST-PSAT1 and tagged PSAT1 was induced in BL21 cells with IPTG. GST-PSAT1 was incubated with one milligram of pre-cleared A549 lysate and columns were washed 3X and eluted with reduced glutathione. Dialyzed elutes were separated by SDS-PAGE and protein bands were detected by silver stain. Bands enriched in the GST-PSAT1 samples were excised and sent for protein identification by mass spectrometry.

LC/MS data collection and analysis

Tryptic peptides were prepared from excised gel bands and analyzed using a liquid chromatograph tandem mass spectrometry (LC-MS/MS) approach as previously described (145). Briefly, peptides were separated on a 10cm C-18 (Jupiter 5-µm RP300A (Phenomenex) packed needle tip using a 5% to 40% acetonitrile gradient at a flow rate of 200nl/min prior to nanoelectrospray into an LTQ linear ion trap mass spectrometer (Thermo Fisher Scientific). Data were acquired in a data-dependent fashion with a full MS scan (300-2000 m/z) followed by six MS/MS scans (35% collision energy) and a 1-min dynamic exclusion window. MS/MS data were searched by ProteomeDiscoverer (version 1.4) as previously described against a human refseq protein database (version HumanRef140722.fasta with 88,942 entries) using SEQUEST (version 1.4.0.288) and Mascot algorithms (version 2.4) assuming 1.0Da fragment mass tolerance and 1.2Da parent mass tolerance, fixed modification of cysteine (+57 for carbamidomethylation),

variable oxidation of methionine (+16 to methionine) and maximal two missed trypsin cleavages(146). High-probability peptide and protein identifications were assigned using the Peptide-/Protein-Prophet algorithms (http://tools.proteomecenter.org/software.php) and result quantitatively using Scaffold v4.3.4 (ProteomeSoftware) using a spectral counting method.

Cell culture

A549 NSCLC adenocarcinoma cells (ATCC) and HEK293T human embryonic kidney cells (provided by Dr. Geoffrey Clark after STR profiling) were maintained in DMEM (Gibco) supplemented with 10% FBS and 50 µg/ml gentamicin (Gibco). PC9 NSCLC adenocarcinoma cells (provided by Dr. Levi Beverly after STR profiling) were maintained in RPMI media (Gibco) supplemented with 10% FBS and 50 µg/ml gentamicin (Gibco). All cells were cultured in humidified incubators at 37 ^{0}C and 5% CO_2.

Plasmid construction and mutagenesis

Full-length human PKM2 cDNA was amplified from A549 cells using primers forward:5'-CTGGGGATCCATGTCGAAGCCCCATAGTGAAG-3' and reverse:5'-GATCGAATTCTCA CGGCACAGGAACAACACGC-3' and sub-cloned into the pcDNA 3.1/FLAG vector [FLAG-wild-type (WT) PKM2]. FLAG-PKM2 WT plasmid was used to generate mutant PKM2 expression constructs using either the QuikChange site-directed mutagenesis kit (Stratagene) or Q5 site-directed mutagenesis kit (New England Biolabs), respectively. Primers utilized for the PKM2 site-directed mutagenesis study are listed in Table 1. All plasmid constructs were verified by sequencing analysis (Eurofins Genomics).

Transient transfection

HEK293T cells were transfected with FLAG-tagged empty vector (FLAG-EV) [FLAG-HA-pcDNA3.1 (Addgene, # 52535)], PKM2 WT, or mutant PKM2 [MT(1-4)] vectors using jetPEI (PolyPlus) transfection reagents according to manufacturer's protocols. Forty-eight hours post-transfection, cells were lysed in IP lysis buffer (Pierce) and co-immunoprecipitation was performed.

Table 1: PCR primers for the site-directed mutagenesis. Point mutations are indicated in bold letters and underlined.

Primer ID	Sequence (5'-3')	Mutagenesis Kit
MT1-PKM2-F MT1-PKM2-R	cagaggctgccatctaccac**agga**aattatttgaggaactccgc gcggagttcctcaaataatt**tcct**gtggtagatggcagcctctg	QuikChange mutagenesis XL kit
MT2-PKM2-F MT2-PKM2-R	ctccgccgcctggcg**agcca**taccagcgaccccac gtggggtcgctggta**tggct**cgccaggcggcggag	
MT3-PKM2-F MT3-PKM2-R	**gcgagccat**accagcgaccccacagaa **caggcggac**gagttcctcaaataattgcaagtggtag	Q5 Site-Directed Mutagenesis
MT4-PKM2-F MT4-PKM2-R	tgaggaactc**gtc**cgcctggcgc aataattgcaagtggtagatggc	
K433Q-PKM2-F K433Q-PKM2-R	cgtcctcacc**c**agtctggcag attatggccccactgcag	
shRNA-resistant-PSAT1		
PSAT1-F PSAT1-R	**tac**tgttagagatacaaaaggaattattagactacaaaggagttggcattag **cac**tgtgcggcagcttggcgggg	

Generation of stable cell lines

PSAT1 stable knockdown: A549 or PC9 cells were transfected with shRNA (PSAT1 shRNA or Non-targeted Mammalian Control shRNA) using jetPEI and clonal cells were selected in 1 µg/ml puromycin.

PSAT1 genetic knockout: PC9 cells were transfected with the PSAT1 CRISPR/Cas9n(D10A)-Puromycin nickase plasmid using jetPEI. Stably transfected cells were selected in 1 µg/ml puromycin. To achieve PSAT1 genomic deletion, puromycin selected PC9 cells were transfected with the PSAT1 CRISPR/Cas9n(D10A)-GFP nickase plasmid. PSAT1 knockout cells were clonally expanded from GFP-positive cells and validated by immunoblotting. Puromycin selected cells without GFP-nickase transfection served as control knockout cells.

Ectopic FLAG-tagged PSAT1 expression: PSAT1 cDNA (Forward: 5'-TGGGATCCATGG ACGCCCCCAGGCAGGTG-3' and reverse: 5'-TGGAATTCTCATAGCTGATGCATCTCCAA-3') was cloned into pcDNA 3.1/FLAG vector. PC9 cells were transfected with FLAG-tagged PSAT1 or FLAG-EV using jetPEI and selected in 200 µg/ml geneticin (Gibco).

PSAT1 rescue studies: An shRNA-resistant FLAG-tagged PSAT1 expression plasmid was generated by site-directed mutagenesis (primers listed in Table 1). For these studies, the shRNA-

resistant FLAG-PSAT1 expression vector was co-transfected with PSAT1 shRNA into parental PC9 cells. Alternatively, PC9 cells were co-transfected with either FLAG-EV and non-targeted shRNA or PSAT1 shRNA to serve as control and PSAT1-silenced PC9 cells, respectively. Stably transfected cells were selected in 200 µg/ml geneticin (Gibco) and 1 µg/ml puromycin (Sigma).

Nuclear PKM2 overexpression: PKM2 cDNA (Forward: 5'-TATTTAGGCGCG CCATGTCGAAGCCCCATAGTGAAG-3' and reverse: 5'-GCCCGTTAATTAATCAC GGCACAGGAACAACACGC-3') was subcloned into pcDNA-3xFLAG-NLS vector (Addgene, #53585). FLAG-PKM2NLS-K433Q expression plasmid was generated by site-directed mutagenesis (primers listed in Table 1). All constructs were verified by sequencing analysis. shPSAT1 PC9 cells were transfected with FLAG-PKM2^{NLS-WT}, FLAG-PKM2$^{NLS-K433Q}$, or FLAG-EV using jetPEI. Control PC9 cells were transfected with FLAG-EV only. Stably transfected cells were selected in 200 µg/ml geneticin and 1 µg/ml puromycin.

FLAG-PKM2 WT or MT3 expression: Stable FLAG-PKM2 WT or MT3 expressing PC9 cells were generated via transfection and clonal expansion under 200 µg/ml geneticin (Gibco). Transient knockdown of endogenous PKM2 in these stable cells was performed by transfection with a pool of three siRNA duplex oligonucleotides against PKM2 3'UTR region (sense: 5'-ccagatggcaagagggtgatt-3', 5'-gatcaacgcctcactgaaatt-3', and 5'-gagcctacctgtatgtcaatt-3') (Dharmacon) using jetPEI.

EGF and erlotinib treatment

EGF Treatment: Stable A549 Control and shPSAT1 cells were serum-starved in serum-free DMEM for 24 hours and subsequently treated with 100 ng/ml EGF or vehicle (10mM acetic acid) for 6 hours. Cells were then collected for subcellular fractionation or co-immunoprecipitation analysis.

Erlotinib Treatment: Stable PC9 Control and shPSAT1 cells were treated with 1 µM of erlotinib or vehicle (DMSO) in serum-free RPMI media for 48 hours prior to sub-cellular fractionation analysis.

Subcellular fractionation

Cytosolic and nuclear proteins were isolated using the NE-PER kit (Thermo Scientific, 78835). 15 μg of cytoplasmic protein and 25 μg of nuclear protein were used for immunoblotting analyses.

Co-immunoprecipitation (Co-IP)

One milligram of cell lysate was incubated with 1 μg of anti-PSAT1 or anti-rabbit IgG (negative control) antibody. Immunoprecipitates were collected using Protein G Dynabeads (Invitrogen, 10004D) and the immunoprecipitated proteins were analyzed by immunoblot.

For recombinant Co-IP experiments, 50 ng of recombinant PSAT1 protein was mixed with 500 ng of recombinant PKM1 or PKM2 protein. Recombinant PSAT1 in IP lysis buffer alone was used as a negative control.

Immunoblotting

Protein extracts or co-immunoprecipitations were separated by SDS-PAGE and transferred to PVDF membrane. Blocked membranes were then incubated with the indicated primary antibodies. Protein detection was performed using HRP-conjugated secondary antibodies and visualized by chemiluminescence (GE Healthcare).

Immunofluorescence staining

Cells were plated in 4-well chamber slides, incubated in serum-free media for 24 hours, and fixed in 4% paraformaldehyde. After blocking, cells were incubated with primary anti-PKM2 and Alexa Fluor 488- conjugated secondary antibodies. Slides were then mounted with SlowFade Diamond Antifade Mountant with DAPI (S36964) reagent. Images were captured by Olympus FV-3000 confocal microscope equipped with Fluoview software under 40X magnification.

Wound-healing assay

All PC9 cell lines were plated at 10^6 cells/ well in 6 well-plate and grown in complete media overnight. Experimental conditions for motility assays were used to minimize the contribution of cell proliferation on wound healing, as described previously (147). After plating, cells were incubated in serum-free media for 24 hours. Confluent monolayer of cells was then wounded with a pipette tip, washed three times, and cultured in low serum-RPMI media (1%). Images were captured at 0 and 24 hours and analyzed using Image J software with MRI wound healing tool (148). The migrated

area was calculated by subtraction of wound area (arbitrary unit) at 24 hours from the initial wound area.

Transwell migration assay

A549 Control and shPSAT1 stable cell lines were plated at 70% confluency and cultured in complete media for 24 hours. Cells were then serum-starved for 24 hours and 10^5 cells were plated in serum-free media in the Boyden chamber. Serum-free media supplemented with 100 ng/ml EGF or vehicle (10 mM acetic acid) was added to the bottom chamber. After 24-hours, cells were fixed with 100% ice-cold methanol and non-migrated cells were removed. Migratory cells were stained with 0.05% crystal violet and washed with ddH20. The area of stained cells was quantified using Image J threshold tool as described (149).

Pyruvate kinase activity assay

Both A549 and PC9 Control and shPSAT1 stable cells were cultured to 70% confluency in 6 well-plate. Intracellular pyruvate kinase activity was assessed using the Pyruvate Kinase Activity assay kit (Sigma, MAK072) according to the manufacturer's protocol.

Computational homology modeling of PKM1 and PKM2

The human PKM1 sequence was obtained from the PKM1 crystal structure (Protein Data Bank entry 3SRF) and was mapped to the human PKM2 structure (Protein Bank entry 4FXJ) using the Prime-based Homology Modeling Module of the Schrödinger Software Suite (150). The image was created within Schrödinger Maestro with the sequence differences between PKM1 and PKM2 identified.

Bioinformatic analysis of PSAT1 in EGFR mutant lung cancers:

The GSE32863, GSE75037, GSE31548, GSE31210, and GSE11969 data sets encompassing gene expression analysis from EGFR mutant lung cancer with clinical information were downloaded from the GEO database through using BRB-ArrayTool software (151). PSAT1 expression (probe IDs: ILMN_1692938 for GSE32863 and GSE75037, 223062_s_at for GSE31210 and GSE31548, and 5144 for GSE11969) was retrieved from EGFR mutant tumor and normal lung specimens with clinical information. Differential expression analyses were carried out for tumor vs.

normal and stage II-III vs. stage I, while Kaplan-Meier analyses were performed for overall survival and relapse-free survival rates on the indicated data sets.

Statistical analysis

All data were statistically analyzed using Prism 8 software (GraphPad Software). Statistical significances were assessed based on the number of groups with one or more independent variables. Paired t-tests were used for the analysis of two groups, with the exception of an unpaired t-test for the pyruvate kinase assay. While one-way ANOVA with Tukey's multiple comparison test for three groups was performed for PC9 cell variants, two-way ANOVA with Tukey's multiple comparison test was used for A549 cell variants with or without EGF treatment. Experimental replicates for each analysis are stated within the respective figure legend. Values of $p < 0.05$ were considered statistically significant.

<div align="center">**Results**</div>

PKM2 is a novel binding partner of PSAT1

        Non-canonical functions of metabolic enzymes that directly involve protein-protein interactions have previously been reported in promoting tumorigenesis (109, 152). To determine PSAT1-associating proteins, we used a GST-PSAT1 pull-down assay coupled to LC-MS/MS analysis (Fig. 6A). Among the resolved proteins, we identified pyruvate kinase M (PKM) with approximately 22% sequence coverage (Fig. 6B). PKM1 and PKM2 are two alternatively spliced isoforms of the *PKM* gene and exhibit differential enzymatic properties (153). Utilizing co-immunoprecipitation (co-IP) analysis encompassing only recombinant PKM1, PKM2, and PSAT1, we found that PSAT1 directly binds to the PKM2 isoform (Fig. 6C). Thus, these results identify PKM2 as a novel direct binding partner of PSAT1.

        Based on this interaction, we hypothesized that a PKM2-specific region may contribute to PSAT1 association. Three-dimensional modeling of human PKM1 and PKM2 demonstrate that they have 95.8 % sequence homology and have the same overall structure. As depicted in Figure 7A, an isoform-specific region (cyan) is localized to a loop structure that lies towards the exterior of the monomer. We mutated amino acid residues in wild-type (WT) PKM2 to the corresponding PKM1 residues by site-directed mutagenesis (Fig. 7A, mutations highlighted in red). Co-IP analysis involving FLAG-tagged PKM2 WT and mutant (MT[1-4]) proteins revealed that mutations in MT 1, 2, & 4 did not substantially affect the interaction with PSAT1 (Fig. 7B). However, the amino acid changes within MT3-PKM2 that are inclusive of mutations in both MT 2 and 4 strongly reduced binding to endogenous PSAT1. Together, the recombinant co-IP and mutational analysis demonstrate a specific PSAT1:PKM2 interaction.

A

MW   Lys   Beads   GST-PSAT1

150
100
75
50
37
25
15

B

Common Amino Acid Sequence of PKM

MSKPHSEAGTAFIQTQQLHAAMADTFLEHMCRLDIDSPPITAR**NT
GIICTIGPASR**SVETLKEMIKSGMNVARLNFSHGTHEYHAETIKN
VR**TATESFASDPILYRPVAVALDTK**GPEIRTGLIKGSGTAEVELK
KGATLKITLDNAYMEKCDENILWLDYKNICKVVEVGSK**IYVDDGL
ISLQVK**QKGADFLVTEVENGGSLGSKK**GVNLPGAAVDLPAVSEKD
IQDLK**FGVEQDVDMVFASFIRKASDVHEVRKVLGEKGKNIKIISK
IENHEGVR**RFDEILEASDGIMVARGDLGIEIPAEK**VFLAQKMMIG
RCNRAGKPVICATQMLESMIKKPRPTRAEGSDVANAVLDGADCIM
LSGETAK**GDYPLEAVR**MQHLiareaeaa--h--lfeel-r--
----d--ea-a-g-veas-kc---a-ivlt-sgrSAHQVA
RYRPR**APIIAVTR**NPQTARQAHLYRGIFPVLCKDPVQEAWAEDVD
LRVNFAMNVGKARGFFKKGDVVIVLTGWRPGSGFTNTMRVVPVP

Common Region (black) | **Matched Peptides** (red) | **Isoform-specific Region** (green)

C

	Input		IP:PSAT1		
recPKM1		+			+
recPKM2	+			+	
recPSAT1			+	+	+	+
IB: PKM1						
IB: PKM2						
IB: PSAT1						

Figure 6. PKM2 is a novel binding partner of PSAT1. A) Silver stain of GST-PSAT1 purified proteins from A549 whole cell lysates. * denotes residual GST-PSAT1 from column purification;← Denotes gel slice encompassing PKM. **B)** Primary amino acid sequence of human PKM. MS identified peptides of PKM are highlighted in red. Black labeled sequences belong to common regions of both PKM1 and PKM2 isoforms and green labeled sequences identify isoform-specificity. **C)** Co-IP of recombinant (rec-) PSAT1 and PKM1 or PKM2. Immunocomplexes were precipitated using anti-PSAT1 antibody and analyzed by immunoblot using anti-PKM1 and anti-PKM2 antibody. RecPKM1 and recPKM2 were used as controls showing antibody specificity and PSAT1 alone was used as IP control. Shown are representative images from two separate experiments.
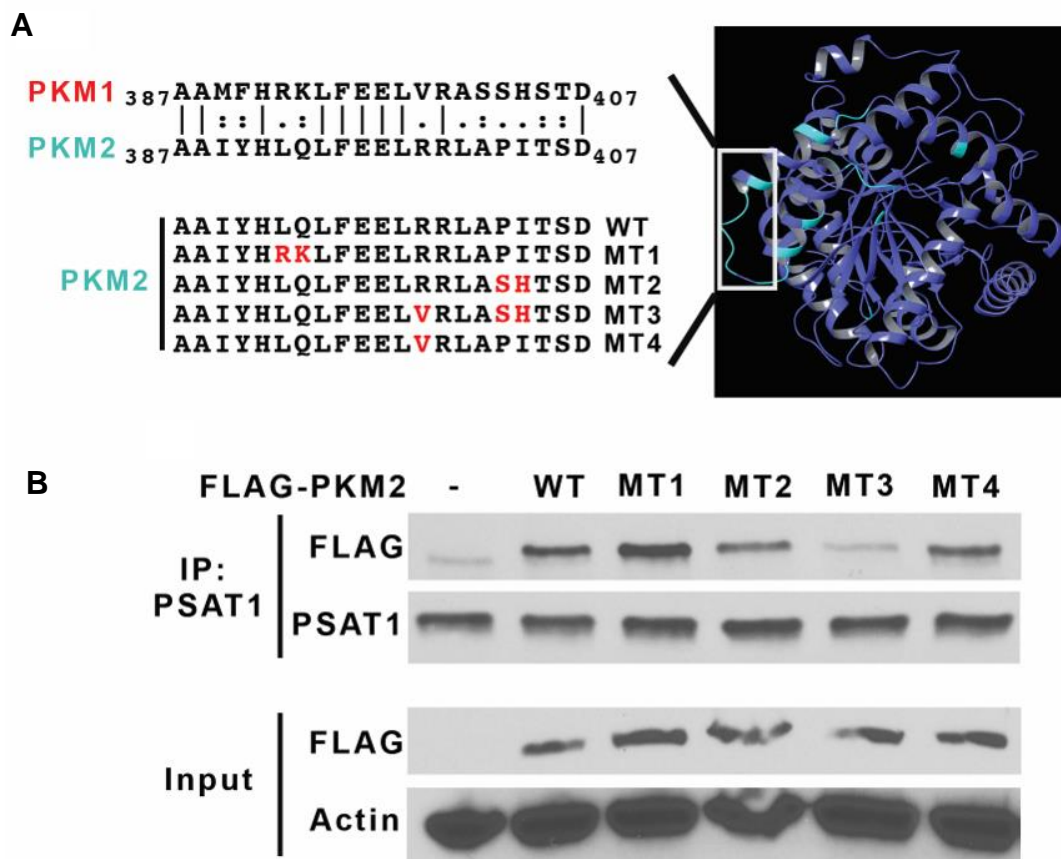
Figure 7. Mutations within an isoform-specific region of PKM2 weakens the PSAT1 interaction. A) Schematic representation of PKM2 specific mutations generated for analysis of PSAT1:PKM2 association. Ribbon representation of the structure of PKM2 colored by PKM1 sequence homology (right panel). Identical regions are shown in purple and divergent regions in cyan. Left panel depicts site directed mutagenesis of amino acids (MT1-4, highlighted in red) in the PKM2 specific region (denoted in white box). **B)** FLAG-PKM2 wild-type (WT), mutants (MT1-4) and FLAG-EV (-) were expressed in HEK293T cells. Endogenous PSAT1 protein complexes were immunoprecipitated and association of PKM2 was assessed by immunoblot. Similar expression of FLAG-PKM2 variants is shown by immunoblot of FLAG fusion proteins from protein lysate input with β-actin used a protein loading control. Shown are representative images from three separate experiments. (-) denotes empty vector.

Suppression of PSAT1 in NSCLC cancer cells does not alter PKM2 expression or pyruvate kinase activity

Previously, the pyruvate kinase activity of PKM2 has been metabolically linked to the serine biosynthetic pathway in human cancers (52, 57, 61, 62). Our pull-down and recombinant protein association studies now suggest that these pathways might also be connected via protein:protein interactions in tumor cells. Co-IP analysis demonstrated an endogenous interaction between PSAT1 and PKM2 in two separate NSCLC cell models (Fig. 8).

To investigate the functional significance of this PSAT1 and PKM2 interaction, PSAT1 expression was stably silenced in PC9 and A549 cells (Fig. 9A). Given the metabolic cross-talk between the glycolytic and serine synthetic pathways (52, 57, 61) and this new PSAT1:PKM2 association, we questioned whether loss of PSAT1 may modulate the metabolic activity of PKM2. As shown in Figure 9B, PSAT1 depletion did not affect pyruvate kinase activity in either cell line. This was not due to altered PKM2 or PKM1 as analysis of PKM isoform expression found no change between control and shPSAT1 cells in both A549 and PC9 cells (Fig. 9C). Taken together, we conclude that while a physiological interaction between PSAT1 and PKM2 exists, suppression of PSAT1 expression fails to alter pyruvate kinase activity and expression of PKM2 in these NSCLC cell lines, indicating that this interaction may be dispensable for cellular pyruvate kinase activity.
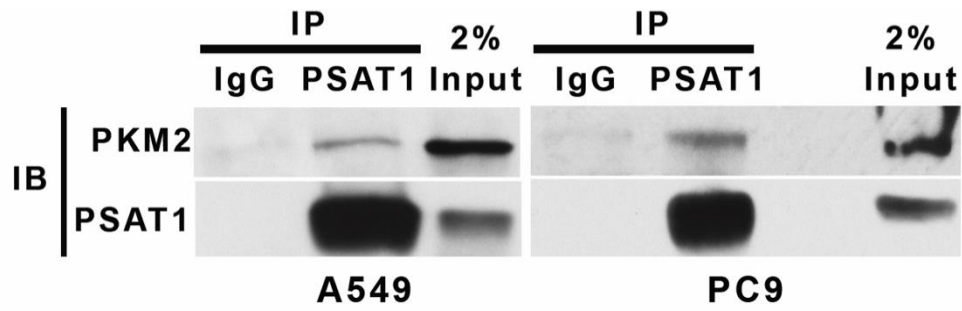
Figure 8. PSAT1 associates with endogenous PKM2 in NSCLC cells. Co-IP of PSAT1 and PKM2 in A549 and PC9 NSCLC cells. PSAT1- specific immunocomplexes were precipitated using anti-PSAT1 from whole cell lysate and analyzed for PKM2 by immunoblot with anti-PKM2 antibody. Shown are representative images from three separate experiments.
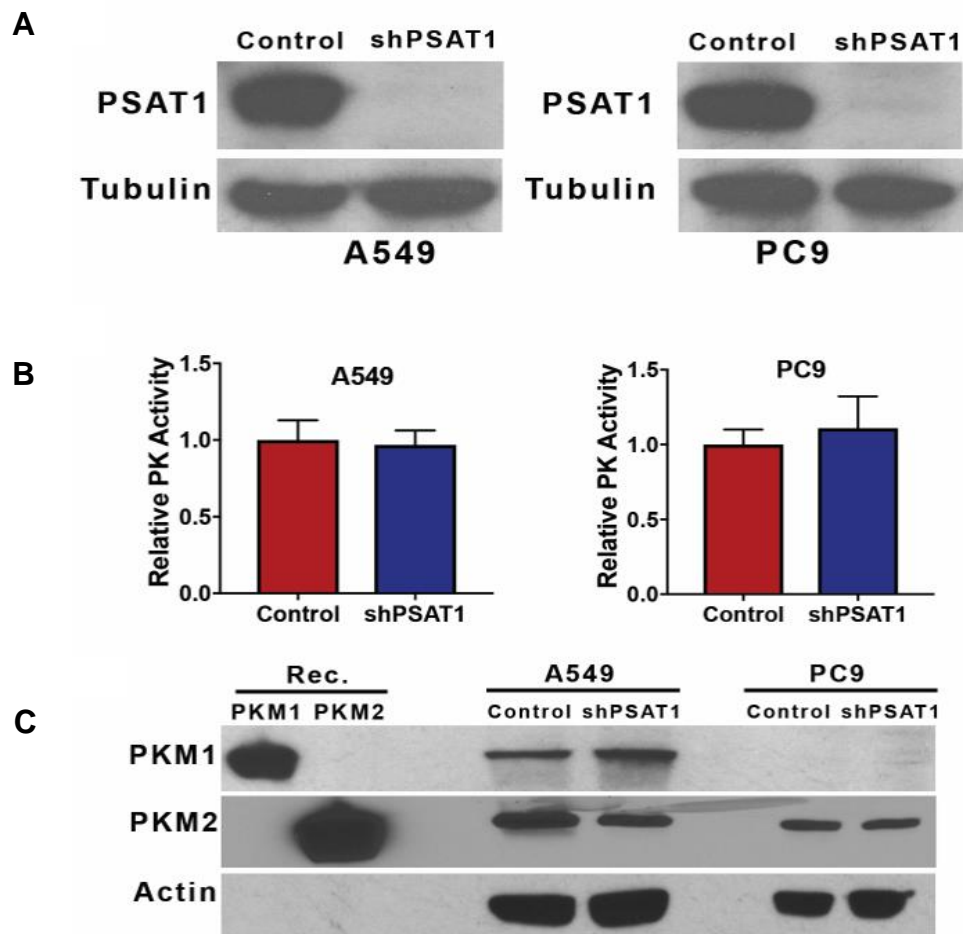
Figure 9. Loss of PSAT1 does not alter pyruvate kinase activity and expression. A) Loss of PSAT1 expression in A549 and PC9 cells stably expressing PSAT1-specific shRNA. PSAT1 expression was determined from whole cell lysates from control or shPSAT1 expressing cells by immunoblot using anti-PSAT1 and anti-α-Tubulin (loading control). **B)** Intracellular pyruvate kinase activity was determined in cell lysates from A549 or PC9 cells with or without PSAT1 expression. Data is represented as relative pyruvate kinase activity (control cells set to 1) and shown are the mean $\pm$ S.D from four independent experiments. **C)** Immunoblot analysis of PKM1 or PKM2 expression in whole cell lysates from control or PSAT1 silenced A549 and PC9 cells. Recombinant human PKM1 and PKM2 proteins were used as positive control for the specificity of antibodies and β-Actin for loading control. Shown are representative images from two separate experiments

Silencing of PSAT1 suppresses the nuclear localization of PKM2 in EGFR activated NSCLC cells

As recent studies have demonstrated EGFR-mediated nuclear localization of PKM2 (113, 114, 154), we examined whether PSAT1 may alter PKM2 nuclear localization under EGFR activation in NSCLC cells. Subcellular fractionation confirmed that the nuclear localization of PKM2 in EGFR-mutant PC9 cells was blocked with the EGFR-TKI, erlotinib (Fig. 10A). Importantly, cellular fractionation and immunofluorescence analysis found that loss of PSAT1 expression by either stable shRNA or CRISPR-mediated knock-out diminished PKM2 translocation under EGFR-activation (Figs. 10A and B and 11). To complement these losses of function studies, conversely, overexpression of FLAG-tagged PSAT1 (Fig. 12A) in parental PC9 cells resulted in higher levels of nuclear PKM2 (Fig. 12B)**.** Unexpectedly, PSAT1 was also found within the nuclear compartment within PC9 cells, which was abrogated with erlotinib treatment and enhanced with FLAG-tagged PSAT1 overexpression (Fig. 10A, 11 and 12B).
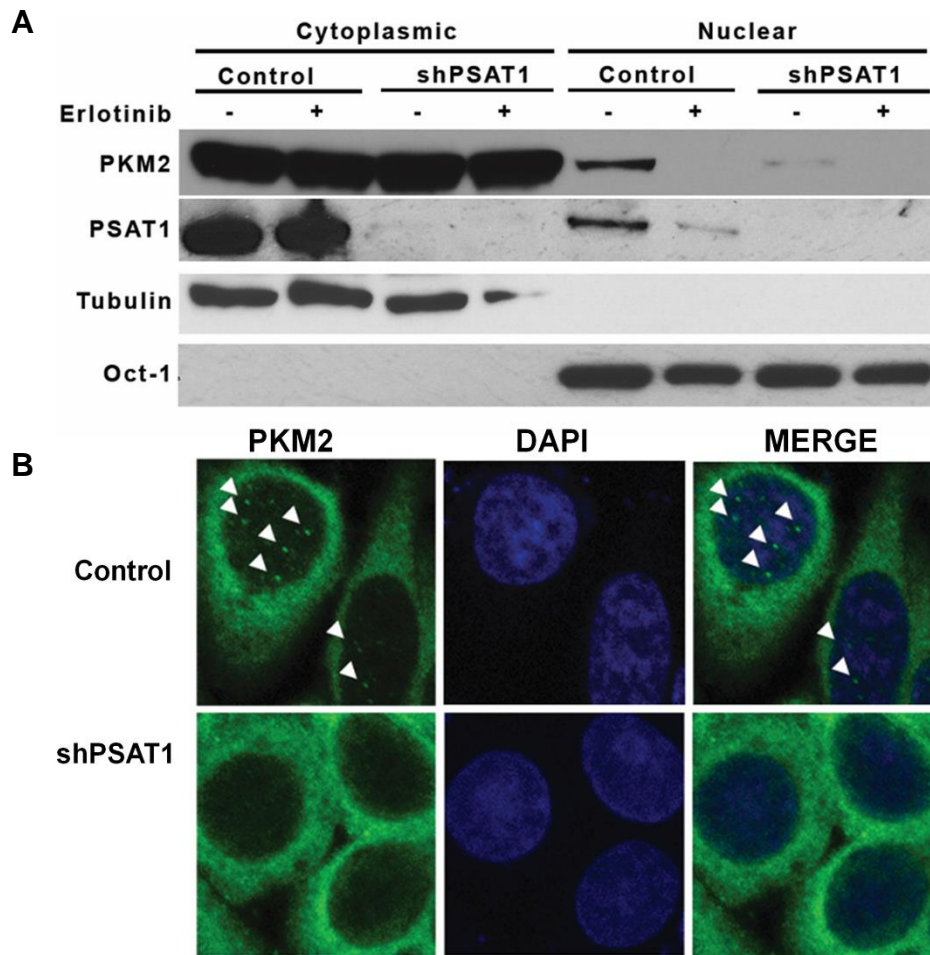
Figure 10. Silencing of PSAT1 suppresses the nuclear localization of PKM2 in EGFR mutant PC9 cells. A) EGFR-mutant PC9 cells stably expressing control or PSAT1 shRNA were treated with 1 µM of erlotinib for 48 hrs. Cytoplasmic and nuclear fractions were examined by immunoblot analysis using anti-PKM2 and anti-PSAT1 antibodies. OCT1 and α-tubulin served as loading controls for nuclear and cytoplasmic compartments, respectively. Shown are representative images from three separate experiments. **B)** Nuclear localization of PKM2 was examined in serum-starved PC9 cells expressing control or PSAT1 shRNA by confocal microscopy. Representative Immunofluorescence image with anti-PKM2 antibody (green) and DAPI nuclei staining (blue). Arrowheads indicate nuclear PKM2 staining.
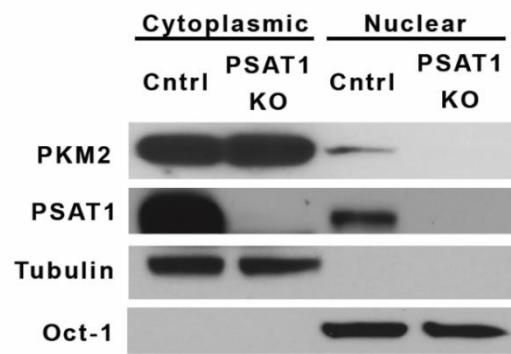
Figure 11. CRISPR-mediated PSAT1 knockout reduces PKM2 nuclear localization in EGFR mutant PC9 cells. Immunoblot analysis of PKM2 and PSAT1 localization after PSAT1 deletion. Cytoplasmic and nuclear fractions from Control and PSAT1 KO PC9 cells were analyzed using anti-PKM2 antibody or anti-PSAT1 antibody. OCT1 and α-tubulin served as loading controls for nuclear and cytoplasmic compartments, respectively. Shown are representative images from three independent experiments.
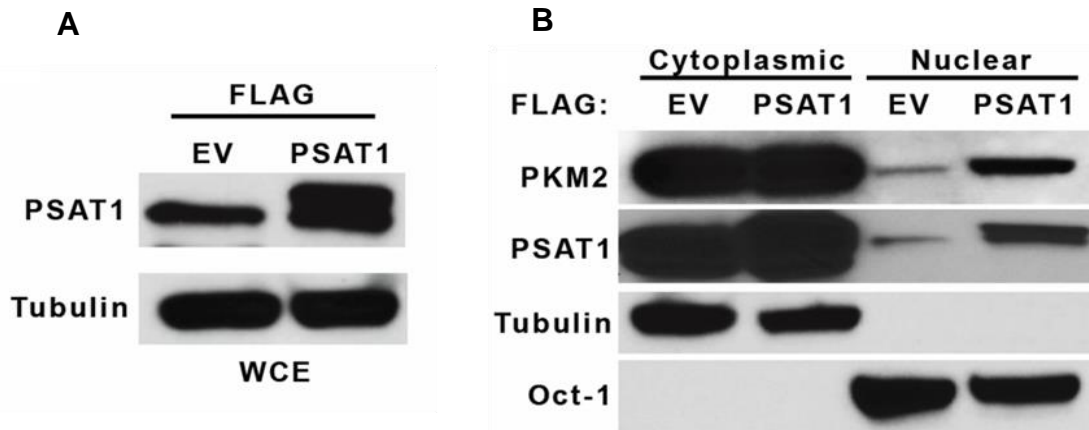
Figure 12. Ectopic expression of PSAT1 induces PKM2 nuclear localization in EGFR mutant PC9 cells. A) Immunoblot analysis of FLAG-PSAT1 expression in PC9 cells. Endogenous and tagged PSAT1 was analyzed using anti-PSAT1 antibody in lysates from PC9 cells expressing empty vector (FLAG-EV) or vector encoding FLAG-PSAT1. α-Tubulin expression was used for loading control. Shown are representative images from three independent experiments. **B)** PKM2 localization in PC9 cells ectopically FLAG-EV or FLAG-PSAT1. Cytoplasmic and nuclear fractions from FLAG-EV and FLAG-PSAT1 expressing cells were analyzed using anti-PKM2 antibody. OCT1 and α-tubulin served as loading controls for nuclear and cytoplasmic compartments, respectively. Shown are representative images from three independent experiments.

We further substantiated these findings in A549 cells harboring wild-type EGFR through EGF stimulation (155, 156). Fractionation analysis revealed enhanced nuclear translocation of PKM2 in EGF-stimulated A549 cells compared to untreated control cells, while the loss of PSAT1 significantly inhibited induced PKM2 nuclear translocation (Fig. 13). Consistent with the findings in PC9 cells, PSAT1 nuclear localization was also observed in EGF-stimulated A549 cells. We then determined whether EGF stimulation alters the PSAT1:PKM2 interaction in A549 cells as a means of promoting enhanced nuclear localization. Co-IP analysis from A549 stimulated with or without EGF found similar PSAT1:PKM2 interactions and the level of PKM2 did not significantly change in response to EGF stimulation (Fig. 14).
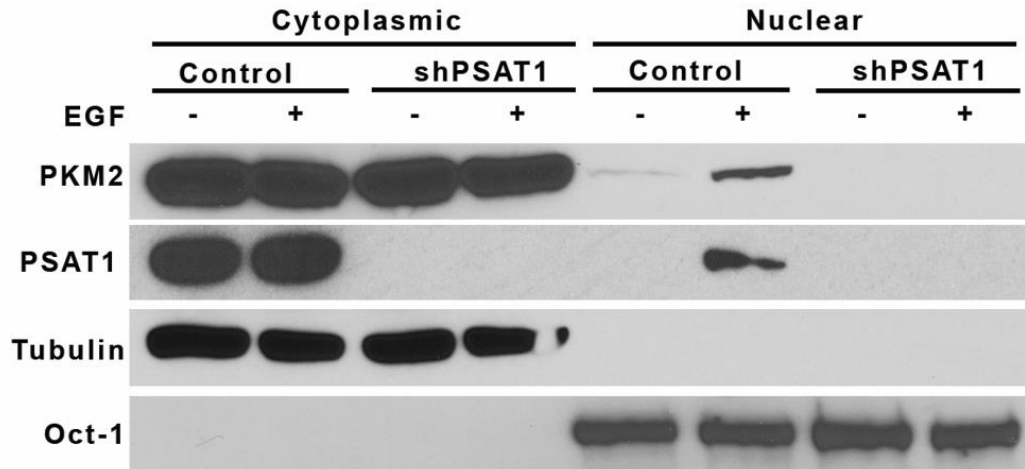
Figure 13. Loss of PSAT1 abrogates EGF-induced nuclear localization of PKM2 in EGFR-WT A549 cells. Serum-starved A549 cells (EGFR-wild-type) stably expressing control or PSAT1 shRNA were treated with or without EGF (100 ng/ml). Cytoplasmic and nuclear fractions were prepared and PKM2 and PSAT1 localization was analyzed by immunoblot. OCT1 and α-tubulin served as loading controls for nuclear and cytoplasmic compartments, respectively. Shown are representative images from three separate experiments.
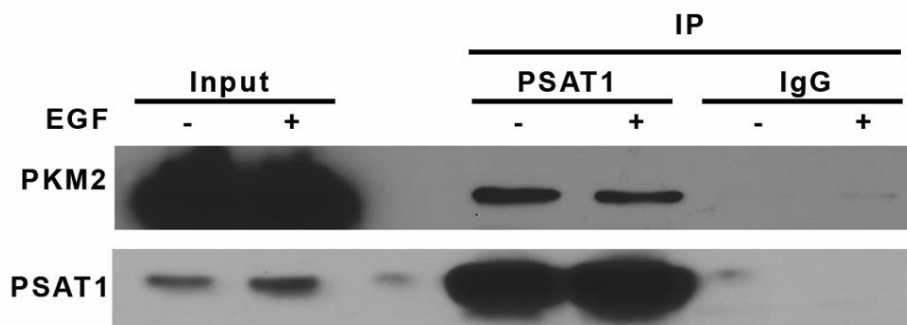
Figure 14. EGF-stimulation does not alter the PSAT1:PKM2 association. Serum-starved A549 cells were treated without or with EGF (100 ng/ml). Shown is a representative co-IP (n = 2) performed using anti-PSAT1 or IgG antibody. PKM2 and PSAT1 were analyzed by immunoblot using anti-PKM2 or PSAT1 antibodies.

The observation that both PSAT1 and PKM2 translocate to the nucleus upon EGFR-activation prompted us to investigate the putative involvement of direct protein-protein interaction in their nuclear localization. FLAG-tagged PKM2 WT or MT3, which has diminished PSAT1 association (Fig. 7B), were stably expressed in endogenous PKM2 depleted PC9 cells. We found that both PKM2 forms were able to localize in the nucleus (Fig. 15). While this may suggest that a direct interaction may not be essential for PSAT1's function in promoting nuclear PKM2, the direct association of PKM2 with these fusion proteins has not yet been defined in the PC9 cells. Further, the co-IP studies in the HEK293T cells showed residual binding of PKM2 MT3 to PSAT1, which may in itself be sufficient in promoting nuclear localization.
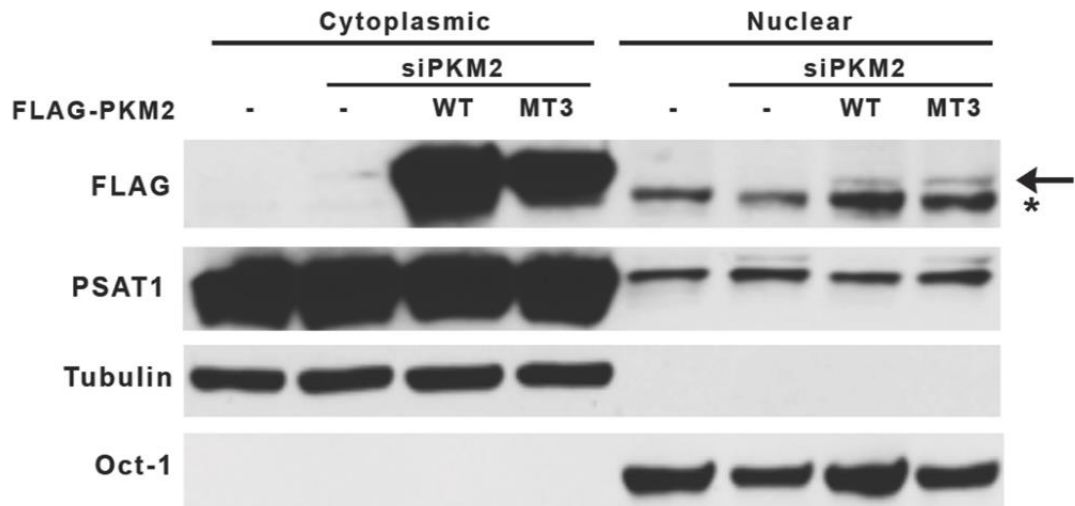
Figure 15. A PSAT1-interaction deficient PKM2 mutant is still able to localize to the nucleus in PC9 cells. Immunoblot analysis of FLAG-PKM2 WT or MT3 localization in PC9 cells stably expressing empty vector (-), FLAG-PKM2 WT, or FLAG-PKM2 MT3. Endogenous PKM2 was silenced via siRNA prior to cytoplasmic and nuclear fractionation of the indicated cell lines. OCT1 and α-tubulin served as loading controls for nuclear and cytoplasmic compartments, respectively. Shown are representative images from three independent experiments. ←indicates FLAG-tagged PKM2, * indicates non-specific band.

Loss of PSAT1 suppresses migration of EGFR-mutant and EGF-induced EGFR-WT lung cancer cells

The oncogenic function of PSAT1 has been investigated in many tumor types and found to play a role in proliferation, migration, and chemo-resistance (1, 43, 71, 74, 77, 79, 81), yet it remains elusive whether PSAT1 may contribute to the cellular response to specific oncogenic signaling, particularly EGFR. Since previous studies have shown that EGF exposure selectively induces cell migration in A549 cells without affecting proliferation (155, 156), we investigated the role of PSAT1 in cell motility in EGFR-activated NSCLC cells. We found that loss of PSAT1 significantly decreased EGFR-mutant PC9 cell motility (Fig. 16 and 17) and observed no impact on cell proliferation with stable shRNA-mediated silencing under these experimental conditions (Fig. 18). In addition, PSAT1 suppression completely inhibited EGF-induced cell migration in A549 cells (Fig. 19).
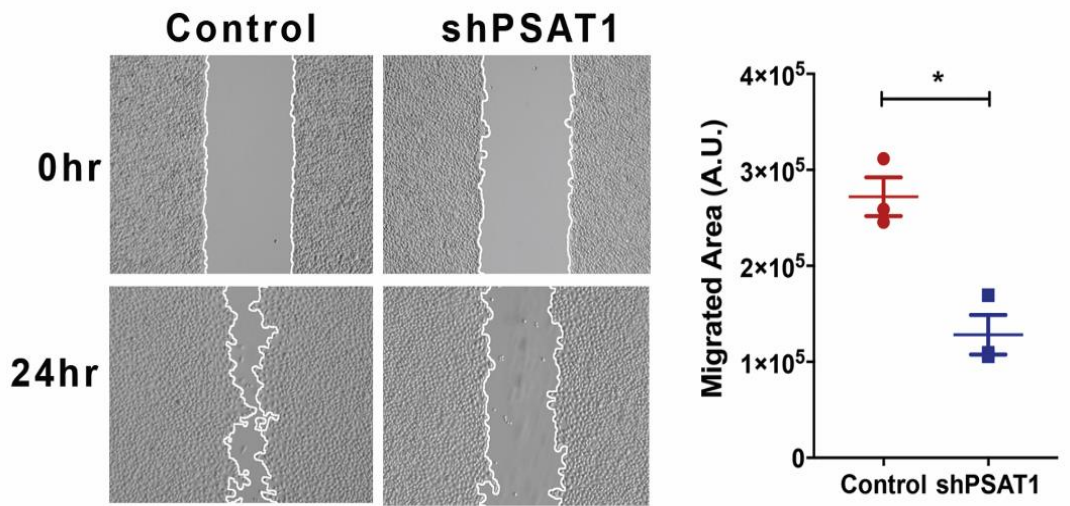
Figure 16. Loss of PSAT1 decreases cell motility in EGFR mutant PC9 cells. Wound healing assay of serum-starved PC9 cells expressing control or PSAT1-specific shRNA. Representative images at 0 hr and 24 hr with migrating cells demarcated by white continuous lines. Data is presented as migrated area after 24 hours and shown is mean $\pm$ SE from three independent experiments. * p < 0.005. A.U.: arbitrary unit.
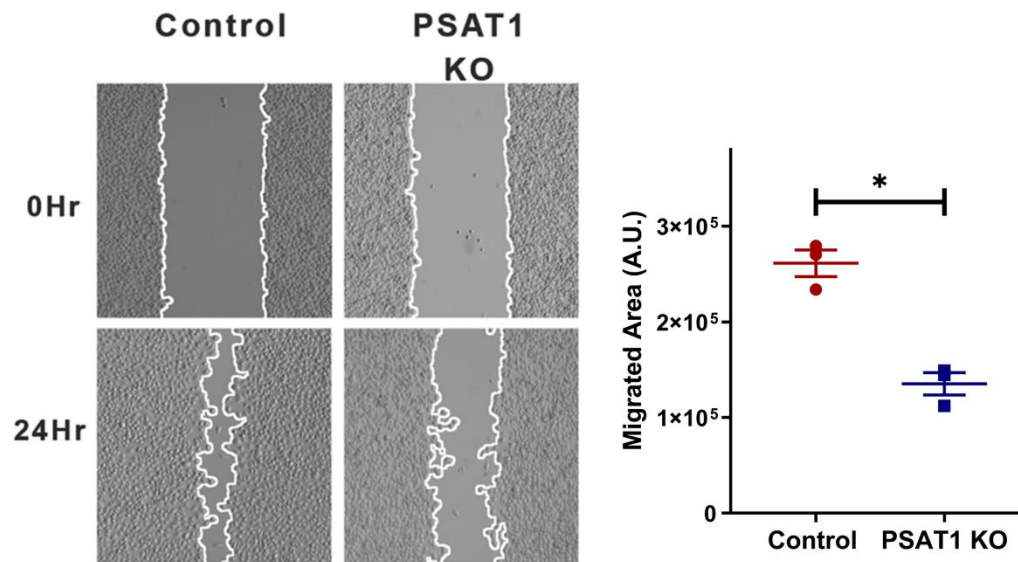
Figure 17. CRISPR-mediated PSAT1 knockout decreases PC9 cell motility. Wound healing assay of serum-starved Control and PSAT1 KO PC9 cells. Shown are representative images at 0 hr and 24 hr with migrating cells demarcated by white continuous lines. Data is presented as mean $\pm$ SE migrated area after 24 hours from three independent experiments. *, p<0.05. A.U.*: arbitrary unit.
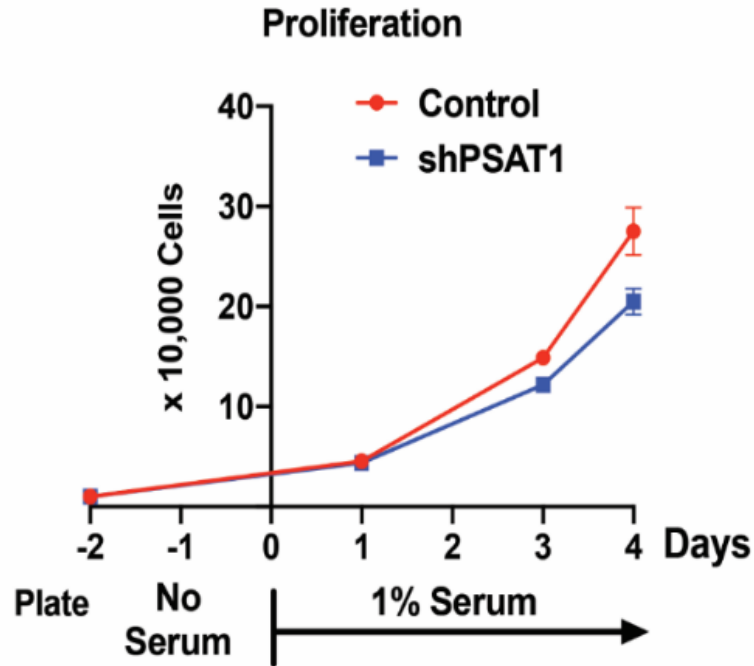
Figure 18. Stable PSAT1 suppression does not impact PC9 cell proliferation under medium conditions and timing used within cell migration assays. PC9 cells (plated at low density -10,000 cells) were serum starved for 24-hours prior to addition of 1% serum. Proliferation was monitored by cell enumeration at the indicated time points. Shown are mean $\pm$ SE from two independent experiments. No effect on cell proliferation was observed at 24 hours and PSAT1 loss had moderate impact at three and four days.
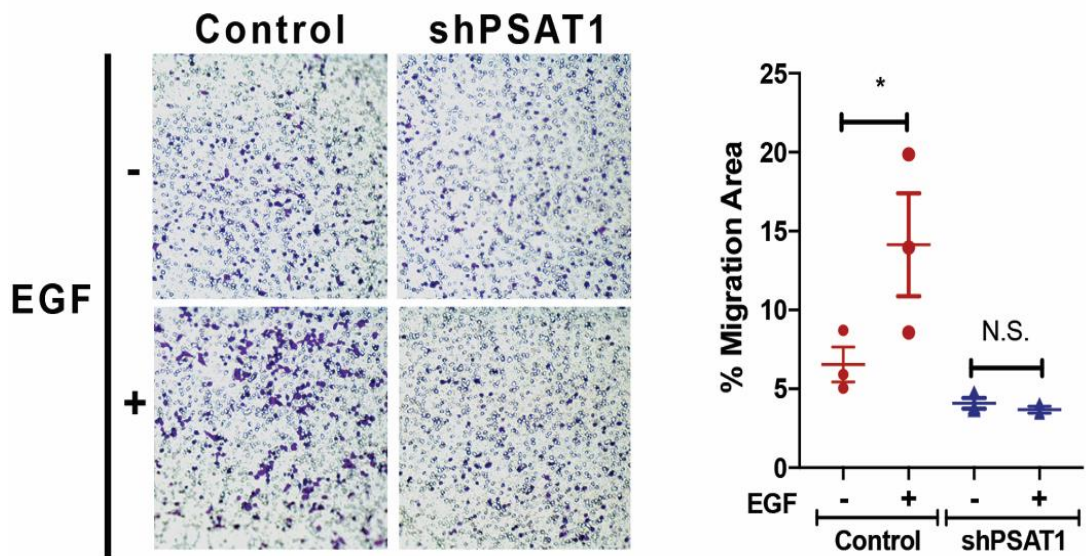
Figure 19. Loss of PSAT1 decreases cell migration in EGF-stimulated A549 cells.
Boyden chamber migration assay on serum-starved A549 cells expressing control or
PSAT1 shRNA. 100 ng/ml EGF serum-free media was used as chemoattractant and
migrated cells were fixed and stained with crystal violet after 24hr. Shown are
representative images of migrated cells and quantification is demonstrated as mean $\pm$
SE of % migration area from three independent experiments. *, p=0.0001. N.S: not
significant.

To demonstrate PSAT1 specificity, we restored expression in silenced PC9 cells (Fig. 20). Re-expression of PSAT1 rescued not only nuclear localization of PKM2 (Fig. 20A and B) but also cell migration (Fig. 21). Increased cell migration upon ectopic PSAT1 overexpression further corroborates these findings (Fig. 22). These results demonstrate a role for PSAT1 in PKM2 nuclear localization and cell migration in these NSCLC models.
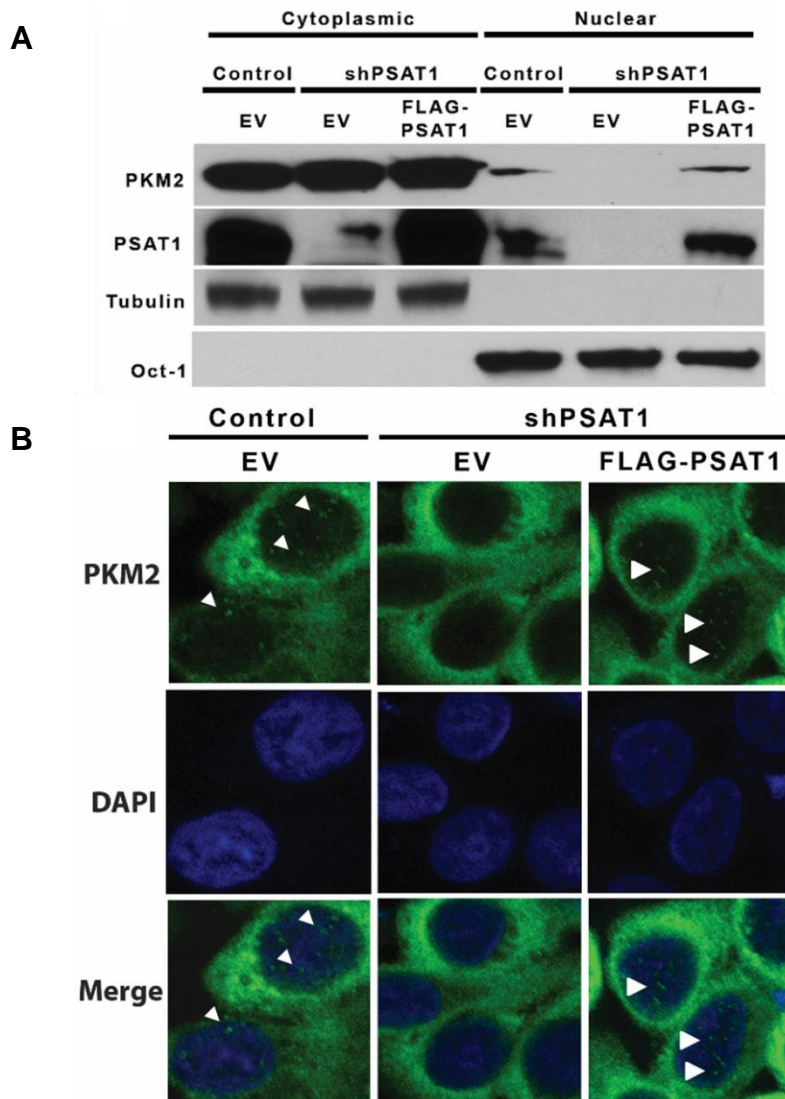
Figure 20. Re-expression of PSAT1 restores the nuclear localization of PKM2 in silenced PC9 cells. A) Immunoblot analysis of cytoplasmic and nuclear fractions from Control-EV, shPSAT1-EV and shPSAT1-FLAG-PSAT1 PC9 cells using anti-PKM2 and anti-PSAT1 antibodies. OCT1 and α-tubulin served as loading controls for nuclear and cytoplasmic compartments, respectively. Shown are representative images from three independent experiments. **B)** Immunofluorescence analysis of PKM2 localization in Control-EV, shPSAT1-EV and shPSAT1-FLAG-PSAT1 PC9 cells by confocal microscopy. Immunofluorescence image with anti-PKM2 antibody (green) and DAPI nuclei staining (blue). Arrowheads indicate nuclear PKM2 staining. EV: Empty Vector.
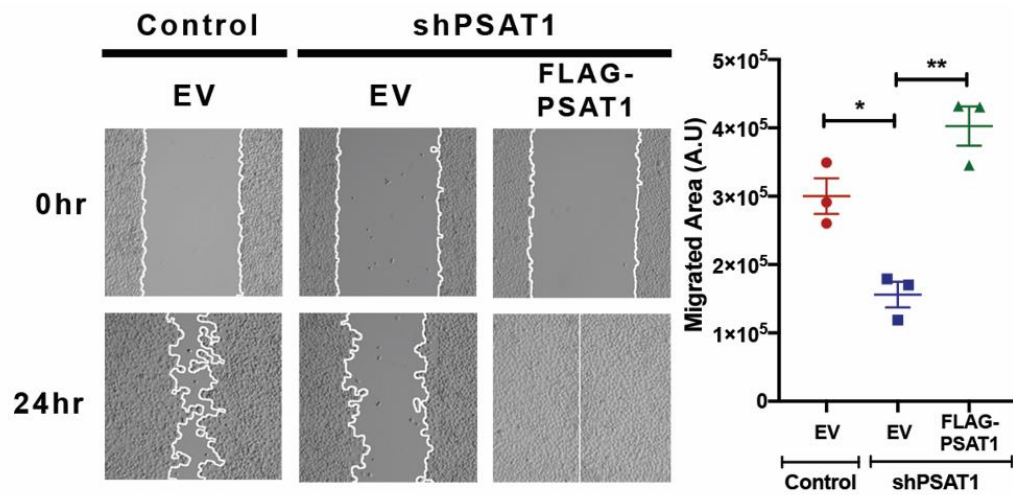
Figure 21. Re-expression of PSAT1 restores cell migration in silenced PC9 cells.
Wound healing assay of Control-EV, shPSAT1-EV, and shPSAT1-FLAG-PSAT1 PC9 cells. Shown are representative images at 0 hr and 24 hr with migrating cells demarcated by white continuous lines. Data is presented as mean ± SE migrated area after 24 hours from three independent experiments. **, $p<0.005$ and *, $p<0.05$. EV: Empty Vector, A.U.: arbitrary unit.
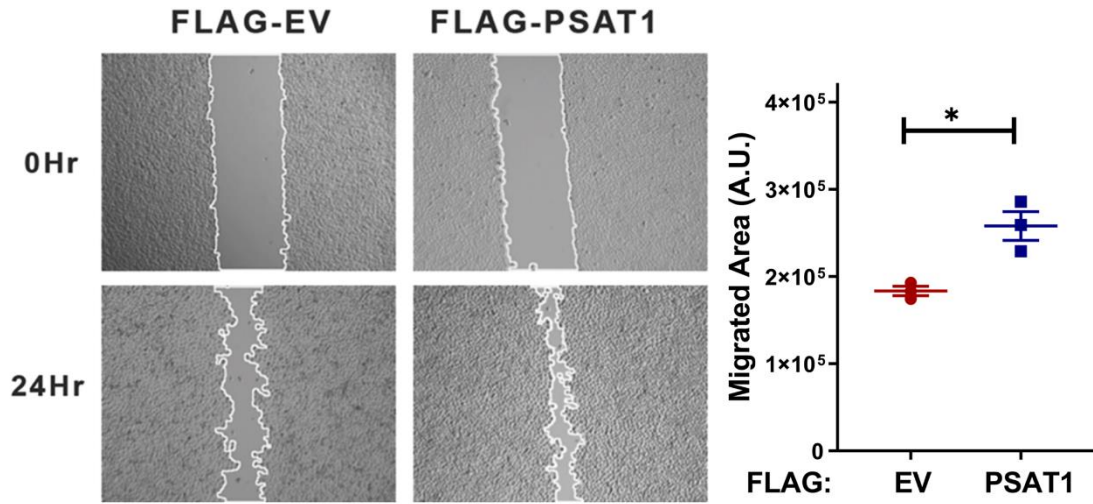
Figure 22. Ectopic expression of PSAT1 induces cell migration in EGFR mutant PC9 cells. Wound healing assay of serum-starved PC9 cells expressing FLAG-EV or FLAG-PSAT1. Shown are representative images at 0 hr and 24 hr with migrating cells demarcated by white continuous lines. Data is presented as mean $\pm$ SE migrated area after 24 hours from three independent experiments. *, $p<0.05$. EV: Empty Vector, A.U.*:* arbitrary unit*.*

Re-expression of nuclear-localized acetyl-mimetic (K433Q) PKM2 partially restores the migration defect due to the loss of PSAT1 in EGFR mutant cells

We then assessed whether nuclear PKM2 may be required for the PSAT1-mediated cell migration in EGFR-mutant cells. Nuclear PKM2 was reconstituted via stable expression of FLAG-tagged PKM2 harboring a nuclear localization signal (FLAG-PKM2^{NLS-WT}) in PC9 cells (Fig. 23A). However, the re-expression of nuclear PKM2 did not restore wound healing in PSAT1 depleted cells (Fig. 23B).
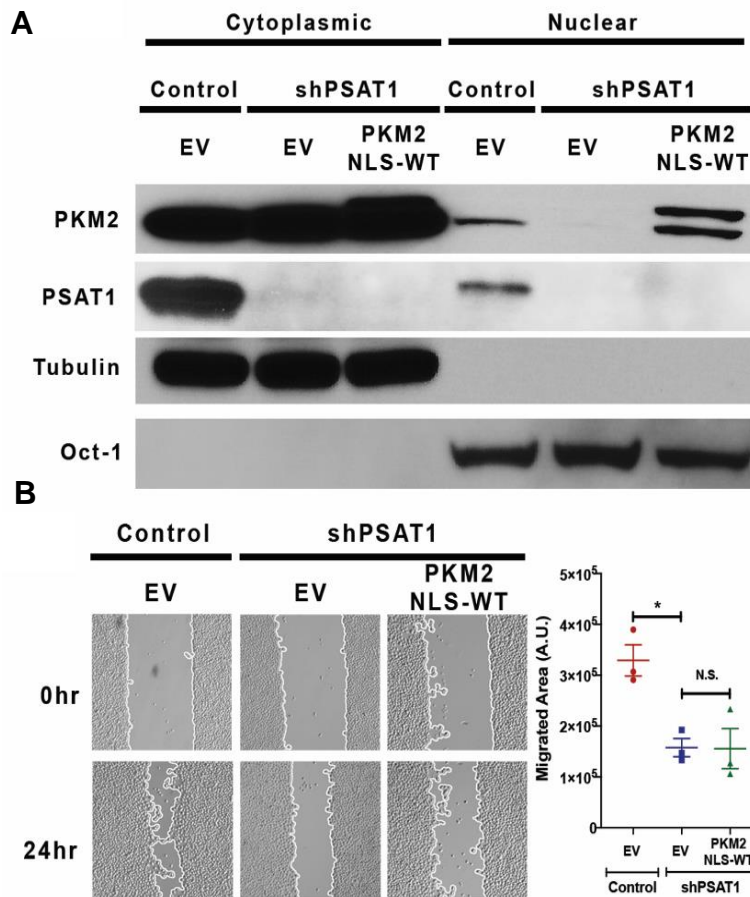
Figure 23. Re-expression of nuclear-localized wild-type PKM2 does not rescue the migration defect due to the loss of PSAT1 in EGFR mutant PC9 cells. **A)** Immunoblot analysis of cytoplasmic and nuclear fractions from Control-EV, shPSAT1-EV, and shPSAT1-PKM2^{NLS-WT} expressing cells using anti-PKM2 and anti-PSAT1 antibodies. OCT1 and α-tubulin served as loading controls for nuclear and cytoplasmic compartments, respectively. Shown are representative images from three independent experiments. **B)** Wound healing assay of serum-starved PC9 cells expressing Control-EV, shPSAT1-EV, and shPSAT1-PKM2^{NLS-WT}. Shown are representative images at 0 hr and 24 hr with migrating cells demarcated by white continuous lines. Data is presented as mean ± SE migrated area after 24 hours from three independent experiments. *, $p < 0.0001$. NS: not significant, A.U.: arbitrary unit, and NLS: nuclear localization signal.

PKM2 can be acetylated at K433 upon EGF stimulation, which localizes in the nucleus and exhibits higher protein kinase activity compared to wild-type PKM2 (110). Consistent with this result, SIRT6-mediated deacetylation of K433 results in the export of PKM2 from the nucleus, suggesting that acetylation of PKM2 at K433 is critical for nuclear localization and function (157). For this, we stably expressed acetyl-mimetic nuclear PKM2 (FLAG-PKM2$^{NLS-K433Q}$) in cells lacking PSAT1. Fractionation analysis confirmed reconstitution of acetyl-mimetic nuclear PKM2 (Fig. 24A). Unlike wild-type PKM2, nuclear acetyl-mimetic PKM2 significantly rescued (41%) PC9 cell motility in the absence of PSAT1 (Fig. 24B). Together, these results suggest that PSAT1 promotes EGFR-stimulated PKM2 translocation, potentially through regulating PKM2 post-translation modifications. This contributes, in part, to PSAT1 mediated cell motility within these EGFR-activated NSCLC cells.
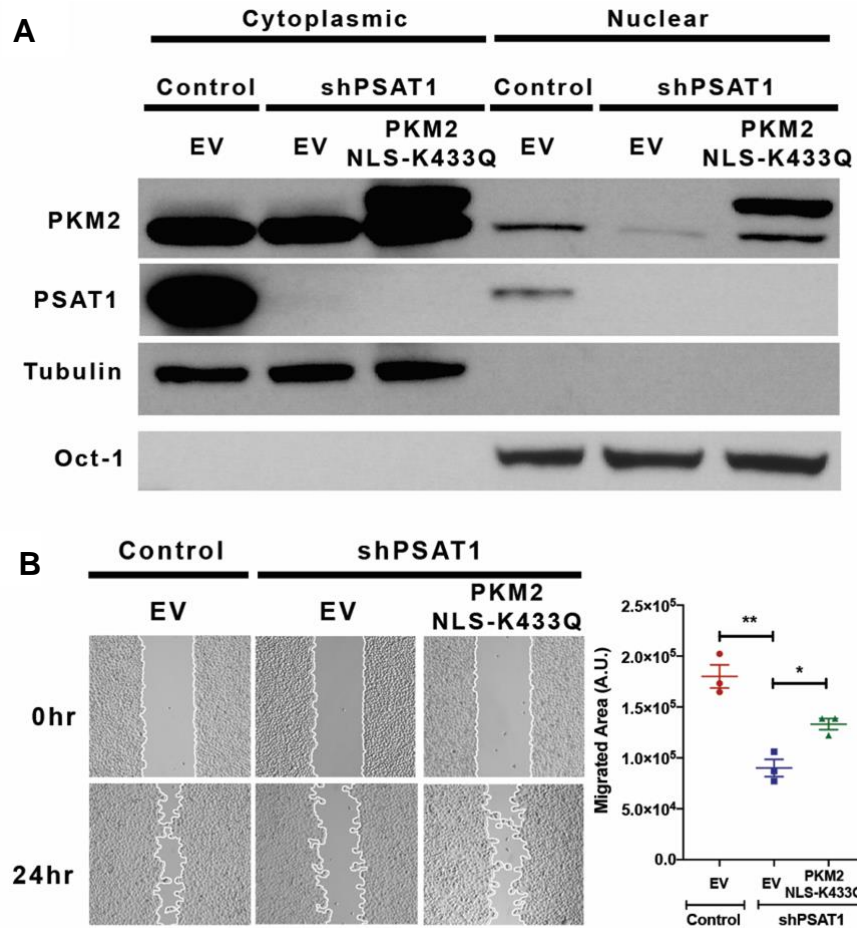
Figure 24. Re-expression of nuclear-localized acetyl-mimetic (K433Q) PKM2 partially rescues the migration defect due to the loss of PSAT1 in EGFR mutant PC9 cells. A) Immunoblot analysis of cytoplasmic and nuclear fractions from Control-EV, shPSAT1-EV, and shPSAT1-PKM2$^{NLS-K433Q}$ expressing cells using anti-PKM2 and anti-PSAT1 antibodies. OCT1 and α-tubulin served as loading controls for nuclear and cytoplasmic compartments, respectively. Shown are representative images from three independent experiments. **B)** Wound healing assay of serum-starved PC9 cells expressing Control-EV, shPSAT1-EV, and shPSAT1-PKM2$^{NLS-K433Q}$. Shown are representative images at 0 hr and 24 hr with migrating cells demarcated by white continuous lines. Data is presented as mean ± SE migrated area after 24 hours from three independent experiments. **, $p < 0.0001$ and *, $p < 0.05$. A.U.: arbitrary unit, and NLS: nuclear localization signal.

PSAT1 expression negatively correlates with survival outcomes in EGFR-mutant NSCLC

We next sought to investigate the clinical relevance of PSAT1 in EGFR mutant lung cancer using microarray datasets and corresponding clinical outcomes from EGFR mutant lung tumors. Expression analysis found elevated PSAT1 expression in both paired and unpaired EGFR mutant lung tumors compared with normal lung (Fig. 25). Furthermore, late-stage EGFR mutant lung tumors tended to exhibit increased PSAT1 expression than early-stage tumors (Fig. 26). Finally, Kaplan-Meier analysis correlated high PSAT1 expression to poorer relapse-free and overall survival rates in this patient population (Fig. 27). These findings suggest that high PSAT1 expression negatively impacts clinical outcomes in EGFR mutant lung cancer.
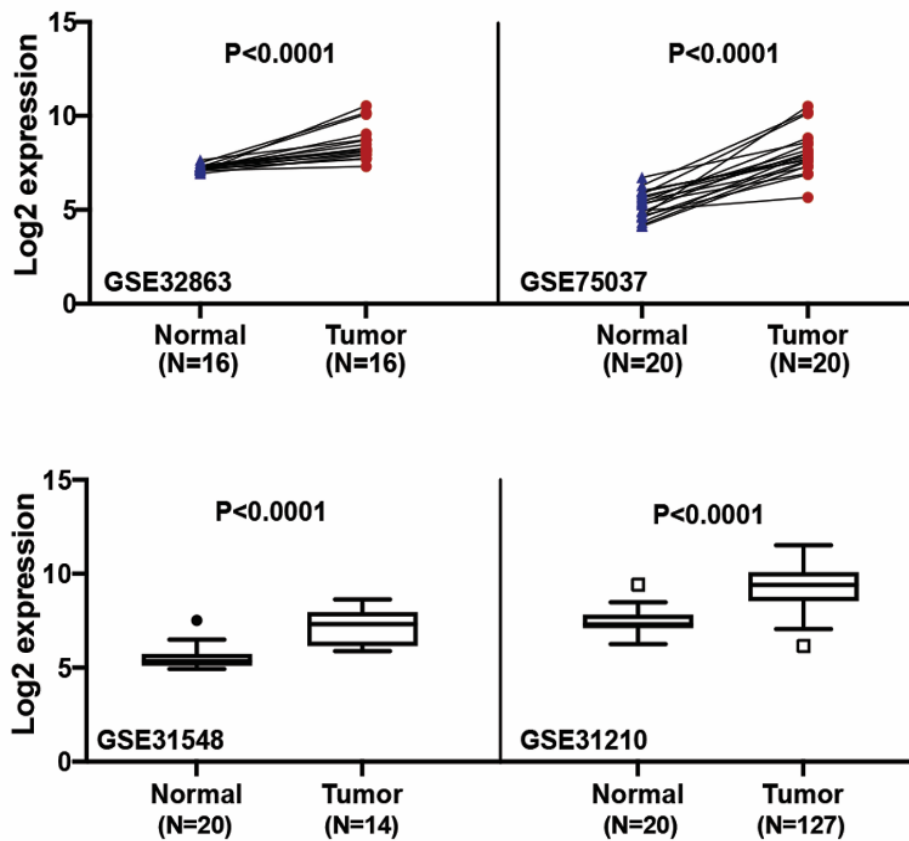
Figure 25. PSAT1 is elevated EGFR-mutant lung cancer compared to normal lung.

Expression analysis of PSAT1 in EGFR mutant lung tumors compared to normal lung in paired (GSE32863 and GSE75037) and unpaired (GSE31548 and GSE31210) datasets. Paired (GSE32863 and GSE75037) and unpaired (GSE31548 and GSE31210) t-tests were performed to determine statistical significance.
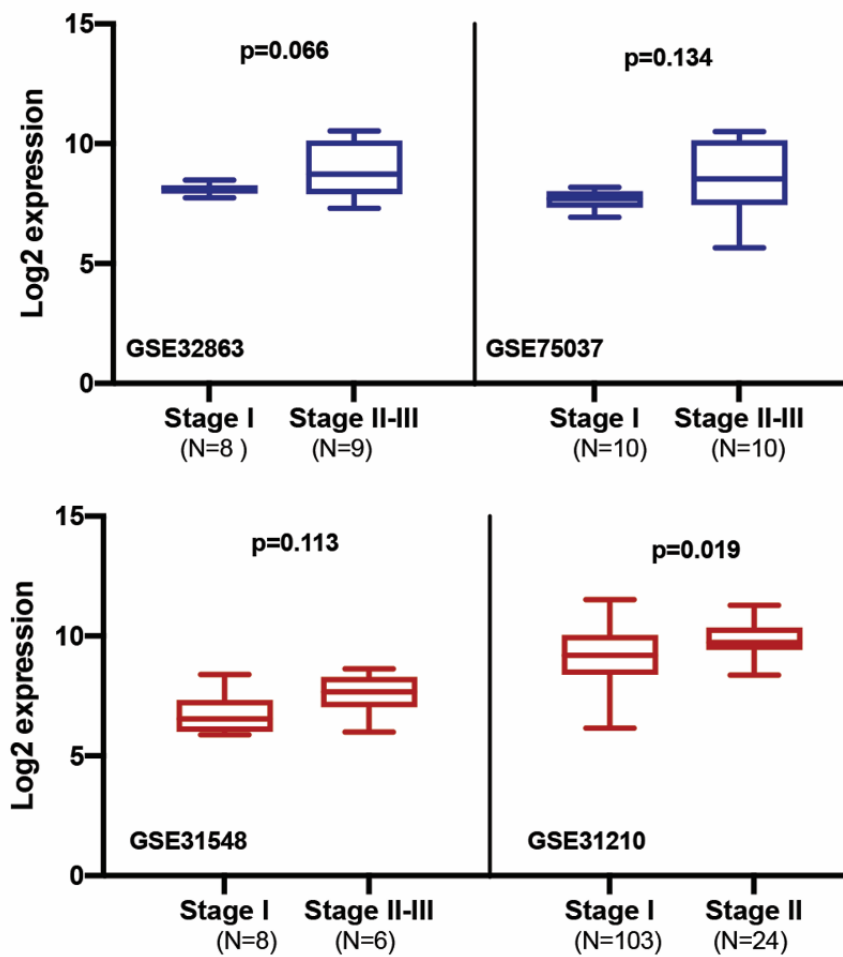
Figure 26. PSAT1 is increased in later stages of EGFR-mutant lung cancer. Expression analysis of PSAT1 in late stage (Stage II and/ or stage III) compared with early stage (Stage I) EGFR mutant lung tumors. Data was statistically evaluated using unpaired t-test.
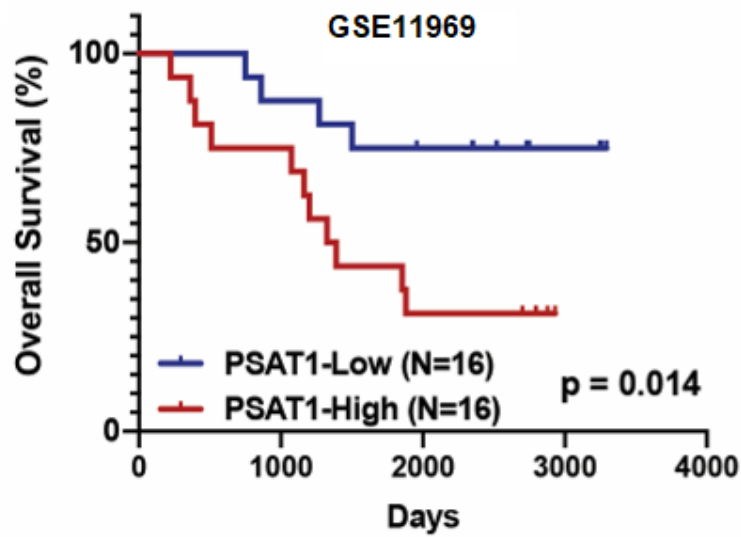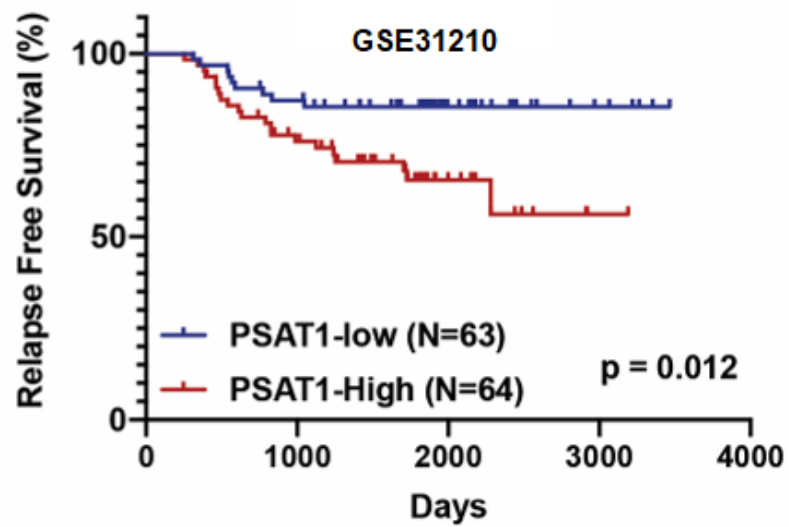
Figure 27. Elevated PSAT1 is associated with poor outcomes in EGFR-mutant NSCLC. Kaplan-Meier analysis was performed to assess the correlation of PSAT1 expression with **A)** overall survival and **B)** relapse-free survival rates in EGFR mutant lung cancer patients.

Discussion

Elevated PSAT1, along with other enzymes within the SSP, has previously been reported in lung cancer (1, 42, 45). Notably, tumor-initiating cells display increased expression of PSAT1, further emphasizing the functional significance of PSAT1 in lung cancer progression (86). While the role of PSAT1 has been investigated in the context of metabolic function, the potential for an alternative role in tumorigenesis remains unclear. Recent discoveries of multifunctionality of metabolic enzymes in tumorigenic processes led us to explore a putative non-canonical function of PSAT1 involved in lung cancer progression (104, 152). In the present study, we identified an interaction between PSAT1 and PKM2 and a need for nuclear PKM2 in PSAT1-driven motility of EGFR-activated NSCLC cells.

PKM2 functions as the predominant pyruvate kinase in many tumor types and promotes growth by various different mechanisms, including regulating anabolic reactions (153). For example, flux through serine biosynthesis is partially controlled through a feedback loop involving PKM2 activity (52, 57). In line with this, small-molecule activators of PKM2 predominantly exert their anti-tumorigenic effect under serine deprivation conditions *in vitro* (60, 61). As these findings indicate a metabolic cross-talk between PKM2 activity and serine, we speculated that depletion of PSAT1 in the cells may alter intracellular pyruvate kinase activity of PKM2 either through reduced serine levels or potentially through disruption of the protein:protein interaction. However, both A549 and PC9 cells did not display a significant change in PKM2 expression or activity in response to PSAT1 silencing, suggesting that PSAT1 association does not influence intracellular PKM2 activity. As our studies were performed in a serine-proficient medium, we postulate that serine import may have sustained intracellular serine levels, which may have contributed to the lack of effect on pyruvate kinase activity in the absence of PSAT1.

Among the oncogenic-drivers of lung adenocarcinoma, activating mutations within the EGFR tyrosine kinase domains account for approximately 17% of these diagnoses (90). Like GBM, nuclear PKM2 has been detected in EGFR mutant NSCLC cancer cells but not in EGFR wild-type NSCLC cells (113, 130, 154). While nuclear PKM2 mediates EGFR-induced proliferation, epithelial-mesenchymal transition (EMT), migration, and invasion in GBM, HCC, and nasopharyngeal

carcinoma cells, EGFR-mediated nuclear function of PKM2 in lung cancer remains elusive, despite a finding as a predictor for response to PARP inhibitor treatment in EGFR-mutant NSCLC cells (113, 154, 158-160). In addition, prior work has also demonstrated that EGF-stimulation promotes cell migration in A549 NSCLC cells that express wild-type EGFR (155, 156). Based on these studies, we speculate that PSAT1 might participate in cell migration under EGFR-activation through facilitating nuclear localization of PKM2. While suppression of PSAT1 decreased EGFR-induced nuclear localization of PKM2, nuclear PKM2 was rescued upon PSAT1 restoration or elevated in ectopic FLAG-PSAT1 overexpressing PC9 cells, implicating a requirement for PSAT1 for PKM2's translocation. Accordingly, cell migration decreased upon PSAT1 suppression and increased when PSAT1 was expressed. Various signals, including EGF, can stimulate PKM2 acetylation at K433, which is required for nuclear function and contributes to tumor progression (110, 157). Consistent with these previous studies, we found that restoration of acetyl-mimetic nuclear PKM2, but not wild-type PKM2, partially reverts the migratory defect due to the suppression of PSAT1. Therefore, our results indicate a correlation between PSAT1-mediated cell migration and nuclear localization of PKM2 upon EGFR-activation.

Although we are able to demonstrate an interaction between PSAT1 and PKM2, our findings yield new unanswered questions. For instance, it is still unclear how PSAT1 may regulate the nuclear localization of PKM2. Similar to PKM2, we also observed EGFR-activation dependent nuclear translocation of PSAT1. However, the requirement of this interaction for nuclear localization is still unclear as a PKM2 mutant that exhibits reduced binding with PSAT1 was still able to localize to the nuclear compartment. Alternatively, PSAT1 may be an essential mediator of EGFR-signaling to PKM2. Upon EGFR activation, cytosolic to nuclear translocation of PKM2 requires multiple steps, including phosphorylation by ERK2, isomerization by PIN1, and then importin α5 mediated nuclear import (114). Subsequently, nuclear retention of PKM2 is aided through binding to poly ADP-ribose (PAR) (154). Given the complexity of nuclear localization of PKM2 mentioned above, it is worth identifying which step or steps are influenced by PSAT1, which is the focus of on-going studies.

The subcellular location in which PKM2 is acetylated by p300 at K433 remains obscure despite the acetylated form being localized in the nucleus and deacetylation resulting in nuclear

export (110, 157). Therefore, it is intriguing whether PSAT1 loss inhibits the nuclear localization of PKM2 by disrupting its acetylation. As p300 acetylates PKM2 in response to oncogenic stimuli, including EGF (110), we postulate that PSAT1 depletion may disrupt the p300:PKM2 interaction or alter EGFR-downstream signaling pathways that regulate p300 activity (161). While nuclear PKM2 is required for EGF-involved EMT-mediated cell migration in HCC, oral squamous carcinoma, and colon cancer, further work is also needed to fully define the mechanisms by which nuclear PKM2 promotes cell motility under EGFR-activation in NSCLC (158, 162, 163).

The partial rescue observed within the PKM2 expression studies indicates that other PSAT1 activities contribute to EGFR-activated NSCLC motility independent of nuclear PKM2, which may include putative nuclear-specific PSAT1 function(s). As the metabolic function of PSAT1 has not yet been thoroughly examined in this context, its enzymatic activity on cell migration and nuclear localization of itself and PKM2 needs further investigation, potentially through the use of metabolic deficient PSAT1 mutants. In summary, we have identified PKM2 as a new PSAT1 associating protein in NSCLC cells. Whereas PSAT1 appears to be dispensable for PKM2's pyruvate kinase activity, it is essential for PKM2 nuclear localization in EGFR-activated NSCLC cells. This supports, in part, PSAT1's ability to promote cell migration under EGFR signaling, which may be a contributing determinant for its negative correlation with patient outcomes in EGFR-mutant NSCLC.

CHAPTER 3

DELINEATING THE FUNCTIONAL LINK BETWEEN A PSAT1-ASSOCIATED GENE
EXPRESSION SIGNATURE AND EGFR-MUTANT LUNG CANCER

Introduction

Genome-wide gene expression profiling has become routine since the discovery of microarray technologies and the completion of the human genome project. Gene expression patterns have allowed for determining the mechanisms that drive diseases, identifying disease sub-types, predicting disease progression, and providing functional information about the differentially expressed genes that can be grouped into functional pathways (164, 165). More recently, RNA sequencing (RNA-seq) has taken the place of microarrays as the cost of sequencing has fallen. This change has also facilitated the discovery of new fusion transcripts involved in tumorigenesis (166).

Analysis of these technologies has also required the development of bioinformatics tools to help researchers handle these large datasets and extract any biological information. MSigDB and WebGestalt are both well-known web-based integrated data-mining systems that can explore large gene sets (167, 168). They are user-friendly bioinformatics tools that help users in the management, information retrieval, organization, visualization, and statistical analysis of gene sets.

The Gene Expression Omnibus (GEO) database was founded to serve as a public repository for high-throughput gene expression and other functional genomics datasets (169). Researchers can easily access either the raw or processed data that may benefit their own studies. Furthermore, biostatisticians of the Biometric Research Branch of the National Cancer Institute have developed the BRB-ArrayTools software package, which is non-commercial and user-friendly

sequence profiling analysis tool (151). In addition to the normalization of the genomics data, it has many plugins to help in performing further analysis. For example, these include class comparison analysis for determining differentially expressed genes between groups as well as survival risk prediction tools for identifying gene signatures that may predict patients outcomes (170). In addition, it has many statistical tools such as cluster, ANOVA, and time-series analysis.

In the previous chapter, we demonstrated a requirement for PSAT1 in EGFR-mediated cell migration. The partial rescue in cell migration with the restoration of nuclear PKM2 implies the potential presence of other PSAT1-dependent mechanisms. As we also found nuclear localization of PSAT1 upon EGFR activation, this prompted us to carry out genome-wide RNA-seq expression profiling under PSAT1 loss. Through analysis of differentially expressed genes, our intent was to identify other unknown mechanisms for PSAT1 in contributing to tumorigenesis. Further, to take advantage of the many genome-wide datasets focused on EGFR mutant lung cancer, we also compared our PSAT1-associated genes with differentially expressed genes in EGFR mutant lung tumors using the BRB-Array tools. This was done with the intent of identifying an EGFR related PSAT1 gene signature, which may have potential clinical application.

<center>**Methods and Materials**</center>

Reagents and antibodies

Antibodies against PKM2 (4053), β-catenin (8480), OCT1(8157), and α-Tubulin (3873) were obtained from Cell Signaling Technology. Anti-PSAT1 (10501-1-AP) antibody was purchased from Proteintech Group Inc. β-actin (A2228), 100x EmbryoMax Nucleosides (ES-008-D), and Dimethyl 2-oxoglutarate(349631) were obtained from Sigma. pGL4.49[luc2P/TCF-LEF/Hygro] Vector (E4611) and Dual-Luciferase Reporter Assay System (E1960) were purchased from Promega. Difco Noble Agar (214220) from BD Bioscience and 100X NEAA (non-essential amino acid) (25-025) were purchased from Corning.

Cell culture

Generation of stable PC9 cells (Control and shPSAT1 PC9, Control-EV, shPSAT1-EV, shPSAT1-FLAG-PSAT1, and shPSAT1-PKM2$^{\text{NLS-K433Q}}$) were previously discussed in chapter 2. Control and shPSAT1 PC9 cells were maintained in RPMI media (Gibco) supplemented with 10% FBS, 50 μg/ml gentamicin (Gibco), and 1 μg/ml puromycin. Control-EV, shPSAT1-EV, shPSAT1-FLAG-PSAT1, and shPSAT1-PKM2$^{\text{NLS-K433Q}}$ PC9 cells were maintained in RPMI media (Gibco) supplemented with 10% FBS, 50 μg/ml gentamicin (Gibco), 1μg/ml puromycin, and 200ug/ml geneticin. All cells were cultured in humidified incubators at 37°C and 5% CO_2.

RNA isolation and reverse transcription

RNA was harvested with RNeasy Mini Kit according to the manufacturer's instructions (Qiagen, 74106). RNA quality and concentration were measured with Nanodrop RNA 6000 nano-assays (for reverse transcription PCR (RT- PCR)). 2 μg of isolated total RNA was reverse transcribed by High-Capacity RNA-to-cDNA according to manufacturer's instructions (ThermoFisher Sci., 4387406). The cDNA sample was diluted by adding 60 μl Nuclease-free water to make an estimated final concentration of 25 ng/μl.

Real-time PCR for mRNA

<center>77</center>

10 µl of reaction mix was prepared by adding 1 µl of cDNA. 0.5 µl target probe (FAM conjugated), 0.5 µl of ACTB(VIC), and 5 ul of TaqMan Fast Advanced Master Mix (Thermo Fischer Sci, 4444557) and reactions were carried out according to Taqman Fast Reaction Protocol using AB StepOnePlus Real-Time PCR System (Applied Biosystems). Data were analyzed using Ct method and β-actin (ACTB) was used as a reference gene. The list of Real-time PCR Taqman probes is presented in Table 2.

Table 2. Taqman probe list

Gene Name	# PROBE
USP14	Hs00193036_m1
VAPA	Hs00427749_m1
NDUFV2	Hs00221478_m1
TYMS	Hs00426586_m1
METTL4	Hs01559838_m1
SEH1L	Hs01031566_m1
IMPA2	Hs00274110_m1
MYL12B	Hs01050560_m1
S100A4	Hs00243202_m1
TMSB4X	Hs03407480_gH
FHOD1	Hs01077922_m1
ACTB	Hs01060665_g1

Soft agar assay and metabolite supplementation

For both Control and shPSAT1 PC9 cells, 2 assays for each of the 8 conditions were prepared: No supplement (-); NEAA; Nucleoside; 500 µM α-ketoglutarate (α-KG); NEAA + 500 µM α-KG; NEAA + Nucleoside; Nucleoside + 500 µM α-KG; ALL (NEAA+ Nucleoside+ 500 µM α-KG). Dimethyl 2-oxoglutarate served as α-KG supplement.

i. *Base agar:* 18 ml of warmed 2% noble agar were mixed with 42 ml of warmed 10% FBS media. 3ml of the mixture was then added to individual 6-cm cell culture plates and incubated at room temperature until solidified.

ii. *Top agar:* (Each condition, 2 plates) 1.3 ml of warmed 2% noble agar were mixed with 8 ml of warmed 10% FBS media containing 3000 cells and supplemented with the indicated metabolite(s). 3 ml were then added to the top of the base agar and incubated at room

temperature until solidified. Cells were cultured in humidified incubators at 37^0 C and 5% CO_2 for 21 days and maintained with feeder layers every 3-4 days, as described below.

iii. *Maintenance of culture with feeding media (4 plates/metabolite addition):* 1.25 ml of warmed 2% noble agar were mixed with 8.75 ml of warmed 10% FBS media supplemented with the indicated metabolite(s). Cells were then fed with 1.5 ml of feeding media every 3-4 days during 21-day incubation. At the end of the study, whole plate images were captured, and colonies were counted via Image J cell counting tool.

Soft agar assay for rescue study

In both PSAT1 and nuclear PKM2 rescue study, 4 plates were prepared for each condition (Control-EV, shPSAT1-EV, shPSAT1-FLAG-PSAT1, or shPSAT1-PKM2[NLS-K433Q]).

i. *Base agar:* Prepared as described above.

ii. *Top agar:* (Each condition, 4 plates) 1.9 ml of warmed 2% noble agar were mixed with 12 ml of warmed 10% FBS media containing 4500 cells. 3 ml of the mixture was then added to the top of the base agar and incubated at room temperature until solidified. Then, cells were cultured in humidified incubators at $37\ ^0$C and 5% CO_2 for 21days.

iii. *Maintenance of culture with feeding media:* 2.5 ml of warmed 2% noble agar were mixed with 27.5 ml of warmed 10% FBS media. Cells were then fed with 1.5 ml of feeding media every 3-4 days during 21-day incubation. At the end of the study, whole plate images were captured, and colonies were counted via Image J cell counting tool.

Wound-healing assay with metabolite supplementation

Control and shPSAT1 PC9 cell lines were plated at 10^6 cells / well in 6 well-plate and grown in complete media overnight. Culture media was then changed to serum-free media for 24 hours. A confluent monolayer of cells was wounded with a 200 µl pipette tip in two different areas in each well. Cells were washed three times with PBS and cultured in 4 ml of low serum-RPMI media (1% FBS) with or without metabolites (1XNEAA + 1XNucleoside + 500 µM α-KG). Six different images (4x magnification) were captured from wounded areas at 0- and 24-hour time points and analyzed

using Image J software with MRI wound healing tool. The migrated area was calculated by subtraction of wound area (arbitrary unit) at 24 hours from the initial wound area.

Whole-cell protein extracts and subcellular fractionation

Whole-cell lysate protein extraction was performed via Pierce IP lysis buffer supplemented with PMSF, protease inhibitor, and phosphatase inhibitor according to manufacturer protocol (Thermo Fischer Sci, 87787).

Cytosolic and nuclear proteins were isolated using the NE-PER kit (Thermo Fischer Sci., 78835). 15 µg of cytoplasmic protein and 25 µg of nuclear protein were used for immunoblotting analyses.

Immunoblotting

Proteins within whole-cell lysates, cytosolic and nuclear fractions were separated by SDS-PAGE and transferred to PVDF membrane. Blocked membranes were then incubated with the indicated primary antibodies. Protein detection was performed using the appropriate HRP-conjugated secondary antibody and visualized by chemiluminescence (ECL Prime, GE Healthcare).

Luciferase reporter assay

Control-EV, shPSAT1-EV, and shPSAT1-FLAG-PSAT1 PC9 cells were plated into 6-well plates and transfected with 2 µg of pGL4.49[luc2P/TCF-LEF/Hygro] using jetPEI with overnight incubation (media changed after 24 hours). Forty-eight hours post-transfection, stably transfected cells were selected in 200 µg/ml hygromycin (TCF-LEF vector), 200 µg/ml geneticin (pcDNA3.1 vector), and 1 µg/ml puromycin (shRNA vector). For each study, 4 x 10^5 stable cells were plated into each well of a 6-well plate (3 replicates for each condition). Next day, cells were switched to serum-free media and maintained for 24 hours. Cells were then harvested according to Dual-Luciferase Reporter Assay protocol. Firefly luciferase activity was determined using 96-well plate luminometer. Protein concentration of samples was measured by BCA Protein assay and used to normalize the luciferase activity.

Phalloidin staining

Cells were plated into 4-well chamber slides and incubated in serum-free media for 24 hours. They were then fixed with 3.7% paraformaldehyde in PBS solution for 10 minutes at room temperature and washed three times with PBS. Following washes, they were permeabilized with 0.1% Triton X-100 in PBS for 3 minutes and washed again. For visualization, cells were incubated with a Rhodamine Phalloidin (Invitrogen, R415) working solution (5μl stock/200 μl PBS) for 20 minutes in the dark at room temperature. After additional washing with PBS (3X), slides were covered with SlowFade Diamond Antifade Mountant with DAPI (S36964) reagent. Images were captured by Olympus FV-3000 confocal microscope equipped with Fluoview software (Olympus America Inc) under 40X magnifications.

RNA-seq transcriptomic profiling

Three sets of RNA for RNA-seq profiling were prepared from 24 hour- serum-starved Control and shPSAT1 PC9 cells. Samples were submitted to the UofL Genomics Facility, which performed the library preparation and sequencing reactions. Sequencing was performed on the Illumina NextSeq 500 using the High Output Kit v2 with 75 cycles (cat# FC-40402005) within the CGeMM facility. Initial data analysis was performed by the KBRIN Bioinformatics core. Normalized FPKM (Fragments Per Kilobase of transcript per Million mapped reads) expression values and statistical analysis results, including p- and q-value with ENSEMBL gene ID, were downloaded for further investigation.

The following parameters served as the selection criterion for differentially expressed genes, $|log_2[FC]| \geq 0.48$, FPKM value (Control or shPSAT1) ≥ 5, and q-value ≤ 0.05. Genes were divided into two groups: down-regulated genes (termed shPSAT1-down-regulated) and up-regulated genes (termed shPSAT1-up-regulated) as identified in comparisons between shPSAT1 PC9 cells and control cells. As MsigDB v7.2 (Molecular Signatures Database) (https://www.gsea-msigdb.org/gsea/msigdb) provides several categories for gene set analysis, KEGG pathway analysis, CGP (chemically and genetically perturbed data sets), gene ontology (GO) analysis with GO_BP (biological process) and GO_CC (cellular component), and positional gene set analysis

tools were utilized in this project based on TOP 20 list for KEGG pathway analysis and TOP 50 for others with FDR ≤0.05 (167). Potential transcription factors involved in the alteration of gene expression were identified by the transcription factor analysis tool of WebGestalt 2013 (WEB-based GEne SeT AnaLysis Toolkit) (http://www.webgestalt.org/2013/) using the hypergeometric test with adj-p≤0.001 with at least 10 gene targets (168).

Public microarray datasets analysis

i. *Data search and import*

The EGFR mutant lung cancer datasets were chosen based on the number of EGFR mutant tumor samples (n>10) with paired or unpaired normal tissue samples and the availability of relevant clinical information. According to these selection criteria, GSE31210, GSE27262, GSE31547, GSE31548, GSE32863, and GSE75037 datasets were imported to BRB-ArrayTool using its NCBI GEO Series tool (151).

ii. *Identification of common gene sets and survival analysis*

shPSAT1-mediated down-regulated and up-regulated gene lists obtained from the RNA-seq analysis were prepared separately as text files and saved under the user gene list folder under the program files of ArrayTool. Expression of these genes was filtered using the ArrayTool- re-filter option and normalized. Data was utilized with the exclusion of those genes whose expression was less than 20% of expression data and less than 1.5- fold change in either direction from the gene's median value options. Differentially expressed genes from our RNA-seq profiling were directly compared to those gene changes between EGFR mutant tumor and normal lung samples using the ArrayTool-Class Comparison plugin and the significance threshold of univariate analysis with p≤0.05 served as statistical analysis criteria. This was done to identify PSAT1 regulated genes that are also differentially expressed in EGFR-mutant NSCLC. Importantly, up-regulated genes in EGFR tumors would be down-regulated by shPSAT1 and vice-versa. Genes with fold-changes (EGFR mutant tumor/ Normal lung) ≥ 1.4 found in our shPSAT1-down-regulated genes list and genes with fold-changes (EGFR mutant tumor/ Normal lung) ≤ 0.71 found in our shPSAT1-up-

regulated genes list were assigned as PSAT1-associated genes linked with EGFR mutant lung cancer. This procedure was repeated for each dataset: GSE31210, GSE27262, GSE31547, GSE31548, GSE32863, and GSE75037.

The common gene sets were determined via Venn diagram comparisons using http://bioinformatics.psb.ugent.be/webtools/Venn/. The expression of common genes from each dataset was extracted using the ArrayTool-Class Comparison tool. Cluster analysis and heatmap generation were performed with dChiP software using the following criteria: Euclidean distance with average linkage analysis (171).

Among the datasets, GSE31210 was the only set encompassing all of the following clinical information on defined NSCLC genotypes: KRAS mutant and EGFR/KRAS wild-type tumor data in addition to EGFR mutant lung tumors and their pathological stage, relapse and survival events, and duration data. Therefore, survival predictions using the expression data of the PSAT1-associated common gene lists were performed by the BRB-ArrayTool survival risk prediction function (170). Principal component analysis with leave-one-out cross-validation and log-rank statistics with 100 permutation tests were used for analysis and $p \leq 0.05$ was considered statistically significant. This analysis calculated the prognostic indexes and classified the patients based on this index as high risk and low risk groups.

iii.   Identification of a potential PSAT1-associated metastatic gene signature

GSE14107 was imported as described above due to the presence of a genome-wide expression profile of both parental PC9 cells and its metastatic brain subline of PC9-BrM3 (172). Differentially expressed genes were determined by ArrayTool- Class comparison plugin using the significance threshold of univariate analysis with $p \leq 0.05$. Down-regulated and up-regulated gene lists were assigned based on fold-change (PC9-BrM3/PC9-Parental) $0.71 \geq$ and $1.4 \leq$, respectively. The GSE14107 gene list was compared with the differential expression gene list from our PC9-shPSAT1 RNA sequencing analysis by http://bioinformatics.psb.ugent.be/webtools/Venn/ to find common genes. Cluster analysis and heatmap generation of common gene expression derived from the GSE14107 dataset were performed by dChiP software.

Statistical analysis

All data were statistically analyzed using Prism 8 software (GraphPad Software). Statistical significances were assessed based on the number of groups with one or more independent variables. Repeated Measure one-way ANOVA with Tukey's multiple comparison test for three groups was performed for both PSAT1 and nuclear PKM2 rescue study. Two-way ANOVA with Tukey's multiple comparison test was used for wound-healing assay with metabolite supplementation. The statistical significance for soft agar assay with metabolite supplementation was determined by two-step analysis: firstly, two-way ANOVA with Dunnet's multiple comparison test was performed with raw data to examine the effect of metabolite supplementation on both control and shPSAT1 cells. Then, the ratio of colony number (shPSAT1/Control) within each treatment was used for repeated measure one-way ANOVA with Dunnet's multiple comparison test to assess the rescue effect. Experimental replicates for each analysis are stated within the respective figure legend. Values of $p \leq 0.05$ were considered statistically significant.

Results

Determination of differentially expressed genes (DEG) in PSAT1 silenced PC9 cells

In the previous chapter, we used biochemical approaches to examine the role of PSAT1 in NSCLC tumorigenesis. We found that PSAT1 interacts with PKM2 and contributes to PKM2's nuclear localization in EGFR-activated NSCLC cells. Unexpectedly, we also observed PSAT1 within the nuclear compartment of the EGFR-activated cells. Thus, we conducted a genome-wide gene expression profiling study using RNA-seq technology to potentially uncover unknown cellular processes that are impacted by PSAT1 loss.

Three separate sets of RNA were extracted from distinctly grown control and shPSAT1 PC9 cells and submitted for sequencing and statistical analysis to the genomics core facility within the James Graham Brown Cancer Center in partnership with the Kentucky Biomedical Research Infrastructure Network (KBRIN). Their initial analysis provided normalized expression values of genes in FPKM (fragments per kilobase of transcript of million mapped reads) with annotation tables, log2(FC) (log2(foldchange)), p-values, and q-values (adjusted p-value). From this, we determined the differentially expressed genes (DEG) based on the following criteria: FPKM≥ 5, fold-change ≥ 1.4 ($|\log_2(FC)| \geq 0.48$), and q-value ≤ 0.05. Heatmaps of both down-regulated and up-regulated genes resulting from PSAT1 silencing were created by dChiP software and presented in Figures 28 & 29, respectively (171). In sum, we found 279 down-regulated and 211 up-regulated genes for further analysis.

Pathways and biological processes affected by PSAT1 suppression

Molecular signature database (MSigDB) is a user-friendly database created and maintained by the Broad Institute (https://www.gsea-msigdb.org/gsea/msigdb/index.jsp) (167). MSigDB stores more than thirty thousand annotated gene sets under 9 different subjects for gene set analysis including, hallmarks of gene sets, positional gene sets, curated gene sets, regulatory target gene sets, computational gene sets, ontology gene sets, oncogenic signature gene sets, immunologic gene sets, and cell type signature gene sets. These major subjects have been further

Figure 28. Heatmap demonstrating down-regulated genes upon PSAT1 silencing.

Color key (Blue, Red)→ (-2,2).

Figure 29. Heatmap demonstrating up-regulated genes upon PSAT1 silencing.

Color key (Blue, Red)→ (-2,2).

divided into sub-groups. For example, curated gene sets consist of gene sets for pathway analysis, including KEGG, BIOCARTA, PID, and REACTOME. Users are able to upload individual gene sets for comparison to the curated sets within MSigDB. The overlapping genes are then identified along with statistical analysis values: p and FDR, which can be downloaded in a text format.

Down-regulated and up-regulated gene lists obtained from our RNA-seq studies were uploaded separately to MSigDB for KEGG pathway analysis based on Top 20 pathways with FDR≤0.05. Results were plotted as number genes in the indicated pathways and presented in Figure 30. The affected pathways identified with the down-regulated gene set included cell cycle, pathways in cancer, and MAPK signaling pathway (Fig. 30A). These are commonly dysregulated pathways involved in tumorigenesis and confirm the oncogenic effect of PSAT1 at the transcriptional level. Down-regulated genes within folate biosynthesis, glutathione metabolism, and purine and pyrimidine metabolism linked dysregulation of serine biosynthetic pathway with loss of PSAT1 metabolic function. Paradoxically, KEGG pathway analysis of up-regulated genes also found cancer-related pathways involving MAPK signaling pathway, ERBB signaling pathway, pathways in cancer, and endometrial cancer (Fig. 30B). However, we found that 20.7 % of down-regulated genes were attributed to cancer-related pathways, while only 11.84 % of up-regulated genes were included in this pathway analysis.

Next, we performed gene ontology (GO) analysis using MSigDB- GO_BP (Biological Process) and GO_CC (Cellular Component) tools to gain deeper insight into PSAT1-associated gene signatures. Top 50 signatures with FDR ≤0.05 served as our selection criteria. GO terminologies were grouped under general biological process titles in order to highlight the overall cellular changes upon PSAT1 silencing. GO_BP and GO_CC analysis of down-regulated genes were summarized in Tables 3 and 4. Similarly, GO_BP and GO_CC of upregulated genes were presented in Tables 5 and 6.
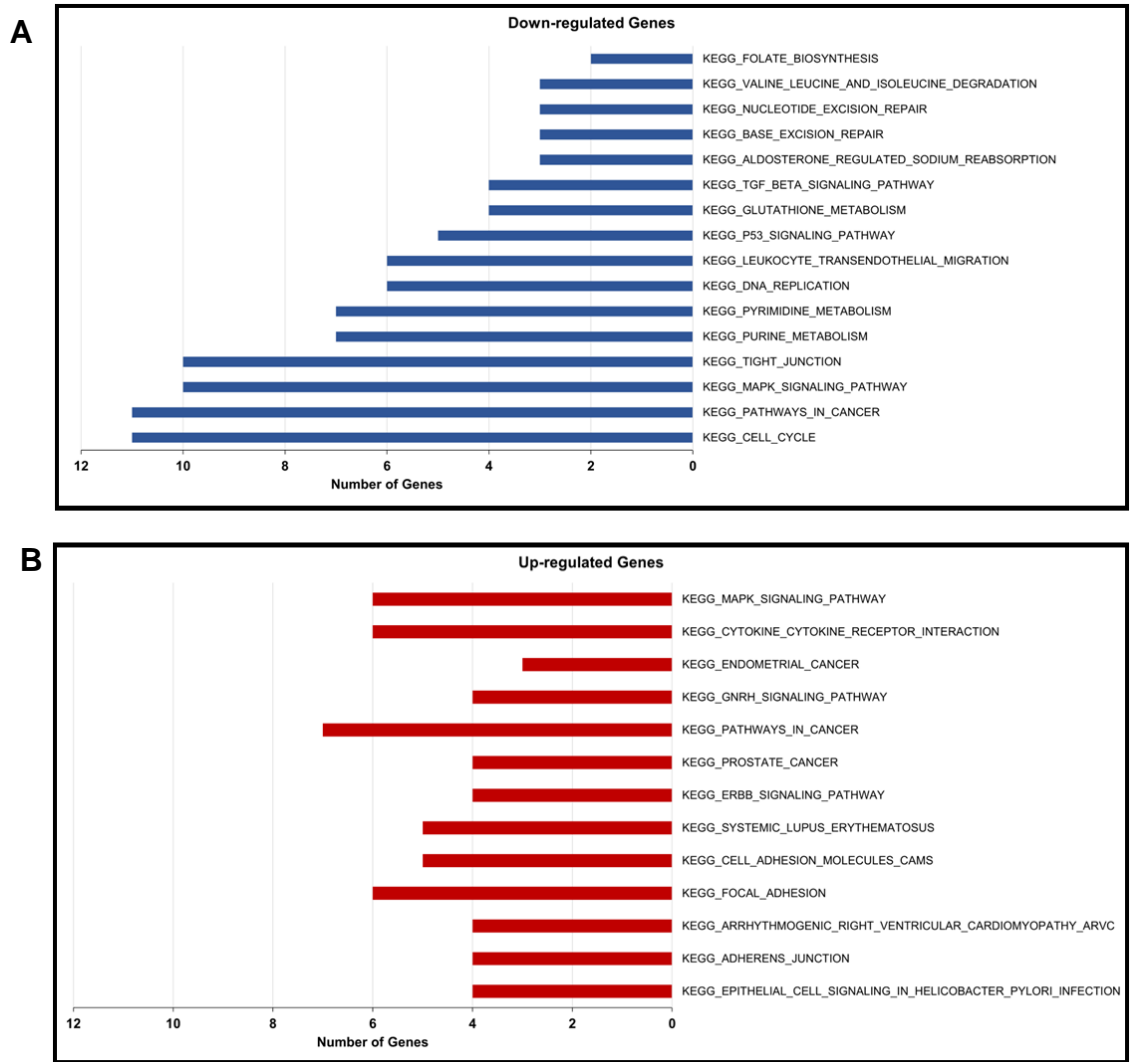
Figure 30. KEGG pathway analysis of differentially expressed genes. A) shPSAT1-down-regulated genes and **B)** shPSAT1-up-regulated genes. FDR≤0.05.

Table 3. GO_BP analysis of shPSAT1-down-regulated genes

Biological Process	GO_BP terms	Genes
Regulation of Molecular Function	GO_REGULATION_OF_PROTEIN_MODIFICATION_PROCESS GO_POSITIVE_REGULATION_OF_MOLECULAR_FUNCTION GO_REGULATION_OF_PHOSPHORYLATION GO_POSITIVE_REGULATION_OF_CATALYTIC_ACTIVITY GO_REGULATION_OF_HYDROLASE_ACTIVITY	CDC6, CCNE1, MCM2, DSCC1, GMNN, CLSPN, CDKN2D, DUSP1, SFN, BMP4, GADD45A, HSPA1A, HSPA1B, TGFA, CEP85, SEH1L, RFC2, CCN2, MAP2K6, TGFB2, MAP2K1, BIN1, HES1, UHRF1, ACD, ARRB2, SGK1, PLAUR, CCN1, TIMP3, BIRC3, ALOX15, TMSB4X, ARHGDIB, INPP5F, MLKL, MAP3K21, IGFBP6, NDRG4, IL11, PTPRR, UCHL1, RALBP1, PPP2R1B, SERPINE1, OCLN, TWSG1, DDX58, YES1, MMD, PPIL4, PPP1R16A, FBXO2, POM121, CLDN4, USP14, ATP1B3, MTCL1, PCOLCE2, RGS7, RP2, MMP15, CYB5B, NCF2, SERPINB7, WFDC2
Regulation of Organization	GO_REGULATION_OF_ORGANELLE_ORGANIZATION GO_REGULATION_OF_TRANSPORT GO_CYTOSKELETON_ORGANIZATION GO_CHROMOSOME_ORGANIZATION	CDC6, CCNE1, MCM2, POLE3, POLE2, MCM6, MCM3, DSCC1, GADD45A, DUSP1, SFN, E2F1, PSMG2, NDC80, BMP4, HSPA1A, HSPA1B, TGFA, GNAI1, CEP85, CHMP1B, SEH1L, DSN1, CENPK, NAA50, SBDS, RFC2, CCN2, MAP2K6, TGFB2, MAP2K1, BIN1, RASSF1, SLC16A1, CENPQ, CETN3, SKA1, TUBB6, UHRF1, EPB41L2, RECQL4, METTL4, EYA4, ACD, SMCHD1, ARRB2, CHRAC1, SGK1, BAZ1B, PLAUR, ADA, ALOX15, IQCJ-SCHIP1, TMSB4X, ARHGDIB, INPP5F, NDRG4, IL11, WLS, SERPINE1, PCSK9, SLC25A4, NUAK2, SRGN, OCLN, LCP1, NAV3, FHOD1, KATNBL1, DDX58, YES1, ATP1B3, RIPOR1, LOXL2, MTCL1, GJA5, RAB12, RHBDF2, CACNG6, CLIC3, NETO2, SMTN, INA
Metabolism	GO_DNA_METABOLIC_PROCESS GO_REGULATION_OF_PHOSPHORUS_METABOLIC_PROCESS GO_DNA_BIOSYNTHETIC_PROCESS GO_POSITIVE_REGULATION_OF_PROTEIN_METABOLIC_PROCESS GO_NUCLEOSIDE_PHOSPHATE_BIOSYNTHETIC_PROCESS	CDC6, CCNE1, TIPIN, MCM2, POLE3, POLE2, MCM6, MCM3, MCM10, ORC6, GINS1, DSCC1, CLSPN, RRM2, GADD45A, CDKN2D, DUSP1, TYMS, SFN, BMP4, HSPA1A, HSPA1B, TGFA, CEP85, SEH1L, RFC2, RMI1, CCN2, MAP2K6, TGFB2, MAP2K1, HES1, THOC1, UHRF1, SAMHD1, RECQL4, METTL4, CGAS, EYA4, UNG, ACD, SMCHD1, ARRB2, GLRX2, CHRAC1, EXOSC4, PLAUR, CCN1, TIMP3, BIRC3, ADA, C1QBP, ALOX15, TMSB4X, INPP5F, MLKL, MAP3K21, IGFBP6, NDRG4, IL11, PTPRR, UCHL1, PPP2R1B, CTSC, PCSK9, OCLN, TWSG1, YES1, MMD, PPIL4, PPP1R16A, POM121, CLDN4, PCOLCE2, EIF5A2, NSUN5, PAPSS2, PNP, CYC1, SCD5, CTPS1, SLC26A2, UPP1, PAICS
Cell Cycle/ Proliferation	GO_CELL_CYCLE GO_DNA_REPLICATION GO_DNA_METABOLIC_PROCESS GO_REGULATION_OF_CELL_POPULATION_PROLIFERATION	CDC6, CCNE1, TIPIN, MCM2, POLE3, POLE2, MCM6, MCM3, MCM10, ORC6, GINS1, DSCC1, E2F8, GMNN, CLSPN, RRM2, GADD45A, CDKN2D, DUSP1, TYMS, SFN, E2F1, PSMG2, NAE1, NDC80, CEP78, BCAT1, BMP4, HSPA1A, HSPA1B, TGFA, GNAI1, CEP85, CHMP1B, SEH1L, DSN1, CENPK, NAA50, SBDS, RFC2, RMI1, CCN2, MAP2K6, TGFB2, MAP2K1, BIN1, APBB2, RASSF1, SLC16A1, CENPQ, CETN3, HES1, SKA1, TUBB6, THOC1, ID3, UHRF1, WDR76, MRPL41, EPB41L2, SAMHD1, RECQL4, METTL4, FAM111B, CGAS, EYA4, UNG, ACD, SMCHD1, ARRB2, GLRX2, CHRAC1, EXOSC4, SGK1
Apoptosis	GO_APOPTOTIC_PROCESS GO_REGULATION_OF_CELL_DEATH	MCM2, GADD45A, CDKN2D, DUSP1, SFN, E2F1, PSMG2, NAE1, BMP4, HSPA1A, HSPA1B, CCN2, MAP2K6, TGFB2, BIN1, APBB2, THOC1, ID3, MRPL41, EYA4, UNG, ARRB2, GLRX2, SGK1, PLAUR, CCN1, TIMP3, BIRC3, ADA, C1QBP, ANKRD2, PPP2R1B, CTSC, SERPINE1, MITF, PCSK9, SLC25A4, ANXA5, NUAK2, TNFSF9, SRGN, CDCA7
Cell Motility	GO_CELL_MOTILITY GO_RESPONSE_TO_WOUNDING	GADD45A, DUSP1, BMP4, SBDS, CCN2, TGFB2, MAP2K1, APBB2, SLC16A1, HES1, ID3, ARRB2, SGK1, PLAUR, CCN1, ADA, C1QBP, ALOX15, TMSB4X, ARHGDIB, INPP5F, IGFBP6, NDRG4, PTPRR, SERPINE1, MITF, ANXA5, OCLN, LCP1, NAV3, DDX58, FGFBP1, SLC1A3, YES1, CLDN4, MACIR, ATP1B3, RIPOR1, LOXL2, OLR1, ARTN, IGSF8, S100A2, PROCR, PAPSS2, MYL12A
Signaling	GO_REGULATION_OF_INTRACELLULAR_SIGNAL_TRANSDUCTION GO_POSITIVE_REGULATION_OF_SIGNALING	GADD45A, CDKN2D, DUSP1, SFN, E2F1, BMP4, HSPA1A, HSPA1B, TGFA, GNAI1, SEH1L, RFC2, RMI1, CCN2, MAP2K6, TGFB2, MAP2K1, HES1, CGAS, ARRB2, PLAUR, CCN1, TIMP3, BIRC3, ADA, C1QBP, ANKRD2, ALOX15, IQCJ-SCHIP1, TMSB4X, ARHGDIB, INPP5F, MLKL, MAP3K21, IGFBP6, NDRG4, IL11, WLS, VAPA, S100A4, PTPRR, UCHL1, RALBP1, TAF13, PPP2R1B, CTSC, TWSG1, DDX58, FGFBP1, SLC1A3, CALB2
Other Functions	GO_REGULATION_OF_RESPONSE_TO_STRESS GO_SECRETION	GADD45A, CDKN2D, DUSP1, HSPA1A, HSPA1B, SEH1L, DSN1, CCN2, MAP2K6, TGFB2, MAP2K1, SLC16A1, THOC1, WDR76, SAMHD1, CGAS, EYA4, SMCHD1, ARRB2, SGK1, PLAUR, TIMP3, BIRC3, ADA, C1QBP, ALOX15, TMSB4X, INPP5F, MLKL, MAP3K21, IL11, WLS, VAPA, CTSC, SERPINE1, SLC25A4, ANXA5, SRGN, OCLN, DDX58, SLC1A3, POM121, CLDN4, MACIR, USP14, EFHD1, OLR1, GJA5, RAB12, RHBDF2, PNPSNX10, STX2, SLC2A3, TVP23B

Table 4. GO_CC analysis of shPSAT1-down-regulated genes

Cellular Component	GO_CC terms	Genes
Nucleus	GO_CHROMOSOMAL_REGION GO_REPLICATION_FORK GO_ORIGIN_RECOGNITION_COMPLEX GO_CHROMOSOME_CENTROMERIC_REGION GO_CHROMOSOME_TELOMERIC_REGION GO_KINETOCHORE GO_NUCLEAR_BODY GO_CHROMATIN	E2F1, HSPA1A, HSPA1B, MCM3, NDC80, DSN1, MCM2, SKA1, RP2, CYC1, SGK1, SEH1L, BAZ1B, CENPK, MCM6, THOC1, ACD, SMCHD1, CENPQ, DSCC1, RECQL4, POLE2, POLE3, CHRAC1, TIPIN, MCM10, UHRF1, BHLHE40, E2F8, NFATC3, ZNF114, MITF, ZNF331, ZNF83, TGIF1, ORC6, RFC2, LOXL2, CLIC3, ANKRD2, GADD45A, RMI1, EXOSC4, WDR76, HMGN4, FAM111B
Microtubule	GO_MICROTUBULE_CYTOSKELETON GO_MICROTUBULE_ORGANIZING_CENTER GO_SPINDLE_POLE	E2F1, HSPA1A, HSPA1B, MAP2K1, MCM3, NDC80, DSN1, MCM2, SKA1, CETN3, CTSC, SLC16A1, SNX10, GNAI1, CEP85, PROCR, CCNE1, CEP78, HSPB11, RP2, RASSF1, YES1, SMTN, VAPA, NAV3, MTCL1, KATNBL1, SBDS, CDC6, GRAMD2B, TUBB6
Vesicle	GO_SECRETORY_VESICLE GO_SECRETORY_GRANULE GO_VESICLE_LUMEN GO_VACUOLE	HSPA1A, HSPA1B, DSN1, CTSC, SNX10, GNAI1, VAPA, NAPG, SEH1L, BIN1, TGFB2, SERPINE1, TIMP3, PLAUR, OCLN, STX2, RAB12, SLC2A3, OLR1, PCSK9, AP1M2, MMD, SRGN, TMSB4X, PNP, NCF2, ADA
Endoplasmic Reticulum	GO_ENDOPLASMIC_RETICULUM_LUMEN GO_NUCLEAR_OUTER_MEMBRANE_ENDOPLASMIC_RETICULUM_MEMBRANE_NETWORK	CTSC, VAPA, NAV3, NDRG4, PCSK9, FSTL1, ERP27, BMP4, SGK1, POM121, EIF5A2, COL4A6, COL15A1, CCN1, PLAUR, TGFA, WLS, GDPD3, TBL2, FADS2, UCHL1, AADAC, CYP26A1, RHBDF2, SCD5, LPIN2
Mitochondria	GO_MITOCHONDRION GO_MITOCHONDRIAL_ENVELOPE	E2F1, HSPA1A, HSPA1B, MAP2K1, CISD1, BRI3BP, MTERF3, CYB5B, CYC1, NDUFV2, AFG3L2, GRPEL2, MRPL41, TYMS, SLC25A4, SLC25A10, EFHD1, PRELID3A, COA6, NDRG4, NAPG, SGK1, C1QBP, GLRX2, ALDH1B1, HIBCH, LACTB2, METTL4, FAM210A, SFN, ENOSF1, PTS, BCAT1, UNG, MTRF1
Membrane	GO_PLASMA_MEMBRANE_REGION GO_WHOLE_MEMBRANE GO_MEMBRANE_PROTEIN_COMPLEX GO_SUPRAMOLECULAR_COMPLEX	NDC80, DSN1, SKA1, SLC16A1, SNX10, GNAI1, PROCR, RP2, RASSF1, YES1, SMTN, VAPA, NAV3, MTCL1, KATNBL1, GRAMD2B, TUBB6, CISD1, BRI3BP, MTERF3, CYB5B, CYC1, NDUFV2, AFG3L2, GRPEL2, NDRG4, NAPG, C1QBP, SEH1L, CENPK, CENPQ, BIN1, SPAG4, GJA5, ADA, CLIC3, ANKRD2, GNG11, ITGAE, CACNG6, INA, KRT23, USP14, CLEC2B, SLITRK6, ALPP, LY6D, ANXA5, COL4A6, PLAUR, OCLN, TGFA, ATP1B3, WLS, INPP5F, SLC39A4, STX2, LCP1, CALB2, DDX58, CLDN4, SLC1A3, CHRNB1, ARRB2, FCHO1, SLC26A2, RAB12, SLC2A3, OLR1, PCSK9, AP1M2, CHMP1B, PPP2R1B, MMD, SPG21, BIRC3, NCF2, MYL12B, MYH15,FGFBP1
Actin Cytoskeleton	GO_ACTIN_CYTOSKELETON	YES1, SMTN, CENPQ, BIN1, LCP1, CALB2, DDX58, EPB41L2, FHOD1, MYL12B, MYH15, MYL12A
Anchoring Junction	GO_ANCHORING_JUNCTION	HSPA1A, HSPA1B, MAP2K1, PROCR, YES1, VAPA, ANXA5, PLAUR, OCLN, LCP1, CALB2, DDX58, CLDN4, EPB41L2, FHOD1, GJA5
Extracellular Space	GO_COLLAGEN_CONTAINING_EXTRACELLULAR_MATRIX GO_EXTRACELLULAR_MATRIX	CTSC, TGFB2, SERPINE1, TIMP3, ANXA5, COL4A6, COL15A1, CCN1, CCN2, S100A4, LOXL2, MGP, MMP15

**Table 5.** GO_BP analysis of shPSAT1-up-regulated genes

Biological Function	GO_BP terms	Genes
Motility	GO_CELL_MOTILITY GO_LEUKOCYTE_MIGRATION GO_CELL_CHEMOTAXIS GO_CELL_PROJECTION_ORGANIZATION GO_MYELOID_LEUKOCYTE_MIGRATION	EGFR, APP, RAC1, S100A9, HDAC9, PDGFA, ALOX5, TNFRSF11A, GLUL, CSF1R, SMAD3, EFNB2, FOLR1, CCL20, CXCL1, B4GALT1, SDC4, ADGRE2, STC1, GBF1, CLDN1, JAG1, TRIB1, ATP2B4, EPS8, HBEGF, TNS3, RIN2, ITGB8, SPOCK1, MEGF9, PLA2G7, DEFB1, SRGAP1, ARID5B, LRP12, TNC, AREG, ROR1, LCN2, BTG2, SPTBN1, KIDINS220, KLK6, FSTL4, MYLIP, DDX56, FGD4, NUDCD3
Immune Response	GO_CELL_ACTIVATION GO_CELL_ACTIVATION_INVOLVED_IN_IMMUNE_RESPONSE GO_BIOLOGICAL_ADHESION GO_INFLAMMATORY_RESPONSE GO_MYELOID_LEUKOCYTE_MEDIATED_IMMUNITY GO_IMMUNE_EFFECTOR_PROCESS GO_LEUKOCYTE_CHEMOTAXIS GO_DEFENSE_RESPONSE	EGFR, APP, RAC1, S100A9, HDAC9, PDGFA, ALOX5, TNFRSF11A, CSF1R, SMAD3, EFNB2, FOLR1, CCL20, CXCL1, B4GALT1, SDC4, ADGRE2, STC1, GBF1, CLDN1, JAG1, HBEGF, RIN2, ITGB8, SPOCK1, MEGF9, PLA2G7, DEFB1, LRP12, C3, TLR1, ABCA1, IGFBP2, TNC, AREG, GJB2, CACNG4, CALCOCO1, PCDH1, GPRC5B, AOC1, LCN2, FTH1, CDK13, CD22, CFD, QPCT, TCN1, TMEM179B, AGR2, AHR, VTCN1, LFNG, TXNIP, CTSV, FBXO32, NEAT1, CREBRF, PMEPA1, DSC2, TJP2, PI3, RAMP1, LYPD3, SPTBN1, SNX18, HLA-DQB1, CFB, TPCN2, BPIFB1, GBP2, TMPRSS4, ATP9A
Response to Exogenous signals	GO_RESPONSE_TO_OXYGEN_CONTAINING_COMPOUND GO_RESPONSE_TO_ORGANIC_CYCLIC_COMPOUND GO_RESPONSE_TO_LIPID GO_RESPONSE_TO_ENDOGENOUS_STIMULUS GO_RESPONSE_TO_CORTICOSTEROID GO_RESPONSE_TO_STEROID_HORMONE GO_RESPONSE_TO_BIOTIC_STIMULUS	EGFR, APP, RAC1, S100A9, HDAC9, TNFRSF11A, GLUL, CSF1R, SMAD3, FOLR1, CCL20, CXCL1, STC1, GBF1, CLDN1, JAG1, TRIB1, ATP2B4, EPS8, DEFB1, C3, TLR1, ABCA1, ANO1, IGFBP2, TNC, AREG, GJB2, CACNG4, EIF4EBP2, CALCOCO1, LATS2, AOC1, LCN2, CFD, AHR, VTCN1, TXNIP, BTG2, CTSV, FBXO32, DGAT2, CREBRF, PMEPA1, EPG5, PI3, RAMP1, KIDINS220, HLA-DQB1, CFB, BPIFB1, GBP2, LSM5
Cell Signaling	GO_CELL_CELL_SIGNALING GO_RESPONSE_TO_ENDOGENOUS_STIMULUS GO_POSITIVE_REGULATION_OF_SIGNALING GO_ENZYME_LINKED_RECEPTOR_PROTEIN_SIGNALING_PATHWAY GO_REGULATION_OF_INTRACELLULAR_SIGNAL_TRANSDUCTION GO_TRANSMEMBRANE_RECEPTOR_PROTEIN_TYROSINE_KINASE_SIGNALING_PATHWAY GO_EPIDERMAL_GROWTH_FACTOR_RECEPTOR_SIGNALING_PATHWAY	EGFR, APP, RAC1, S100A9, HDAC9, PDGFA, ALOX5, TNFRSF11A, GLUL, CSF1R, SMAD3, EFNB2, FOLR1, CCL20, STC1, GBF1, CLDN1, JAG1, TRIB1, ATP2B4, EPS8, HBEGF, SRGAP1, ARID5B, C3, TLR1, ABCA1, PER2, IGFBP2, TNC, AREG, GJB2, CACNG4, EIF4EBP2, CALCOCO1, ROR1, SCEL, PCDH1, GPRC5B, LATS2, SYNPO, TCF7L1, GABBR2, AOC1, CD22, AGR2, AHR, LFNG, TXNIP, BTG2, CTSV, FBXO32, CREBRF, PMEPA1, RAMP1, SPTBN1, KIDINS220, MAP3K1, GPRC5A, ARHGAP23, KLK6, FSTL4, BMF, SOS2, FGD4, FAM83A, DEPTOR, PIK3IP1
Molecular Function	GO_SECRETION GO_POSITIVE_REGULATION_OF_MOLECULAR_FUNCTION GO_EXOCYTOSIS GO_REGULATION_OF_TRANSPORT GO_REGULATION_OF_CELLULAR_COMPONENT_MOVEMENT GO_POSITIVE_REGULATION_OF_CATALYTIC_ACTIVITY GO_REGULATION_OF_PROTEIN_KINASE_ACTIVITY GO_POSITIVE_REGULATION_OF_PROTEIN_METABOLIC_PROCESS GO_REGULATION_OF_TRANSFERASE_ACTIVITY GO_LIPID_METABOLIC_PROCESS GO_ENDOCYTOSIS GO_REGULATION_OF_PROTEIN_MODIFICATION_PROCESS	EGFR, APP, RAC1, S100A9, HDAC9, PDGFA, ALOX5, TNFRSF11A, GLUL, CSF1R, SMAD3, EFNB2, FOLR1, CCL20, CXCL1, B4GALT1, SDC4, ADGRE2, STC1, CLDN1, JAG1, TRIB1, ATP2B4, HBEGF, RIN2, ITGB8, PLA2G7, DEFB1, SRGAP1, ARID5B, LRP12, C3, TLR1, ABCA1, ANO1, PER2, AREG, CACNG4, ROR1, GPRC5B, LATS2, AOC1, LCN2, FTH1, CDK13, CD22, CFD, QPCT, TCN1, TMEM179B, AGR2, TNFAIP2, LFNG, DGAT2, SGPP2, PMEPA1, DSC2, LIPK, RAMP1, KIDINS220, MAP3K1, GPRC5A, ARHGAP23, SNX18, SNX13, DCP1B, H1-0, MYLIP, CREBL2, TPCN2, TOMM7, ICE1, EEPD1, SLC43A2, TSPAN13, DEPTOR, CCNL2, KPNA7, STX5, PIK3IP1, MTMR1, RBP1, AKR1B15, CYP4V2, ALDH3B2, THNSL2, STARD3NL, TMPRSS4, ATP9A, WDR70
Development	GO_EPITHELIUM_DEVELOPMENT GO_TUBE_MORPHOGENESIS GO_NEUROGENESIS	EGFR, APP, RAC1, S100A9, HDAC9, PDGFA, ALOX5, GLUL, CSF1R, SMAD3, EFNB2, FOLR1, B4GALT1, SDC4, STC1, CLDN1, JAG1, ATP2B4, HBEGF, TNS3, RIN2, ITGB8, SPOCK1, LRP12, C3, PER2, TNC, AREG, GJB2, ROR1, SCEL, GPRC5B, AGR2, TNFAIP2, LFNG, TXNIP, BTG2, CTSV, DSC2, TJP2, PI3, LIPK, KRT6B, RAMP1, SPTBN1, KIDINS220, KLK6, FSTL4, MYLIP, DDX56
Proliferation	GO_REGULATION_OF_CELL_POPULATION_PROLIFERATION	EGFR, APP, PDGFA, ALOX5, TNFRSF11A, GLUL, CSF1R, SMAD3, EFNB2, CXCL1, B4GALT1, SDC4, CLDN1, JAG1, TRIB1, HBEGF, TNS3, PER2, IGFBP2, TNC, AREG, FTH1, CDK13, CD22, AHR, VTCN1, TXNIP, BTG2, NEAT1, SGPP2, H2AC6

Table 6. GO_CC analysis of shPSAT1-up-regulated genes

Cellular Localization	GO_CC terms	Genes
Cell Membrane	GO_INTRINSIC_COMPONENT_OF_PLASMA_MEMBRANE GO_CELL_SURFACE GO_RECEPTOR_COMPLEX GO_WHOLE_MEMBRANE GO_PLASMA_MEMBRANE_REGION GO_APICAL_PART_OF_CELL GO_APICAL_PLASMA_MEMBRANE GO_G_PROTEIN_COUPLED_RECEPTOR_COMPLEX	APP, EGFR, SDC4, FOLR1, ABCA1, TLR1, CACNG4, ITGB8, RAMP1, ROR1, CSF1R, HBEGF, CD22, GABBR2, EPS8, GPRC5A, ANO1, ATP2B4, CLDN1, JAG1, EFNB2, GJB2, PCDH1, SLC28A3, ADGRE2, LRP12, RCE1, LYPD3, EEPD1, OPN3, TSPAN13, CD82, TM4SF1, PDGFA, B4GALT1, RAC1, C3, CTSV, TMEM179B, BMF, AREG, STX5, HLA-DQB1, PMEPA1, SLC29A3, ATP9A, GPRC5B, VTCN1, TNFRSF11A, SMAD3, AHR, SNX18, STARD3NL, TPCN2, SNX13, PEX6, TOMM7, SLC4A11, IGFBP2, STC1, SPTBN1
Junction/Projection	GO_ANCHORING_JUNCTION GO_ACTIN_BASED_CELL_PROJECTION GO_GLIAL_CELL_PROJECTION	APP, EGFR, SDC4, ITGB8, EPS8, CLDN1, JAG1, EFNB2, GJB2, PCDH1, PDGFA, B4GALT1, RAC1, CTSV, AOC1, FGD4, DSC2, SYNPO, TJP2, TNC, TNS3, GLUL
Golgi/Secretion	GO_GOLGI_APPARATUS GO_SECRETORY_VESICLE GO_VESICLE_LUMEN GO_GOLGI_MEMBRANE GO_VESICLE_MEMBRANE GO_ENDOPLASMIC_RETICULUM_GOLGI_INTERMEDIATE_COMPARTMENT GO_ENDOSOME GO_FICOLIN_1_RICH_GRANULE GO_VACUOLE GO_SPECIFIC_GRANULE	APP, EGFR, SDC4, FOLR1, ABCA1, TLR1, CACNG4, HBEGF, CD22, GPRC5A, GJB2, PDGFA, B4GALT1, RAC1, CDK13, C3, CTSV, AOC1, QPCT, CXCL1, TCN1, LCN2, ALOX5, CFD, S100A9, TMEM179B, BMF, FTH1, KLK6, FSTL4, TMPRSS4, AREG, STX5, HLA-DQB1, PMEPA1, SLC29A3, ATP9A, GBF1, MAN1A1, GBP2, LFNG, CHST12, HS6ST2, FGD4, DEFB1, RETREG1, H1-0, SLC39A11, CAPN8, GPRC5B, SNX18, STARD3NL, TPCN2, SNX13, SLC4A11, KIDINS220
Others	GO_NUCLEAR_ENVELOPE_LUMEN GO_LIPID_DROPLET GO_PERINUCLEAR_REGION_OF_CYTOPLASM GO_CORNIFIED_ENVELOPE	APP, EGFR, ABCA1, GJB2, ALOX5, ATP9A, GBF1, GBP2, DSC2, EPG5, DGAT2, ALDH3B2, RBP1, SCEL, PER2, PI3

The serine synthetic pathway provides precursors for anabolic pathways such as nucleotide and lipid biosynthesis to promote tumor growth (Fig. 31A)(16, 28). As mentioned above, KEGG pathway analysis confirmed the decreased SSP activity upon PSAT1 silencing. Accordingly, GO analysis with down-regulated genes implicated genes involved in maintaining chromatin structure, participating in DNA metabolism, and influencing cell proliferation (Tables 3 & 4). As a result, we speculated that the metabolic activity of PSAT1 contributes to the oncogenic capacity of EGFR-mutant NSCLC cells. For this, we performed soft agar assays with or without supplementation of SSP-downstream metabolites, including non-essential amino acids (NEAA), nucleosides, and α-ketoglutarate (α-KG). We observed that depletion of PSAT1 resulted in a 40% reduction in colony formation in comparison with control cells (Fig. 31B). The addition of down-stream metabolites alone did not affect the ratio of colony number (shPSAT1/Control). However, the combination of any metabolite(s) with nucleosides significantly increased the ratio of colony number in comparison with media without supplementation. To further understand the putative metabolic role, soft agar assays were repeated with the genetic rescue of PSAT1 or expression of nuclear acetyl-mimetic PKM2 in PC9 cells, as was done in Chapter 2. Restoration of PSAT1 (Fig. 31D), but not PKM2$^{NLS-K433Q}$ (Fig. 31C), recapitulated the phenotype of control cells. Taken together, these results are consistent with the RNA sequencing analysis and implicate the metabolic function of PSAT1 contributes to anchorage-independent growth.

Next, we investigated the contribution of PSAT1-downstream metabolites on cell migration. A wound-healing assay was performed in the presence or absence of all metabolites (NEAA+ nucleoside + α-KG). Unlike the soft agar assays, we found that the addition of metabolites did not rescue the loss of PSAT1 mediated migration deficiency (Fig. 32). This supports our previous findings that a putative novel non-canonical function of PSAT1, including facilitation of nuclear PKM2 localization, contributes to cell migration.
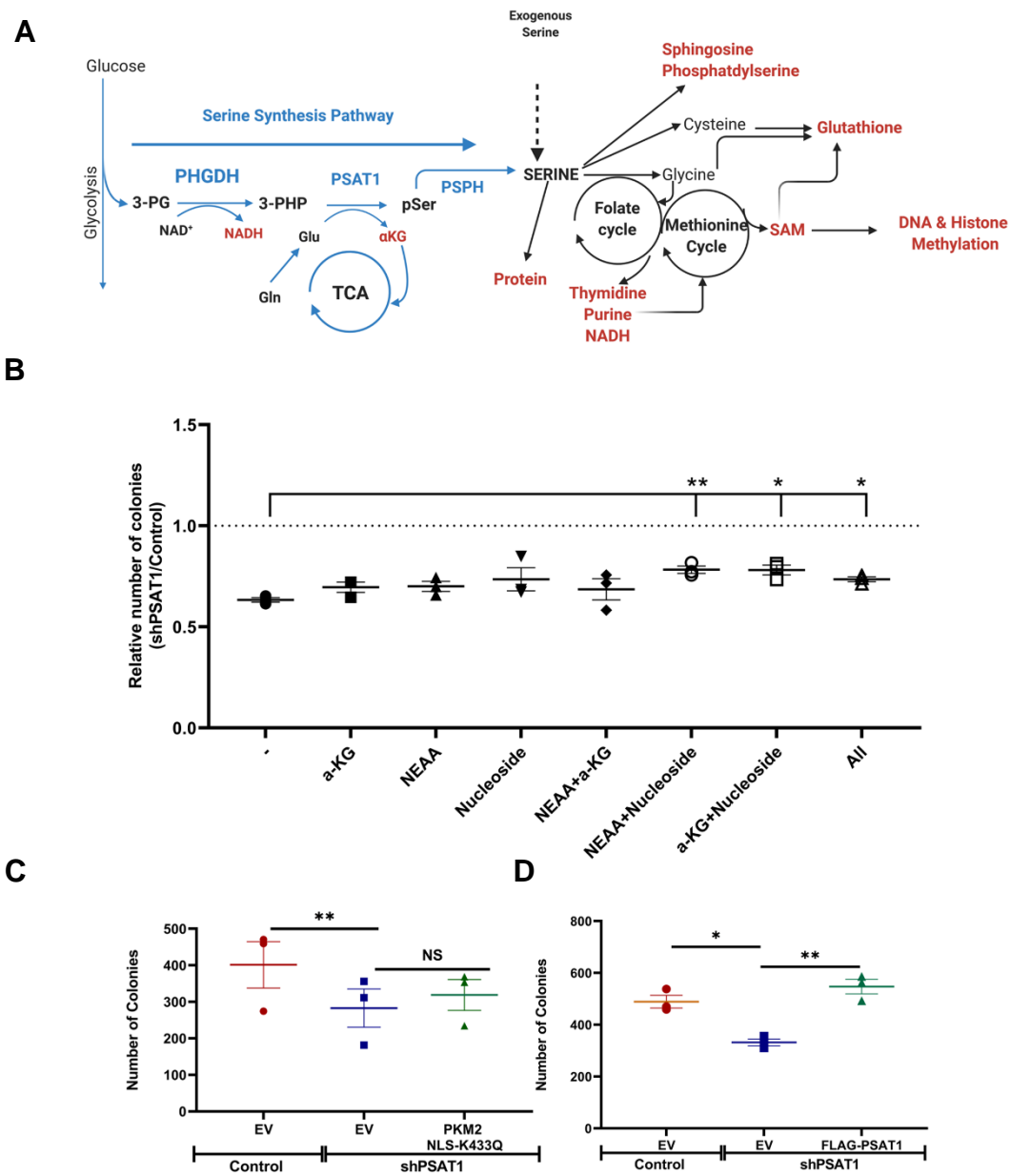
Figure 31. The metabolic activity of PSAT1 contributes to anchorage-independent growth. A) Serine synthetic pathway. **(B-D)** Soft agar assays analysis for **B)** metabolite supplementation, **C)** nuclear PKM2 restoration, and **D)** PSAT1 restoration. N=3, *, $p \leq 0.05$ and **, $p \leq 0.01$. EV: empty vector and NS: Not significant.

A

B
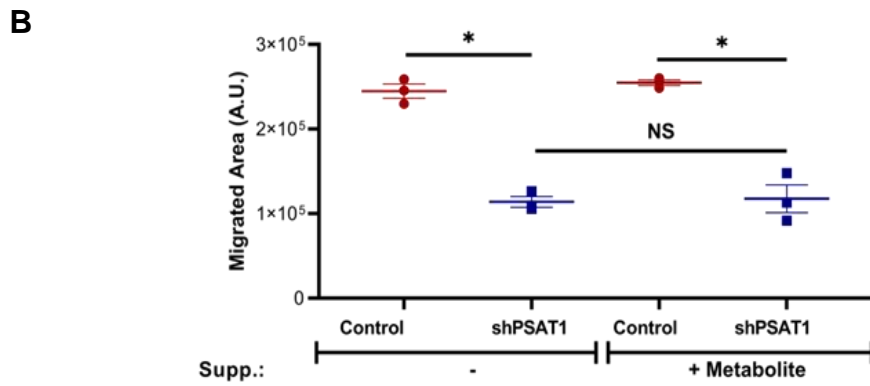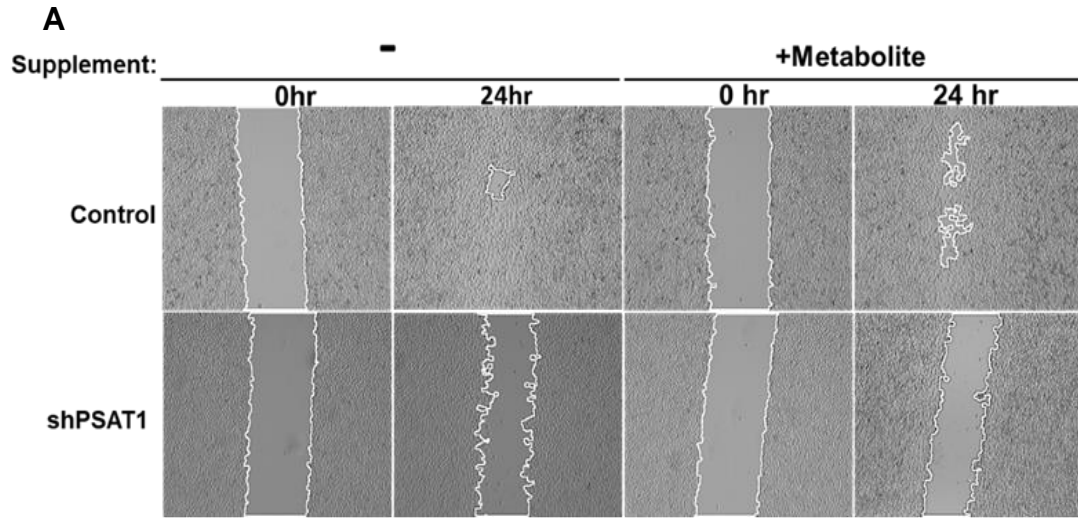
Figure 32. The addition of downstream metabolites fails to induce cell migration in PSAT1 silenced cells. A) Representative images of wound-healing assay. **B)** Quantification of migration. N=3, *, $p \leq 0.0001$, NS: not significant, and A.U,: arbitrary unit.

Validation of PSAT1 mediated gene changes in EGFR-mutant NSCLC cells

Our KEGG pathway analysis described above found significantly altered cell cycle process in the absence of PSAT1 (Fig. 30). To explore genes involved in the RB/E2F pathway's functional role in regulating the cell cycle, we utilized the DEG list from our RNA-seq studies and performed gene set analysis using the MSigDB CGP (chemical and genetic perturbations) tool that harbors curated gene lists from other genome-wide gene expression studies and transcription factor analysis by WebGestalt 2013 (167, 168). The results for the gene set analysis were presented in Figure 33A. We found a high number of downregulated genes that significantly overlapped with genes within "FISCHER_ G1/S_CELL _CYCLE" (30 genes, p= 2.6e-31, FDR= 7.82 e-28) and "CHICAS_RB1_TARGETS_SENESCENT" (37 genes, p= 2.85e-25, FDR= 1.37e-22) that function in RB/E2F pathway. Furthermore, nineteen of the down-regulated genes possessed E2F binding sites within their promoter regions. Expression values of E2F family members and RB1 were extracted from our RNA-seq data and plotted to determine any changes at the transcriptional level. As shown in Figure 33B, E2F1 and E2F8 were significantly downregulated in PSAT1 silenced cells. Taken together, our analysis corroborates previous reports that PSAT1 contributes, in part, to cell cycle progression through modulating the RB/E2F pathway (1).

A

Genes observed in RB-E2F pathway

GSEA-MSIGDB CGP: chemical and genetic perturbations	FISCHER_G1_S_CELL_CYCLE (p= 2.6e-31, FDR=8.72e-28)	• Cell cycle genes with peak expression in G1/S check point • 30 common genes
CHICAS_RB1_TARGETS_SENESCENT (p= 2.85e-25, FDR=1.37e-22)	• Genes up-regulated in senescent IMR90 cells after knockdown of RB1 by RNAi. • 37 common genes
Transcription Factor Analysis (WebGestalt 2013)	• Genes with E2F/E2F1/E2F4 binding site • 19 genes

B

Figure 33. Gene set analysis confirms the link between PSAT1 and RB/E2F mediated cell cycle progression. A) Summary of gene set and transcription factor analyses. **B)** Log transformed FPKM value of E2F family and RB expression. *, q≤0.05; q: Adjusted p-value

***PSAT1 may mediate β-catenin transactivation through regulating protein expression***

EGFR activation promotes the nuclear localization of β-catenin through various mechanisms. While phosphorylation of membranous β-catenin by EGFR or AKT leads to migration of β-catenin away from the membrane, EGFR activation inhibits the proteasomal degradation of cytoplasmic β-catenin protein by GSK3β inactivation. Thus, both EGFR-mediated pathways result in the accumulation of β-catenin in the nucleus (63, 173-175). Nuclear β-catenin is associated with poor overall survival in patients with EGFR mutant lung cancer (174). Although a role for nuclear β-catenin in tumor initiation and cell migration has been shown in EGFR mutant lung cancer models (176, 177), the contribution of nuclear β-catenin activity to the development of EGFR-TKI resistance is of significant interest since EGFR-TKI resistant NSCLC cells developed various mechanisms to promote β-catenin stabilization and activation (176-183). In short, nuclear β-catenin seems to contribute to every step within EGFR-driven tumor progression.

β-catenin is another downstream target of the GSK3β pathway that has previously been examined (43, 79). Reduction in β-catenin level has been observed together with phospho-GSK3β upon PSAT1 silencing, impacting cell cycle and proliferation in ER-negative breast cancer cells and resistance in ovarian cancer cells while inducing apoptosis. However, the connection between β-catenin and PSAT1 remains elusive in EGFR mutant NSCLC cells. Furthermore, nuclear PKM2 requires EGF-induced β-catenin transactivation in EGFR-driven tumor growth of GBM and EGF-induced EMT and invasion in HCC cells (100, 113). Considering these previous reports and our results showing the link between PSAT1 and nuclear PKM2, we speculated that loss of PSAT1 may result in altered β-catenin transactivation.

First, we performed gene set analysis with our PSAT1-mediated DEG list utilizing the MSigDB-CGP tool and transcription factor analysis by WebGestalt 2013. As β-catenin induces transcription via interacting with TCF/LEF1 transcription factor family, genes with LEF1 binding sites were assumed as potential β-catenin targets (162, 164). The summary of our gene comparison analysis was shown in Figure 34A. While overlapping shPSAT1-down-regulated genes within the "FEVR_CTNNB1_TARGETS_DN" gene set suggested a reduction in β-catenin

transactivation in PSAT1 silenced cells, paradoxically, we also found down-regulated genes within the "WANG_RESPONSE_TO_GSK3B_INHBITOR_SB216763_DN" gene set, which indicated a possible activation of β-catenin upon PSAT1 loss. Furthermore, transcription factor analysis found LEF1 promoter binding sites in genes from both down and up-regulated gene lists. In short, these analyses did not provide any clear insight into whether β-catenin transactivation may change upon PSAT1 silencing. Thus, we extracted the expression data of β-catenin (CTNNB1) and TCF(T-cell specific transcription factor) family (TCF7(TCF-1), LEF1, TCF7L2 (TCF-4), TCF7L1(TCF-3)) and compared their transcript levels between control and stable PSAT1 shRNA expressing PC9 cells (162, 173). We did not observe any significant change in the mRNA expression level of β-catenin and TCF/LEF1 transcription factor except TCF7L1 with a 1.47-fold increase in PSAT1 silenced cells (Fig. 34B). As TCF7L1 is a known repressor, this may reduce the β-catenin-TCF/LEF1 target gene expression (173). Overall, our gene set analysis was unable to provide any definitive link between PSAT1 and β-catenin transactivation in our PC9 cell model.

To better understand the connection between PSAT1 and β-catenin, we next assessed whether β-catenin protein expression was altered in the presence or absence of PSAT1. In Figure 35A, immunoblot analysis found that β-catenin expression decreased upon PSAT1 silencing, which can be rescued by re-expression of PSAT1. We then examined whether nuclear PKM2 expression (as assessed by PKM2$^{NLS-K433Q}$) would affect β-catenin expression under PSAT1 silencing. We found no rescue of β-catenin expression with nuclear acetyl-mimetic PKM2, indicating that regulation of β-catenin expression is independent from nuclear PKM2 level in the context of PSAT1 loss (Fig. 35B).
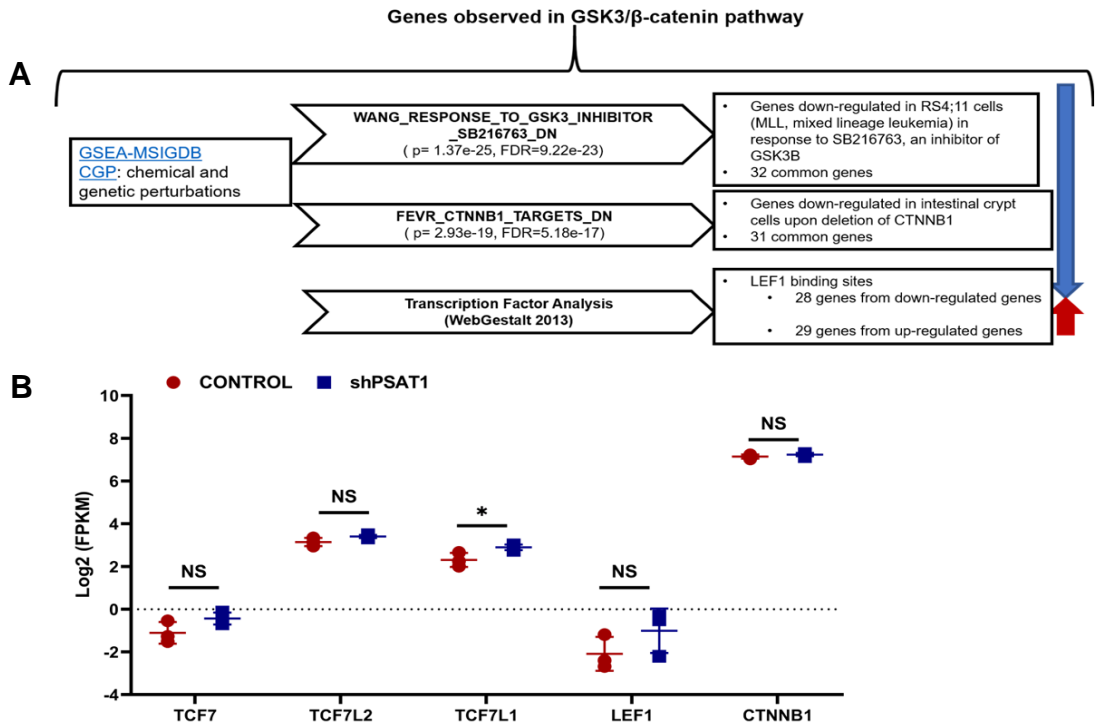
Figure 34. PSAT1 mediated DEG are compared with genes within the GSK3β/β-catenin related pathway. A) Summary of gene set and transcription factor analyses. **B)** Log transformed FPKM value of TCF/LEF1 family and CTNNB1 expression. *, q≤0.05; q: Adjusted p-value.
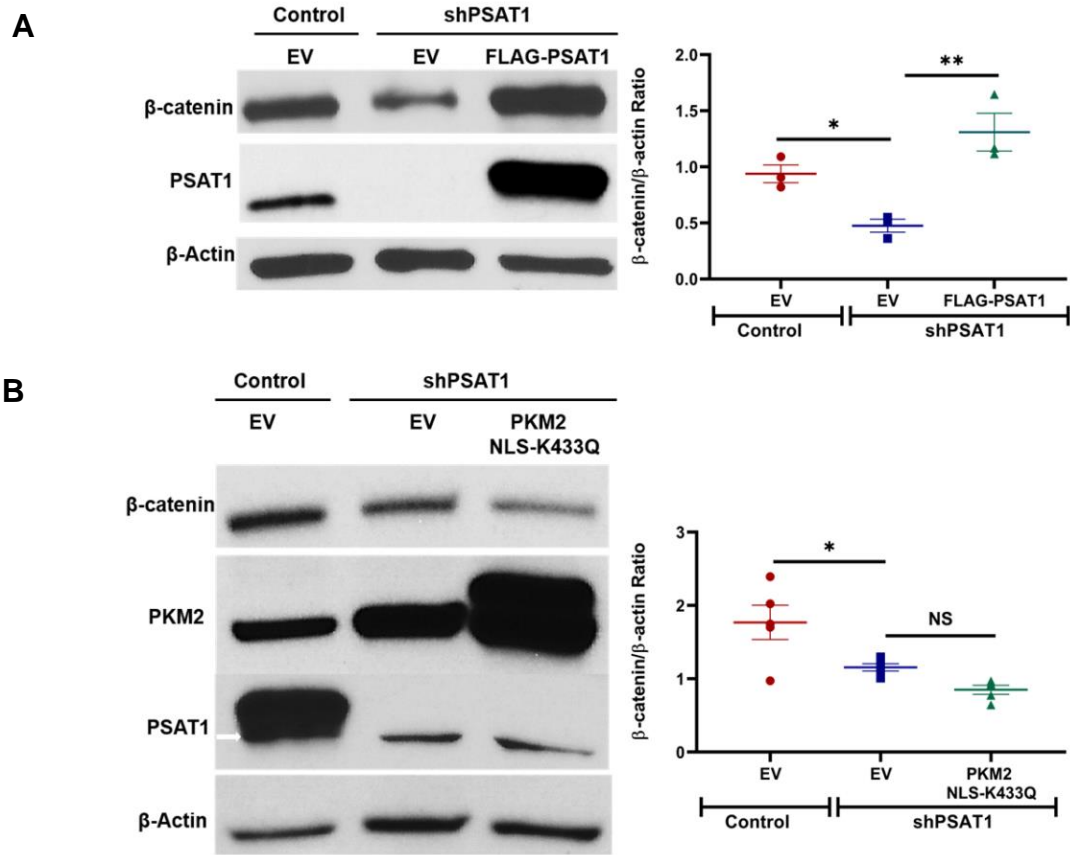
Figure 35. Suppression of PSAT1 reduces β-catenin protein levels. (A-B) Immunoblot analysis of β-catenin expression and quantification in **A)** PSAT1 rescued shPSAT1 PC9 cells (N=3) and **B)** Nuclear PKM2 rescued shPSAT1 PC9 cells (N=5). White arrow: non-specific band. *, $p \leq 0.05$; **, $p \leq 0.01$, and NS: not significant.

Accumulation of cytoplasmic β-catenin due to inhibited proteasomal degradation leads to its nuclear localization and transactivation (83, 175). Since we found a reduction in total β-catenin levels, we next examined its cellular distribution upon PSAT1 silencing. Thus, subcellular fractionation was performed, and the cytoplasmic and nuclear distribution of β-catenin was assessed by immunoblotting. We found that nuclear β-catenin decreased in PSAT1 silenced cells in comparison with control cells, which could be rescued upon re-expression of PSAT1 (Fig. 36A). Yet, we also observed the same pattern of β-catenin expression in the cytoplasmic fraction (SE; short exposure). These results, together with our findings from whole-cell lysates (Fig. 35A) and

mRNA expression profiles (Fig. 34B), imply that PSAT1 contributes to β-catenin stability in PC9 cells, possibly through increasing phospho-GSK3β level.

We then aimed to directly measure β-catenin transcriptional activity with an established luciferase reporter assay system. To achieve this goal, cells were stably transfected with the luc2p/TCF-LEF vector. Cells were maintained in serum-free media for 24 hours in order to directly assess mutant activated EGFR-dependent β-catenin transactivation. Figure 36B demonstrates that loss of PSAT1 significantly decreased luciferase activity compared to control cells, while PSAT1 re-expression completely rescued β-catenin transcriptional activity. Taken together, our findings suggest that PSAT1 affects β-catenin transactivation through regulating its stability.
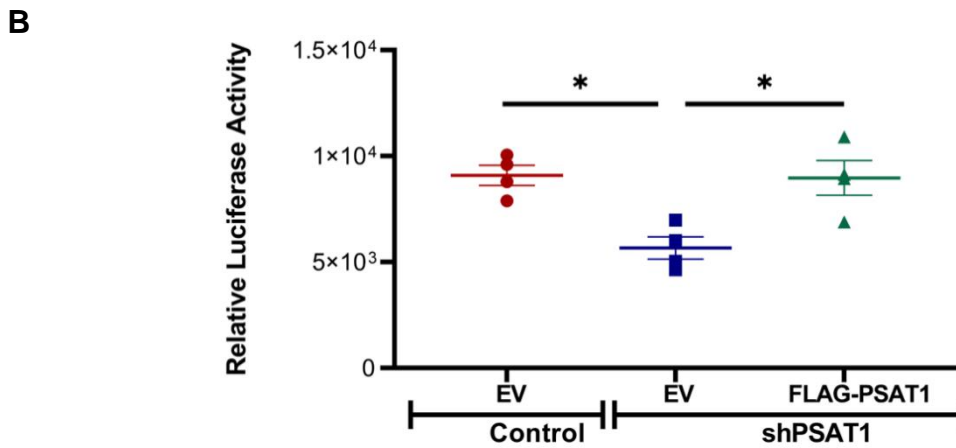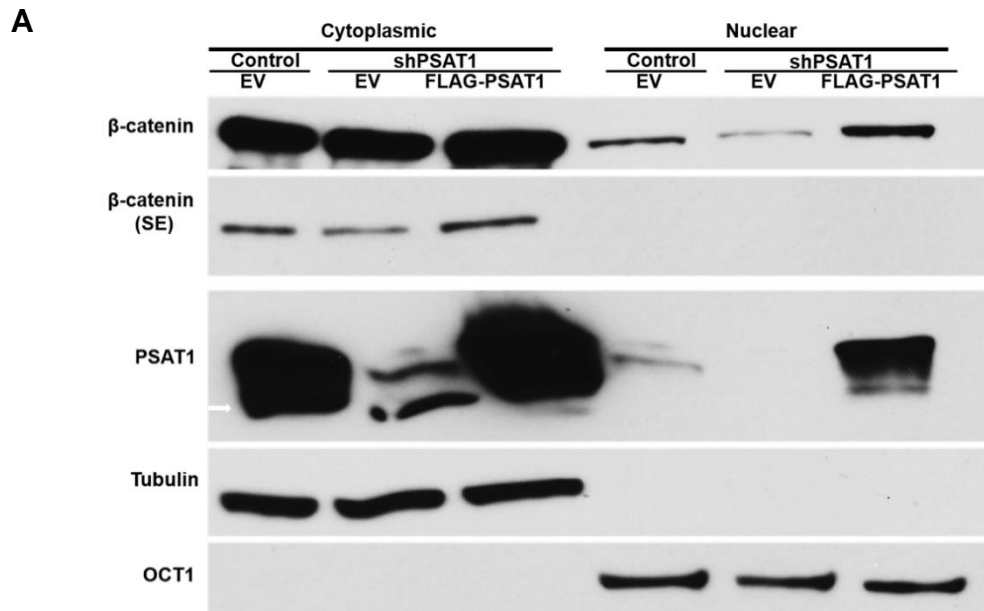
Figure 36. Suppression of PSAT1 reduces β-catenin transactivation. **A)** Immunoblot analysis of cytoplasmic and nuclear β-catenin expression (N=3). **B)** TCF-Luciferase reporter assay for the assessment of β-catenin-TCF transactivation (N=4). *, p≤0.05. White arrow: non-specific band. EV: Empty vector and SE: short exposure

Silencing of PSAT1 impacts the actin cytoskeleton organization via decreasing the expression of actin regulating genes

The actin cytoskeleton not only determines cellular morphology but plays key roles in tumorigenic processes such as migration and invasion due to the requirement for cell movement (184). As our previous results found a requirement for PSAT1 in cell migration, we speculated that loss of PSAT1 may impact the organization of the actin cytoskeleton. To assess this, we used immunofluorescence microscopy with phalloidin staining that is commonly used to visualize actin stress fibers through binding to F-actin (filamentous actin) (185). As shown in Figure 37, confocal microscopy found that control PC9 cells exhibited structured actin fibers spanning the whole cell body, while cells devoid of PSAT1 displayed loss of these actin stress fibers. Yet, re-expression of PSAT1 in silenced cells rescued the long fiber formations, thereby validating PSAT1's on-target effects and confirming a role for PSAT1 in actin cytoskeleton organization.

Next, we further scrutinized our PSAT1-mediated DEG lists to identify genes involved in actin-related processes. Firstly, we extracted gene lists from the MSigDB database stratified under the GO_Actin_ [Binding, Cytoskeleton, Filament Organization] categories and determined overlapping genes with our DEG list. We found 15 genes related to actin cytoskeleton regulation within our shPSAT1-down-regulated gene list (Fig. 38).

Formin Homology 2 Domain Containing 1 (FHOD1) functions as an actin filament capping and bundling protein, unlike other formin members with nucleation and elongation activity (186). It is activated via phosphorylation by the RhoA-ROCK pathway and subsequently promotes stress fiber formation. While depletion of FHOD1 in cells leads to decreased stress fiber formation, thicker actin fibers have been observed in overexpressed cells (187). The gain and loss of function studies have shown differential effects of FHOD1 on cell shape through regulating F-actin bundling (188-190). Co-localization of FHOD1 with F-actin at the cell periphery suggests that FHOD1 enhances cell migration via inducing the formation and stabilization of F-actin at the leading edge. Its role in cancer metastasis is further supported by the observation of elevated expression at the invasive front of squamous cell carcinoma (SCC) (190).

105
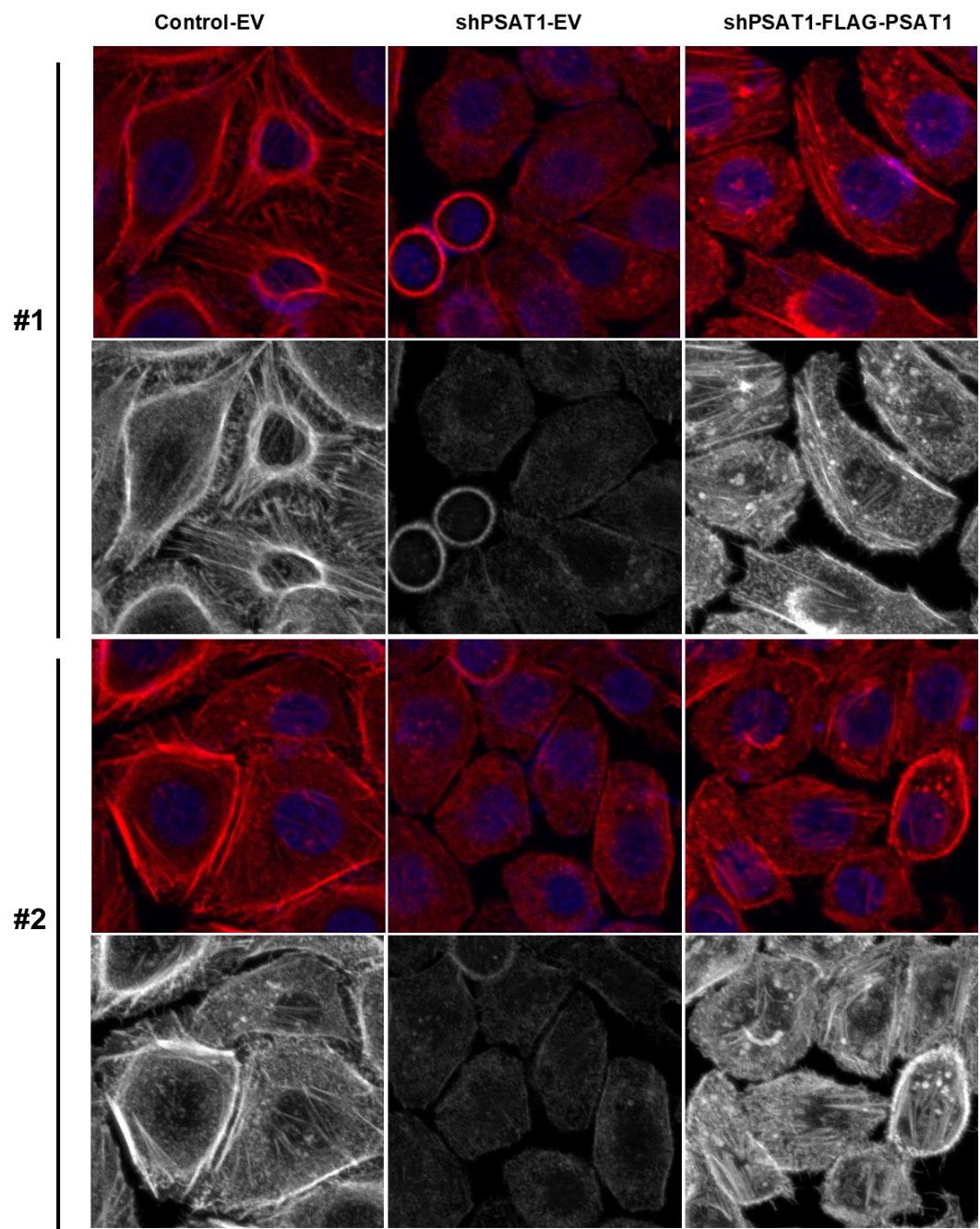
Figure 37. Loss of PSAT1 impacts the actin cytoskeleton. Representative images from two different experiments. Phalloidin staining for F-actin visualization: Real (red) and pseudo-colored (gray) images. DAPI served (blue) served as nuclear staining.
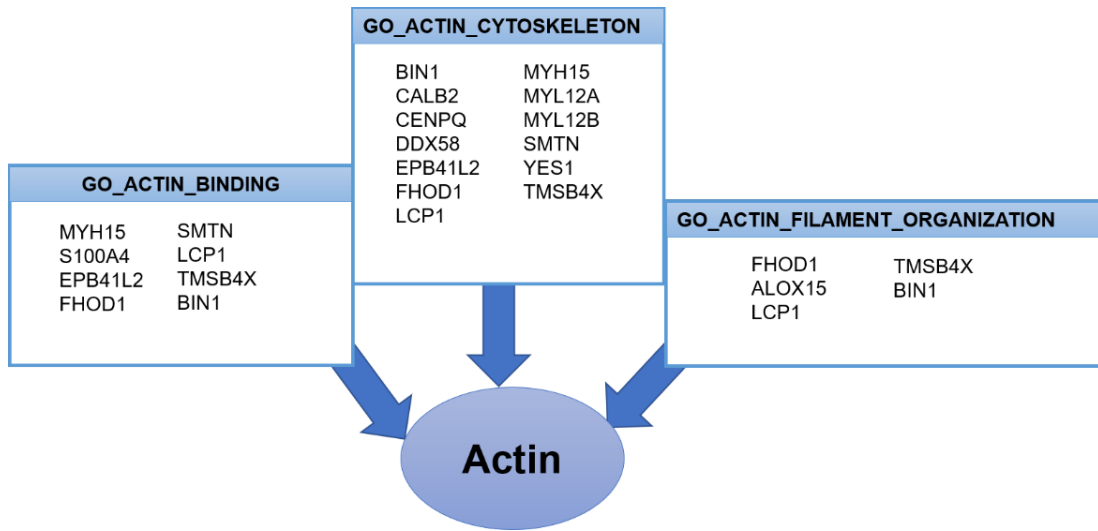
Figure 38. shPSAT1-down-regulated genes involved in actin-related biological functions.

TMSB4X encodes a small peptide that is known as thymosin β4 (Tβ4). Its expression has been linked to aggressive tumorigenic phenotypes such as increased angiogenesis, cell migration, and metastasis (191)**.** Thymosin β4 is recognized as a G-actin sequestering factor that inhibits spontaneous actin polymerization (192). It contributes to cell motility via localizing the monomeric G-actin at the leading edge of lamellipodia for actin polymerization, leading to the formation of membrane protrusions (193). Thymosin β4 has also been reported as a prognostic factor for poor survival and metastasis in patients with early-stage NSCLC (194). Furthermore, decreased cell proliferation, cell migration, and invasion both *in vitro* and *in vivo* have been observed in thymosin β4 silenced A549 and H1299 NSCLC cells (195).

S100A4 is a calcium-binding protein belonging to the S100 family and recognized as a metastasis-associated protein (196). The prognostic value of S100A4 has been shown in a variety of cancers, including lung cancer. S100A4 functions as a metastasis-inducing factor in tumor cells without apparent tumorigenic function. Association with actin-related factors such actin, myosin, and tropomyosin has been reported, but the mechanism in which S100A4 increases the lamellipodia stabilization and actin cytoskeleton re-arrangement to promote cell migration remains elusive (184, 197).

As mentioned above, the common points of FHOD1, TMSB4X, and S100A all share an interaction with actin, contribute to F-actin formation, and play critical roles in cellular motility. As PSAT1 loss results in motility defects and changes in actin polymerization, we confirmed the differential expression of these genes via Real-Time PCR in our NSCLC model. As shown in Figure 39, silencing of PSAT1 reduced the expression of each gene, which was fully restored by re-expression of PSAT1. These results validate our findings from the RNA-seq transcriptomic and implicate a new role for PSAT1 in cell migration through regulating the expression of actin-related factors.
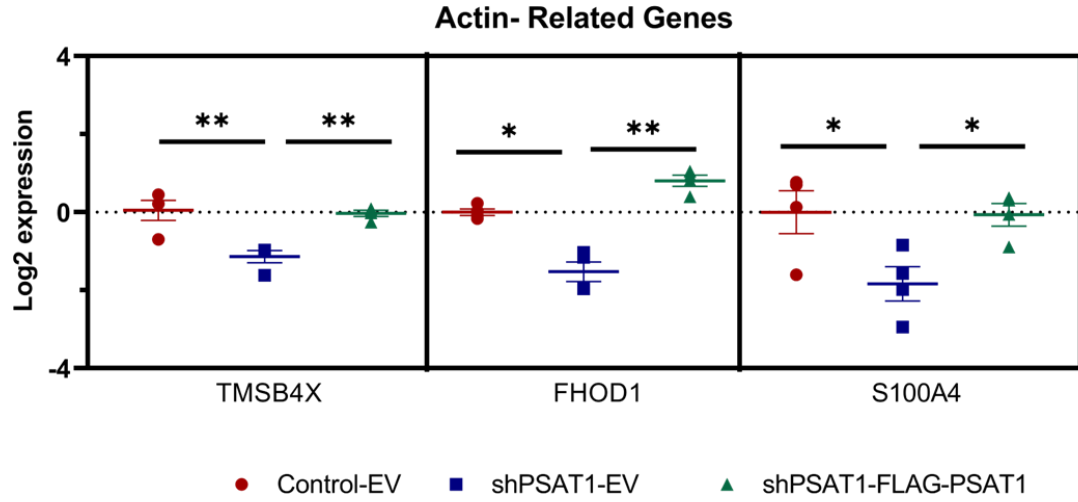
Figure 39. Suppression of PSAT1 reduces the expression of genes involved in F-actin formation. Real-time PCR analysis of gene expression. N= 3-4; *, p≤0.05 and **, p≤0.01

PSAT1 impacts the expression of genes localized in chr18p11

Serine metabolism can potentially contribute to epigenetic regulation due to the involvement of one-carbon metabolism or production of α-KG (38, 136). Kottakis *et al.* has found an epigenetic mechanism for PSAT1 upon the depletion of the tumor suppressor, Lkb1, in a Kras-activated pancreatic cancer transgenic mouse model (46). Increased PSAT1 expression leads to hypermethylation of DNA, which is mainly enriched in retrotransposons. These hypermethylated retrotransposons can promote tumor formation through impacting the host gene expression. In another study, Hwang *et al.* has demonstrated that PSAT1 participates in the maintenance of stem cell properties of mouse ESCs via providing the α-ketoglutarate cofactor for α-KG-dependent dioxygenases that results in hypomethylation of histone and DNA (136). These reports highlight PSAT1's potential role in epigenetic regulation.

As epigenetic regulation generally affects transcriptional expression over a broad chromosomal area, we sought to identify differentially expressed genes located in the same chromosomal region. Results from this analysis using the MSigDB-positional gene set tool were presented in Figure 40. Several shPSAT1-down-regulated genes were localized to the chr18p11 cytogenic band, while the chr7p21 cytogenic band harbored various shPSAT1-up-regulated genes.

A genome-wide association study within a Korean population conducted by Ahn *et al.* found an association of chr18p11 with never-smoker lung cancer susceptibility (198). Consistent with the fact that EGFR activation mutation is more common in the never-smoker Asian population, we chose to examine these genes localized in chr18p11 in response to differential PSAT1 expression (96). First, we utilized the UCSC genome browser (http://genome.ucsc.edu/) to determine the genomic position of the genes on chr18p11 cytogenic bands. As shown in Figure 41A, our identified down-regulated genes were not restricted to a small region but observed spanning the wide-ranging area within chr18p11. We then picked 8 genes to validate their differential regulation observed in our RNA-seq studies upon PSAT1 silencing (Fig. 41A, red color). Real-time PCR analysis confirmed that genes within Chr18p11 were down-regulated upon PSAT1 silencing and partially

restored by re-expression of PSAT1, with the exception of *TYMS* (Fig. 41B). This result suggests

potential PSAT1-mediated epigenetic regulation in this region.

A **Down-regulated Genes**

Gene Set Name [# Genes (K)]	Description	# Genes in Overlap (k)	k/K	p-value ❓	FDR q-value ❓
chr18p11 [197]	Ensembl 101 Genes in Cytogenetic Band chr18p11	29		$3.8\ e^{-30}$	$1.14\ e^{-27}$
chr16q22 [177]	Ensembl 101 Genes in Cytogenetic Band chr16q22	8		$2.92\ e^{-5}$	$4.37\ e^{-3}$
chr7q11 [252]	Ensembl 101 Genes in Cytogenetic Band chr7q11	9		$5.91\ e^{-5}$	$5.29\ e^{-3}$
chr8q24 [320]	Ensembl 101 Genes in Cytogenetic Band chr8q24	10		$7.08\ e^{-5}$	$5.29\ e^{-3}$

B

Up-regulated Genes

Gene Set Name [# Genes (K)]	Description	# Genes in Overlap (k)	k/K	p-value ❓	FDR q-value ❓
chr7p21 [82]	Ensembl 101 Genes in Cytogenetic Band chr7p21	11		$5.73\ e^{-13}$	$1.71\ e^{-10}$
chr11q13 [420]	Ensembl 101 Genes in Cytogenetic Band chr11q13	10		$7.66\ e^{-5}$	$1.15\ e^{-2}$
chr7p13 [50]	Ensembl 101 Genes in Cytogenetic Band chr7p13	4		$1.35\ e^{-4}$	$1.34\ e^{-2}$
chr7p22 [119]	Ensembl 101 Genes in Cytogenetic Band chr7p22	5		$4.06\ e^{-4}$	$3.04\ e^{-2}$

Figure 40. Differentially expressed genes are observed in the same cytogenetic bands.

A) sh-PSAT1-down-regulated genes and **B)** shPSAT1-up-regulated genes.
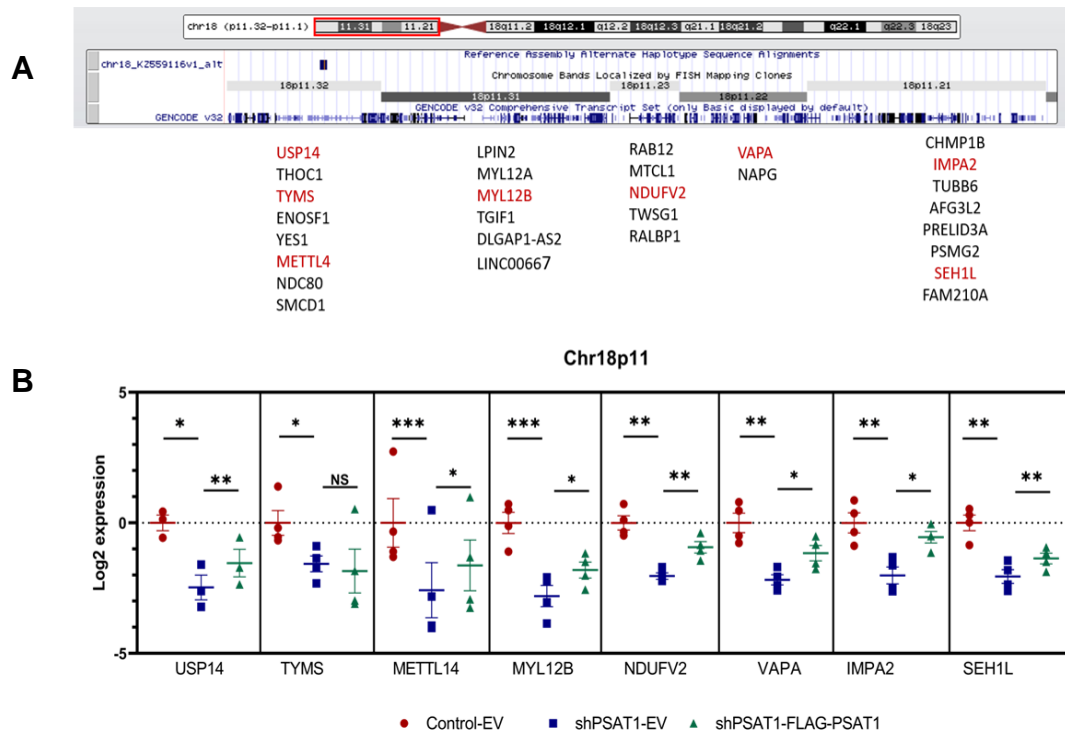
Figure 41. Suppression of PSAT1 results in reduced expression of genes across the chr18p11 cytogenic band, which are partially rescued by re-expression of PSAT1. A) The cartoon showing the map of down-regulated genes on chr18p11 cytogenic bands. Highlighted genes with red color were tested with Real-Time PCR in **B).** N=4; *, p≤0.05; ** p≤0.01; ***, p≤0.0001, and NS: not significant.

Identification of PSAT1-associated genes differentially expressed in EGFR mutant NSCLC

PC9 cells have been frequently used as an *in vitro* model for EGFR mutant lung cancer studies due to the presence of an activation mutation (exon19del) in the EGFR tyrosine kinase domain and its responsiveness to EGFR tyrosine kinase inhibitor treatment (199). Within the above transcriptomic analysis, RNA was collected from serum-starved PC9 cells to assess the EGFR-dependent gene expression alterations while minimizing the contribution of other serum-factors from the media. Therefore, we would expect to observe a subset of PSAT1-mediated genes that have been independently implicated in EGFR-driven lung tumorigenesis. To identify these genes, we designed a bioinformatic approach through a comparative analysis between the differentially regulated genes in our RNA-seq analysis and publicly available microarray datasets obtained from EGFR-mutant patient tumors.

GEO database (https://www.ncbi.nlm.nih.gov/geo/) stores a large number of microarray datasets from various studies and makes them available for other researchers for their independent investigations (169). We searched for gene expression datasets consisting of EGFR mutant lung tumors and normal lung (n≥10, each) derived from untreated patients. Based on these criteria, GSE31210, GSE31547, GSE31548, GSE27262, GSE32863, and GSE75037 were chosen for this analysis. Clinical information on the EGFR mutant lung tumor samples and the microarray chip platform were summarized in Table 7.

We utilized the BRB-ArrayTool, a user-friendly free software package for microarray data analysis, to import the gene expression files of these datasets and perform statistical analysis to determine PSAT1-associated genes in EGFR mutant tumors (151). The flow chart in Figure 42 demonstrates our strategy to determine these PSAT1-associated genes in EGFR mutant lung tumors**.**

Briefly, the series matrix of each dataset, which includes the normalized value of gene expression and the relevant clinical information, was imported by BRB ArrayTool "import data with NCBI GEO series" plugins. After re-filtering, the PSAT1 associated DEG list from our RNA sequencing study was used for a class comparison analysis between EGFR mutant lung tumor

Table 7. The GEO microarray datasets harboring expression profiles from EGFR

mutant lung cancer and normal lung with relevant clinical information used in this study.

Geo Dataset	Array Platform	Number of probe	Number of Array	Pathological Stage	Survival Data
GSE31210	Affymetrix HG-U133_Plus_2	54675	Tumor=127 Normal=20	Stage I= 103 Stage II=24	Relapse Overall
GSE27262	Affymetrix HG-U133_Plus_2	54675	Tumor=19 Normal =19	Stage I= 19	NA
GSE31547	Affymetrix HG-U133A	22277	Tumor=14 Normal =20	Stage I=8 Stage II=4 Stage III=2	Relapse Overall
GSE31548	Affymetrix HG-U133B	22645	Tumor=14 Normal=20	Stage I=8 Stage II=4 Stage III=2	Relapse Overall
GSE32863	Illumina HumanWG-6 v3.0	48803	Tumor=17 Normal=17	Stage I=8 Stage II=4 Stage III=5	NA
GSE75037	Illumina HumanWG-6 v3.0	48803	Tumor=20 Normal=20	Stage I=10 Stage II=6 Stage III=4	NA
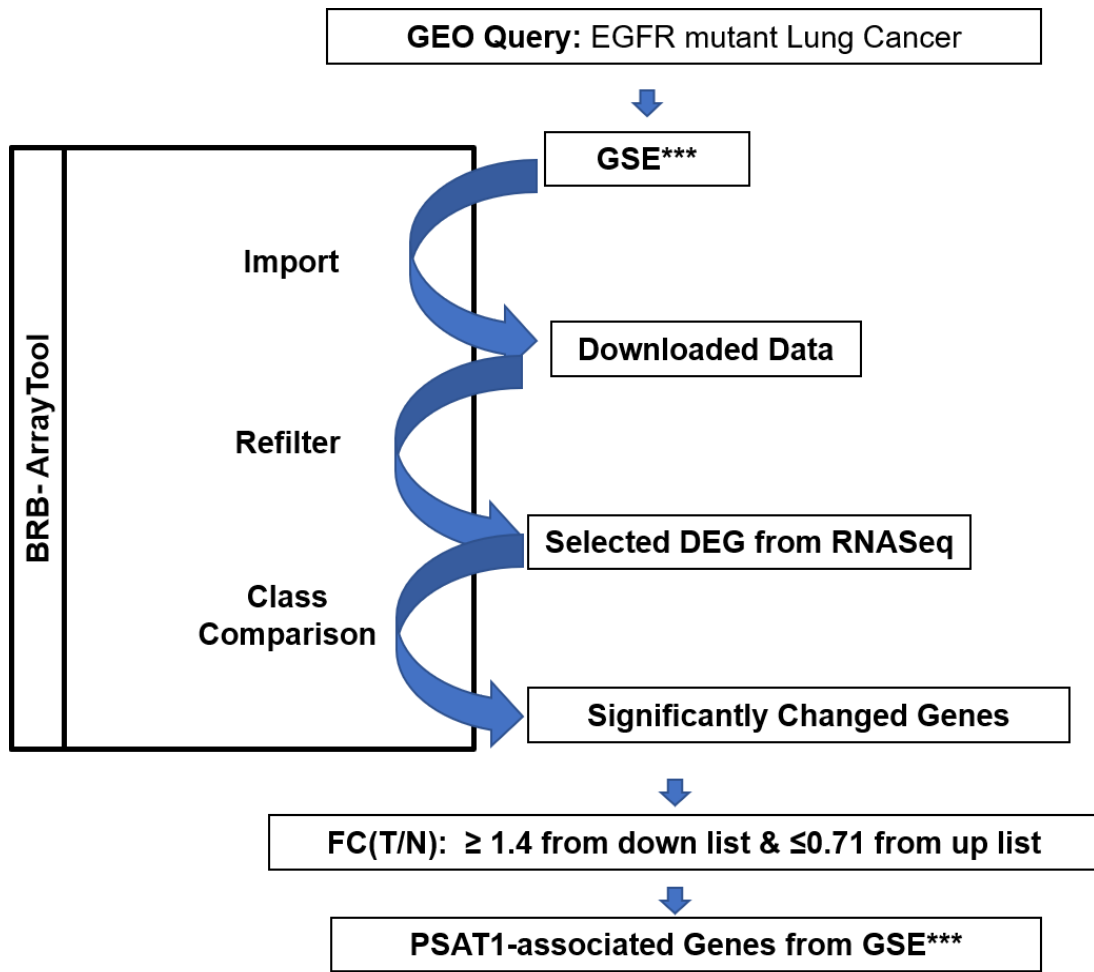
Figure 42. Strategic flow chart to identify PSAT1-associated genes from our PC9 study that are differentially expressed in human EGFR mutant lung tumors. ***, ID number 31210, 27262, 31547, 31548, 32863, or 75037; FC, fold-change; T, tumor; N, normal.

and normal lung to determine the significantly altered genes. **PSAT1-associated genes were defined as those up-regulated in tumor tissues (T/N) that are correspondingly down-regulated upon PSAT1 silencing in our RNA-seq profiling (shPSAT1-down-regulated) and, conversely, down-regulated in tumor tissue (T/N) that are correspondingly up-regulated upon PSAT1 loss (shPSAT1-up-regulated).**

Gene lists derived from the GSE31547 and GSE31548 datasets were combined as "GSE31547-48" since neither Affymetrix-HG-U133A nor Affymetrix-HG-U133B can cover all genes from the RNA-seq list and expression profiles were obtained from the same patients (Table 7) (200). We then compared the PSAT1-associated gene list from each dataset to obtain "common genes" altered in all datasets using web tool: http://bioinformatics.psb.ugent.be/webtools/Venn/. As some genes were represented by several probes, the number of probes was more than the number of genes (Fig. 43A(i) and B(i)). Venn diagrams in Figure 43A(ii) and 43B(ii) highlight 13 genes from our shPSAT1-down-regulated gene list and 12 genes from our shPSAT1-up-regulated genes list from the RNA-seq study, respectively. These were classified as PSAT1-associated genes in EGFR-mutant lung tumors as they were found to be differentially expressed in all the EGFR-mutant lung cancer datasets (Fig. 43A(iii) and B(iii)).

To confirm these findings visually, the expression of these genes was extracted from each dataset by BRB-ArrayTool. Cluster analysis was performed and heatmaps were generated by dChlp software for each dataset. Figure 44 demonstrates that shPSAT1-down-regulated common genes were increased in EGFR mutant tumors compared to normal tissue, while Figure 45 shows shPSAT1-up-regulated common genes that were decreased in EGFR mutant tumor tissues. Together, this bioinformatics approach was able to identify common genes linked through PSAT1 regulation in EGFR mutant lung tumors.

A **(i)**

GSE ID #	# Probes	# Genes
27262	81	61
31210	147	102
31547-48	43	34
32863	39	34
75037	75	59
Overall number of genes		129

(ii)

31547-48 / 31210 / 27262 / 75037 / 32863

37
1
3
3
4 17
0
0 0 4
2 7 6
0
1 0 13 1 0
0 0 6 0 0
2 1
10 5 5 0
1
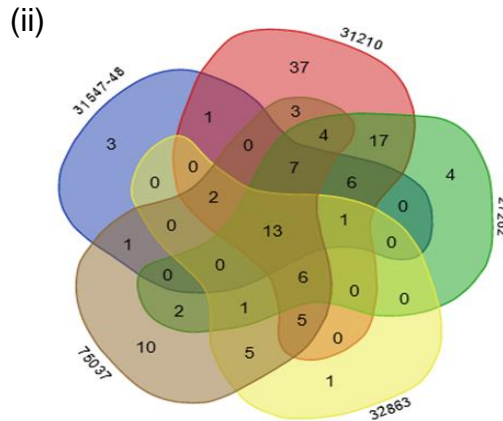
(iii) <u>Down-regulated Genes</u>

PSAT1
TYMS
CDCA7
SFN
SLC39A4
UHRF1
MMP15
NSUN5
NETO2
PAICS
ANKRD22
SPAG4
MCM2

B **(i)**

GSE ID#	# Probes	# Genes
27262	90	51
31210	121	56
31547/48	54	36
32863	36	32
75037	61	50
Overall number of genes		87

(ii)

31210 / 31547-48 / 27262 / 75037 / 32863

2
14
0 2
1 1 1
0 4 8 5
0 0 7
2 0
0 12 0
3 5 3 0 0
1 1 2
6 7 0
0
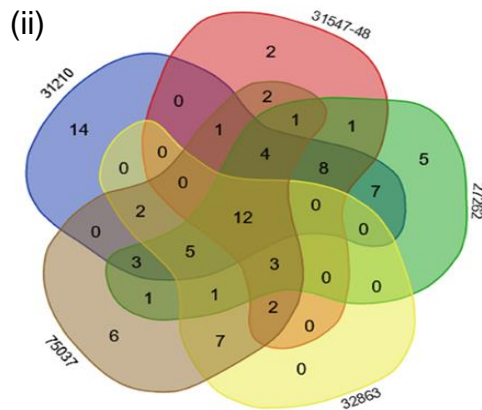
(iii) <u>Up-regulated Genes</u>

HBEGF
BTG2
JAG1
TJP2
CFD
GPRC5A
SPTBN1
SCEL
EFNB2
S100A9
ALOX5
FILIP1L

Figure 43. 13 shPSAT1-down-regulated and 12 shPSAT1-up-regulated genes are defined as PSAT1-associated genes in EGFR mutant lung tumors. Selection of common genes found across all EGFR-mutant tumor datasets that were **A)** shPSAT1-down-regulated or **B)** shPSAT1-up-regulated in response to PSAT1 loss in our RNA-seq analysis.
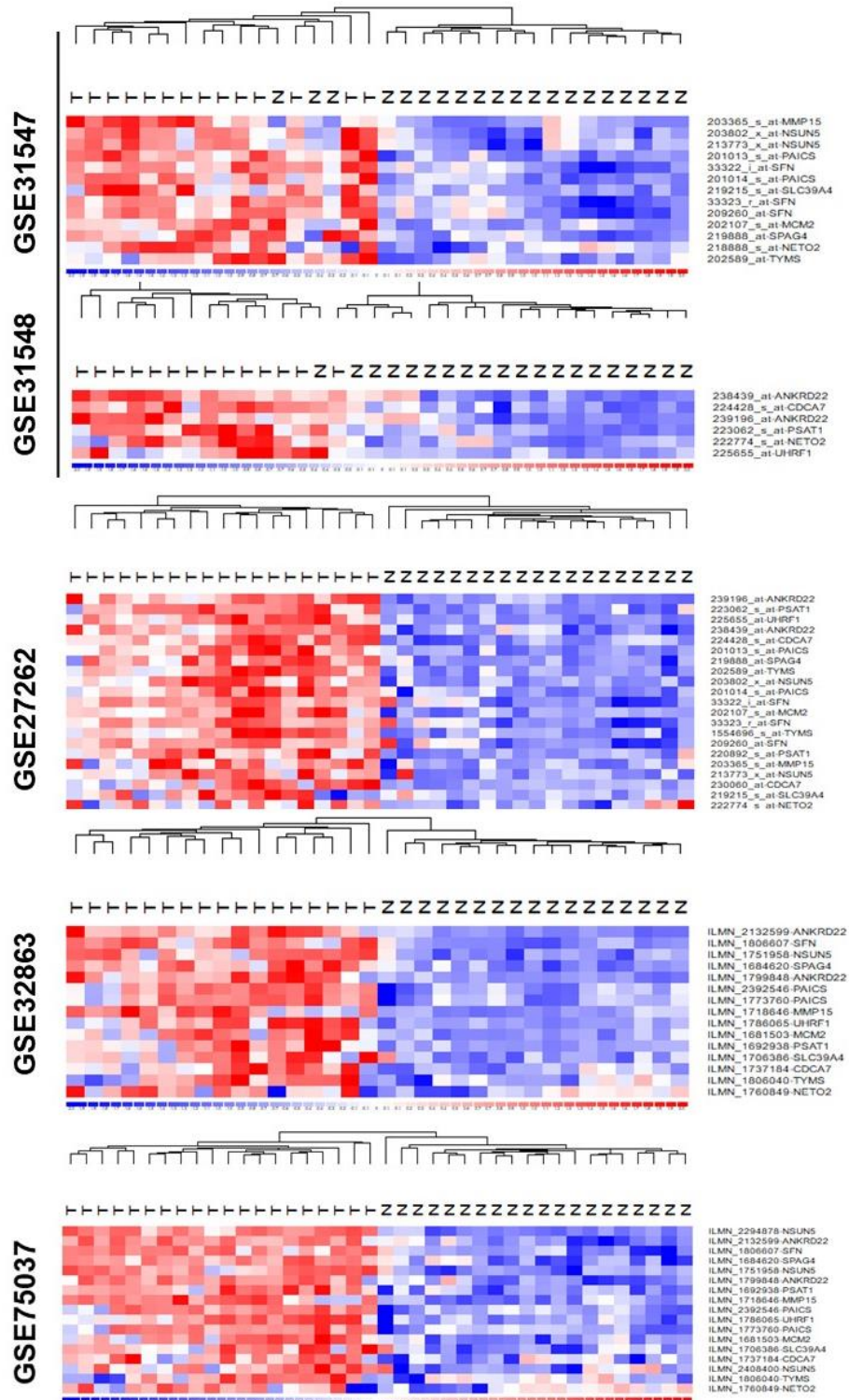
Figure 44. Heatmaps show increased expression of shPSAT1-down-regulated common genes in EGFR-mutant tumor tissues compared to normal lung. T: Tumor and N: Normal. Color key (Blue, Red)→(-2,2).
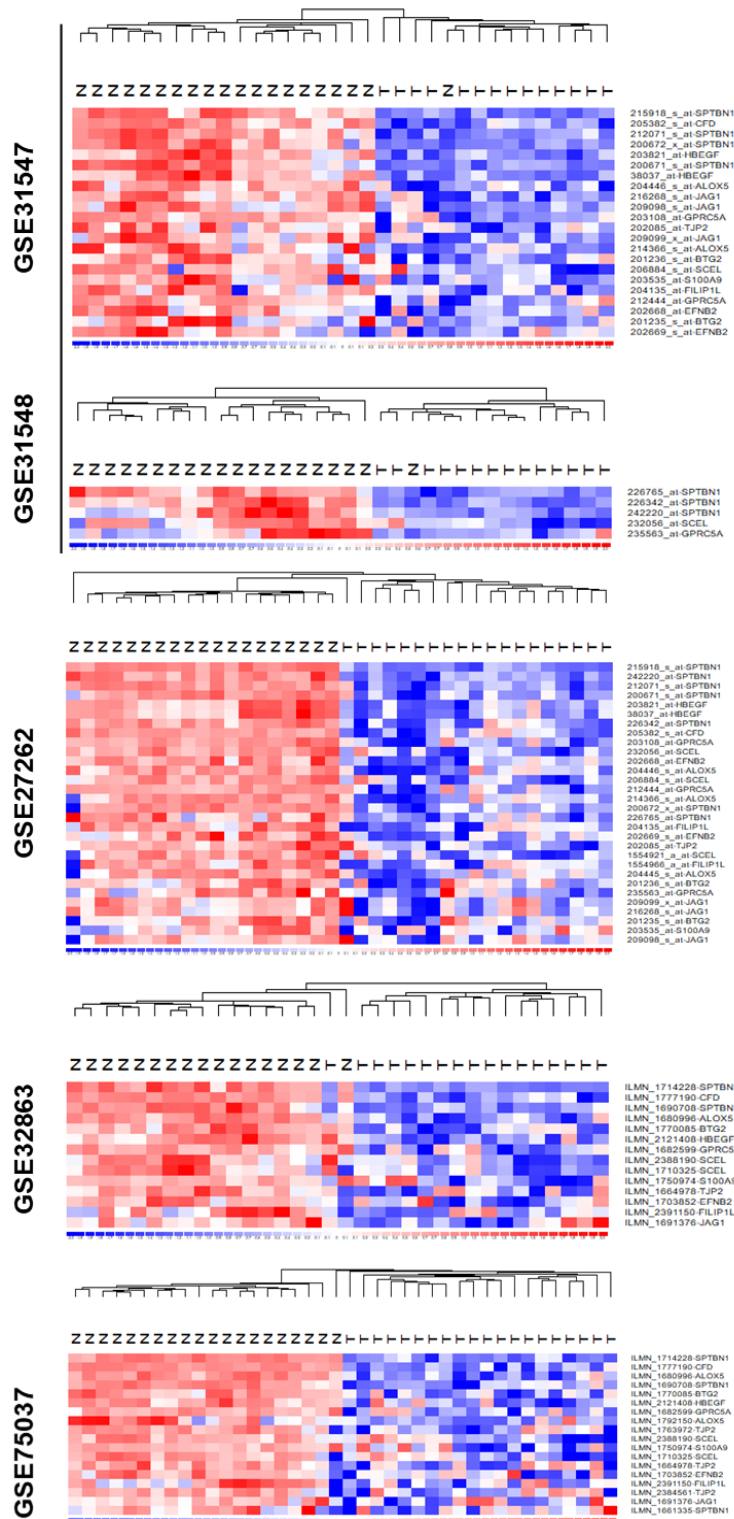
Figure 45. Heatmaps show decreased expression of shPSAT1-up-regulated common genes in EGFR-mutant tumor tissues compared to normal lung. T: Tumor and N: Normal. Color key (Blue, Red)→(-2,2).

A PSAT1-associated gene expression signature is associated with poor outcomes in patients with EGFR mutant lung cancer

The combination of the down-regulated and up-regulated common genes collectively identifies a PSAT1-associated gene signature for EGFR mutant lung cancer. We then wanted to assess the relationship between this gene signature and both relapse-free and overall survival in EGFR-mutant lung cancer patients. Among the datasets we used, GSE31210, GSE31547, and GSE31548 contained patient survival information. However, we focused on GSE31210 dataset as GSE31547 and GSE31548 had a limited number of EGFR mutant lung cancer samples (14 arrays) for survival analysis and could not be combined due to the platform incompatibility.

Survival risk prediction tools from BRB-ArrayTool have been commonly used to test the predictive ability of gene expression on patient outcomes (170, 201, 202). This tool calculates the survival risk score from the sum of gene expression product and corresponding regression coefficient for each gene. Based on this survival risk score, it assigns patients into two groups such as "High Risk" and "Low Risk": High Risk > mean (total survival risk score) > Low Risk. These groups are then utilized to generate a Kaplan-Meier (KM) plot using patient survival information and Receiver Operating Characteristic (ROC) curves. The KM plot demonstrates the predictive ability of gene expression on patient outcomes, while the area under the curve (AUC) in the ROC plot is accepted as the measure of predictive accuracy of the test and AUC above 0.7 is considered significant (170, 203).

Unfortunately, we had only one dataset with survival information (GSE31210) on EGFR-mutant NSCLC patients, so we were unable to validate our findings with another dataset. Therefore, we performed overall survival and relapse-free survival analysis by the leave-one cross-validation method with 100 permutation tests under principal component analysis with p ≤0.05 as previously defined (170). 13 and 17 out of 25 genes were found to predict the overall survival and relapse-free survival rates, respectively (Fig. 46). In addition, 12 genes were observed in both overall survival and relapse-free survival analyses.

KM plot groups	# Probes	# Genes
OS-Genes	19	13
RFS-Genes	26	17
Overall number of genes		18
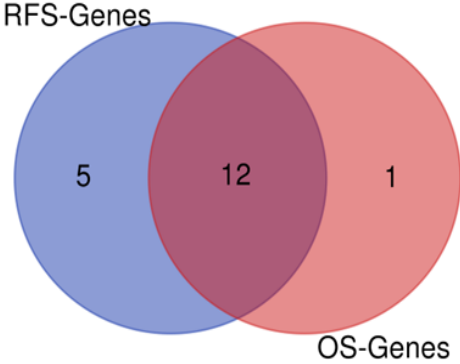
Figure 46. Common genes from the PSAT1-associated gene signature for EGFR mutant lung cancer display predictive ability for both overall survival (OS) and relapse-free survival (RFS).

According to Kaplan-Meier Plot for overall survival, the high-risk group (defined by 13 genes out of 25) exhibited significantly shorter overall survival than the low-risk group (Fig. 47A(i)). In addition, the prediction accuracy was supported by the AUC value (0.77) (Fig. 47A(ii)). Survival risk prediction for relapse-free survival analysis found additional genes (17 genes out of 25) that contributed to RFS. The KM plot demonstrated that the high-risk group correlated with worse relapse-free survival (Fig. 47B(i)) with a prediction accuracy AUC value of 0.72 (Fig. 47(ii)). Taken together, these results suggest that a PSAT1-associated gene signature is associated with poorer outcomes in patients with EGFR-mutant NSCLC.

We then extracted the expression of these 25-genes in GSE31210 for cluster analysis and subsequently heatmap generation. Figure 48 showed that the high-risk group identified by relapse-free survival analysis clustered together and exhibited the opposite expression profile of normal lung. While the high-risk group comprised 21 of 24 stage II samples and 45 of 103 stage I patient samples, the low-risk group derived from 58 stage I and only 3 stage II patient samples. Stage I patients' samples within the high-risk group displayed a similar expression pattern as the stage II samples in the same group yet were different from the stage I patient samples within the low-risk group. This implies that this PSAT1-associated gene signature for EGFR mutant lung cancer may predict high-risk groups within stage I patients.

The probes and their corresponding genes involved in relapse-free and overall survival prediction were summarized in Table 8 with their statistical significance (p-value) and contribution to cross-validation (% CV support). We also added coefficients of each probe (wi) used in survival risk score calculation. Probes/genes with positive coefficient indicate that higher expression is correlated with shorter survival, whereas negative coefficient implies the higher expression is associated with longer survival. Therefore, when looking at the sign of coefficients, we observed that down-regulated genes upon PSAT1 silencing possessed positive coefficients and up-regulated genes had negative coefficients, corroborating the findings above that PSAT1-associated gene signature for EGFR mutant lung cancer is associated with poorer outcomes.
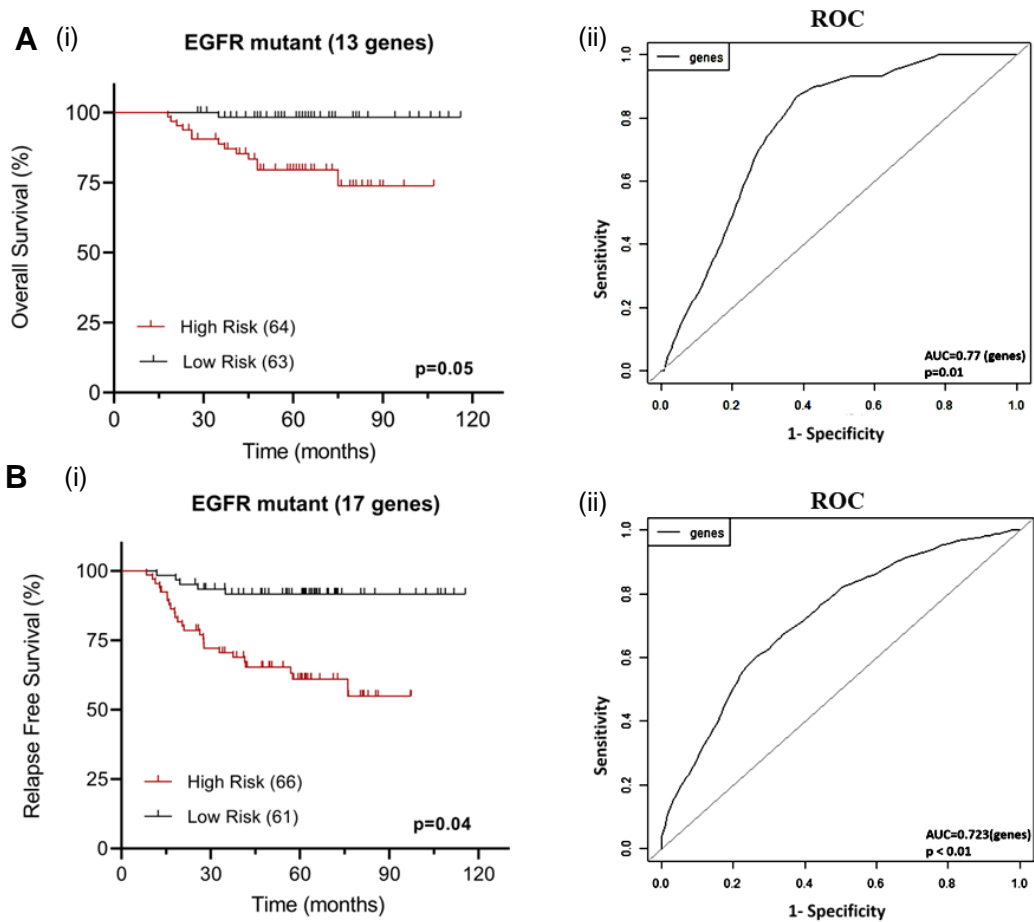
Figure 47. PSAT1-associated genes for EGFR mutant lung cancer are found to be associated with poorer clinical outcomes. (A-B) Cross-validated Kaplan-Meier Curve and log-rank statistics based on permutation (i) and cross-validated ROC curve with AUC value (ii) for **A)** overall survival analysis and **B)** relapse-free survival analysis in patients with EGFR mutant lung cancer. ROC: Receiver Operating Characteristics; AUC: Area under respective ROC curve.
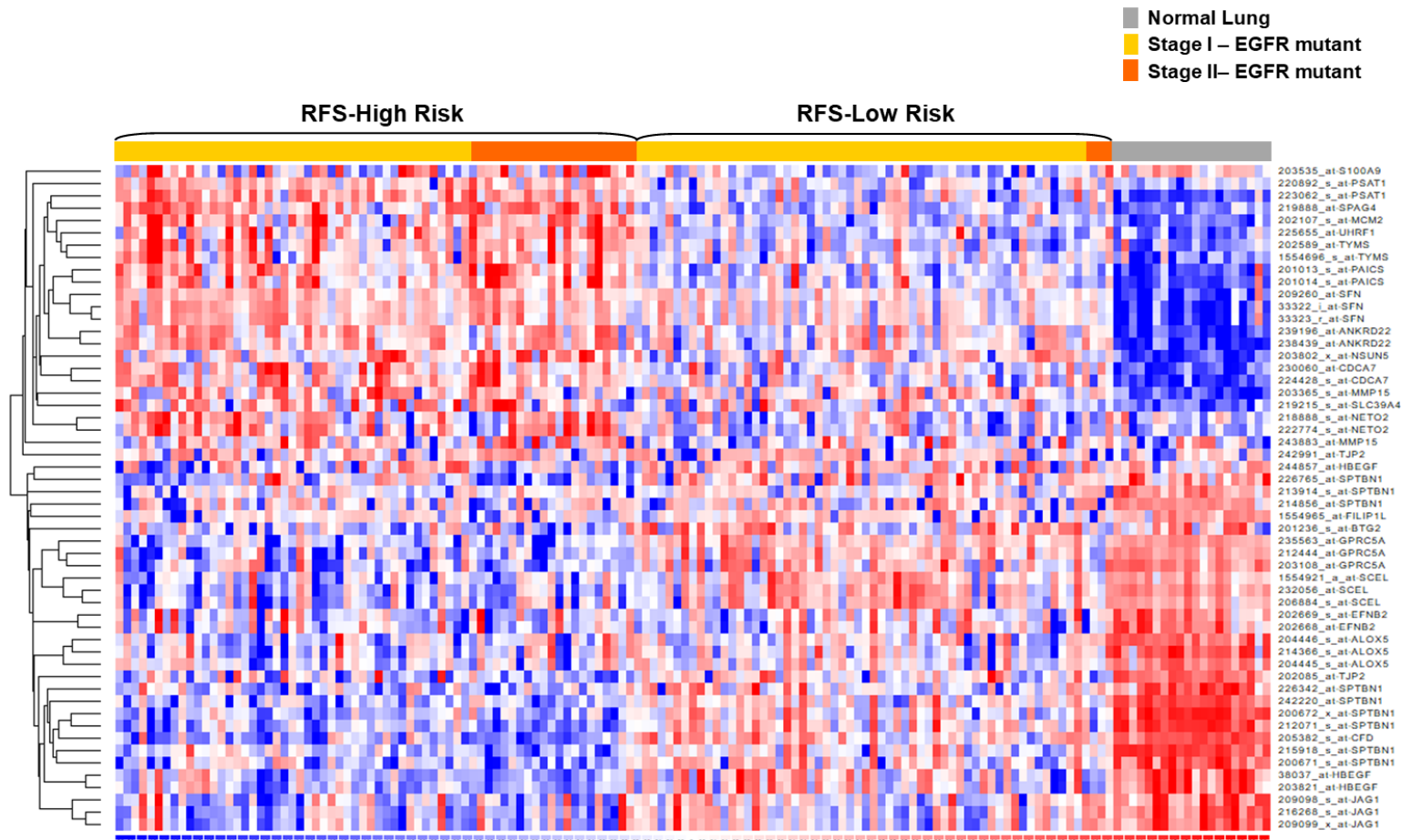
Figure 48. PSAT1-associated genes are able to discriminate a high-risk relapse group within stage I EGFR-mutant lung cancer patients from the GSE31210 dataset. RFS: Relapse-free Survival. Color key (Blue, Red)→ (-2,2).

Table 8. Probe list of genes identified in the relapse-free survival and overall survival analysis of EGFR mutant patients' samples. Shown are the Cox proportional hazards models (p≤0.05), %CV support: cross-validation, and Weight (wi): coefficient of each probe used of survival risk score calculation.

EGFR mutant Tumor (n=127)		Relapse-Free Survival			Overall Survival		
Genes	Probe ID	p-value	% CV Support	Weights (wi)	p-value	% CV Support	Weights (wi)
CFD	205382_s_at	2.055E-04	100	-0.114579	4.63E-04	100	-0.155391
FILIP1L	1554965_at	9.436E-03	100	-0.015713	1.88E-02	96.85	-0.019086
GPRC5A	212444_at	5.962E-03	100	-0.069177	6.06E-03	100	-0.097158
GPRC5A	235563_at	5.228E-03	100	-0.08264	3.23E-02	98.43	-0.113706
HBEGF	244857_at	2.611E-04	100	-0.030123	4.67E-03	100	-0.038612
MCM2	202107_s_at	5.760E-05	100	0.064114	1.93E-04	100	0.090761
MMP15	243883_at	-	-	-	5.07E-03	100	0.029494
PAICS	201013_s_at	6.360E-05	100	0.044286	5.36E-03	100	0.059939
PSAT1	220892_s_at	4.256E-03	100	0.063036	2.30E-02	98.43	0.088233
PSAT1	223062_s_at	1.716E-03	100	0.088942	4.49E-02	92.91	0.121965
SCEL	1554921_a_at	1.656E-02	100	-0.070521	2.97E-02	98.43	-0.107053
SCEL	232056_at	5.110E-03	100	-0.093097	1.23E-02	100	-0.136887
SFN	209260_at	2.136E-04	100	0.054471	5.39E-03	100	0.073341
SFN	33322_i_at	6.670E-05	100	0.034709	1.21E-03	100	0.046443
SFN	33323_r_at	1.390E-03	100	0.040225	7.23E-03	100	0.053199
SLC39A4	219215_s_at	1.350E-02	100	0.025303	2.09E-02	98.43	0.037955
TYMS	1554696_s_at	8.194E-04	100	0.060664	1.37E-02	100	0.083552
TYMS	202589_at	2.288E-03	100	0.086638	7.62E-03	100	0.119874
UHRF1	225655_at	2.998E-02	96.85	0.103476	1.139E-02	100	0.144022
CDCA7	224428_s_at	6.952E-03	100	0.070623	-	-	-
PAICS	201014_s_at	1.116E-03	100	0.048539	-	-	-
BTG2	201236_s_at	3.605E-02	96.06	-0.04939	-	-	-
GPRC5A	203108_at	2.229E-02	100	-0.039503	-	-	-
NETO2	218888_s_at	2.223E-02	100	0.04869	-	-	-
NETO2	222774_s_at	4.979E-02	42.52	0.065235	-	-	-
JAG1	229924_s_at	2.418E-02	99.21	-0.024027	-	-	-
ANKRD22	238439_at	2.015E-02	100	0.044862	-	-	-

We performed a literature search for reported function and/or connection of our survival genes in lung cancer and summarized these findings in Table 9. We observed that shPSAT1-down-regulated genes (conversely increased in tumors) were associated with poor patient outcome and tumor progression and involved in various oncogenic processes, including cell cycle progression, proliferation, migration, and invasion. On the other hand, shPSAT1-up-regulated genes (conversely decreased in tumors) have been linked to good prognosis and played roles in inhibition of cell proliferation, migration, and invasion. Among these genes, BTG2 (B-cell translocation gene 2) and GPRC5A (G Protein-Coupled Receptor Class C Group 5 Member A) have already been accepted as tumor suppressors and GPRC5A acts as a negative regulator of EGFR signaling in NSCLC cells (3, 32, 34). However, we were unable to find the relationship between these genes and EGFR mutant lung tumors in the current literature, implying the novelty of our PSAT1-associated genes in EGFR mutant lung cancer.

Table 9. The role of genes found by relapse-free and overall survival analysis in NSCLC.

shPSAT1-down-regulated Genes (increased in tumors)	
PSAT1	• Shorter overall survival in NSCLC (1, 2) • Cell proliferation, cell cycle progression and tumor growth in vivo (1) • Shedden_Lung_Cancer_Poor_Survival_A6 (4)
TYMS	• Associated with advanced stage, lymph node metastasis, and vasculature invasion in lung adenocarcinoma (8) • Shedden_Lung_Cancer_Poor_Survival_A6 (4)
SFN	• Increased expression in NSCLC by hypomethylation of promoter and further reduced methylation with progression (10, 11) • Early-stage lung adenocarcinoma marker for progression (12) • Role in oncoprotein stabilization (13)
SLC39A4	• Associated with increased tumor size, regional lymph node metastasis, and poor patient outcome (14) • EMT
UHRF1	• Poor overall survival in lung adenocarcinoma(23) • Role in regulation of epigenetic modulation during DNA duplication in S-phase • Hypomethylation of UHRF1-related genes
MMP15	• Associated with lymph node metastasis, tumor stage, and intra-tumoral microvessel density (24) • EMT via degrading adherens and tight junction proteins (25)
NETO2	• Shorter overall survival in lung adenocarcinoma (26) • Shedden_Lung_Cancer_Poor_Survival_A6 (4)
ANKRD22	• Relapse and shorter overall survival in NSCLC (27) • Cell proliferation via increasing the expression of E2F1
MCM2	• Shorter overall survival and progression-free survival in lung adenocarcinoma (29) • Cell proliferation, cell cycle, and migration (30)
PAICS	• Disease progression and poor prognosis in lung adenocarcinoma (31) • De novo purine biosynthesis, cell proliferation, invasion, and modulation of pyruvate kinase activity • Shedden_Lung_Cancer_Poor_Survival_A6 (4)
CDCA7	• Shorter overall survival • Involved in a variety of oncogenic processes (37)

(Continued)

128

Table 9. Continued

shPSAT1-up-regulated genes (decreased in tumors)	
BTG2	• Hypermethylation of promoter is associated with shorter overall survival (3) • Inhibition of cell proliferation and invasion and PI3K/AKT signaling pathway
HBEGF	• Highly expressed in subgroup of lung cancer and associated with advanced tumor growth (7) • Patients with high serum level tend to longer progression-free and overall survival (21)
JAG1	• Better overall survival rate (22)
CFD	NA
SCEL	• Shedden_Lung_Cancer_Good_Survival_A4 (4)
GPRC5A	• Low expression is associated with worse prognosis and advanced TNM stage(32) • Negative modulator of EGFR signaling in NSCLC cells and inhibited by EGFR-dependent phosphorylation(33, 34) • Shedden_Lung_Cancer_Good_Survival_A4 (4)
FILIP1L	• Down in lung cancer by DNA methylation (35) • Inhibition of cell migration • Reduced nuclear β-catenin expression (36)

PSAT1-associated gene signature is unable to predict the risk groups in other NSCLC tumors

In addition to EGFR-mutant lung tumors, the GSE31210 microarray dataset also harbors ALK-fusion positive, KRAS mutant, and EGFR/KRAS/ALK wild-type tumor samples with their corresponding clinical information. Therefore, we investigated whether the predictive ability of PSAT1-associated gene signature is specific to EGFR mutant lung cancer or applies to NSCLC tumors with other oncogenic drivers. Therefore, we performed survival risk prediction analysis for KRAS mutant and EGFR/KRAS/ALK wild-type tumors as described above. Survival analysis for ALK-fusion positive only tumors was excluded due to the limited sample size (n=10). EGFR/KRAS/ALK wild-type tumors were identified as EGFR/KRAS wild-type so as to not lead to confusion.

Expression profiles of JAG1, BTG2, ANKRD22, GPRC5A, and ALOX5 genes in KRAS mutant tumor and ALOX5 expression in EGFR/KRAS wild-type tumor resulted in the Kaplan-Meier overall survival curve construction (Fig. 49A and C, respectively). However, these genes were unable to separate the high-risk groups from the low-risk groups in neither KRAS mutant tumor nor EGFR/KRAS wild-type tumor. Kaplan-Meier relapse-free survival curves were generated from the expression profile of SCEL, MMP15, JAG1, BTG2, and ANKRD22 in KRAS mutant tumor and PSAT1 and SFN in EGFR/KRAS wild-type tumor (Fig. 49B and D, respectively). Although we observed better separation between high-risk and low-risk groups for the relapse-free survival curve in both KRAS mutant and EGFR/KRAS wild-type tumors compared with overall survival curves, they did not reach statistical significance.
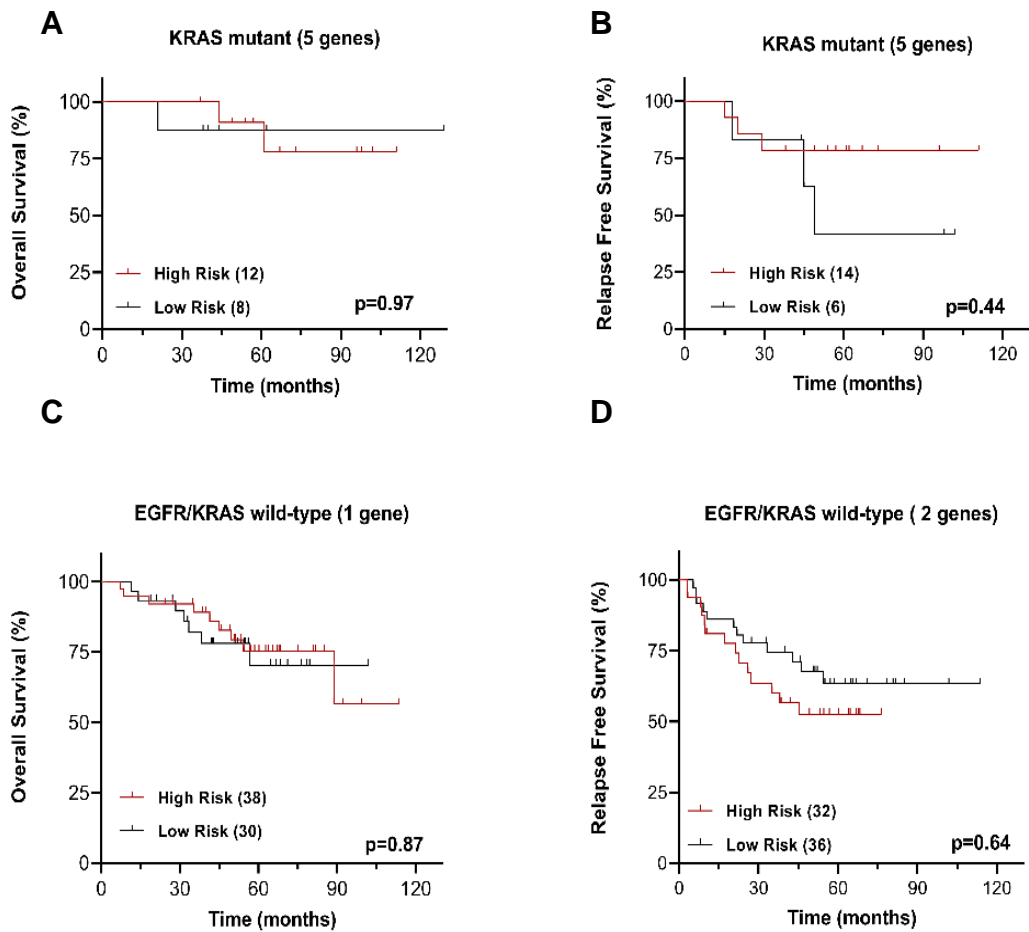
Figure 49. Survival risk predictions with the identified PSAT1-associated genes from EGFR mutant lung cancer against other NSCLC tumors. (A-D) Cross-validated Kaplan-Meier Curve and log-rank statistics based on permutation for overall survival analysis in patient with **A)** KRAS mutant and **C)** EGFR/KRAS wild-type tumor and **B)** relapse-free survival analysis in patients with KRAS mutant and **D)** EGFR/KRAS wild-type tumor.

Identification of potential PSAT1-associated metastatic gene signature

The PSAT1-associated gene signature we have described is mainly dominated by early-stage EGFR mutant lung cancer transcriptomic profiles due to the presence of a high number of stage I patients in GSE31210 (N=103) and GSE27262 (all stage I tumors). These datasets may inform us to the relevance of this PSAT1-associated gene signature for EGFR tumor initiation and early progression, but at the same time, these may hamper the identification of potential PSAT1-associated genes involved in late-stage tumor progression and metastasis as these microarray datasets had a limited number of stage-III and even fewer stage IV samples. Therefore, we decided to analyze the GSE14107 microarray dataset, which encompasses transcriptomic profiles of the PC9-parental line and the PC9-BrM3 brain metastatic sublines (172).

We hypothesized that PSAT1-associated metastatic genes would be upregulated in PC9-BrM3 and correlate with down-regulated genes in our PSAT1 silencing RNA-seq results and vice versa. To identify these genes, the GSE14107 microarray dataset was retrieved by BRB-ArrayTool as described before. Then, differentially expressed genes between PC9 and PC9-BrM3 cells were determined by class comparison plugin based on the same criteria used before: 1.4 fold- change and p≤0.05. Common genes between groups were determined by Venn diagram drawing webtool (http://bioinformatics.psb.ugent.be/webtools/Venn/).

As shown in Figures 50A and B, 51 genes from the sh-PSAT1-down-regulated gene list and 30 genes from the shPSAT1-up-regulated gene list were identified as potential PSAT1-associated metastatic genes. To confirm these findings visually, we extracted the differential expression profile of these genes between PC9-P and PC9-BrM3 cells from GSE14107. After performing cluster analysis, heatmaps were generated by dChIP. Figures 50C and D, respectively, demonstrated the up-regulation of genes in PC9-BrM3 from the shPSAT1-down-regulated gene list and down-regulation of genes in PC9-BrM3 from the shPSAT1-up-regulated gene list. Interestingly, PSAT1 was one of the genes that increased in PC9-BrM3 cells, further supporting our hypothesis that these genes may contribute to PSAT1's metastatic potential in PC9 cells.
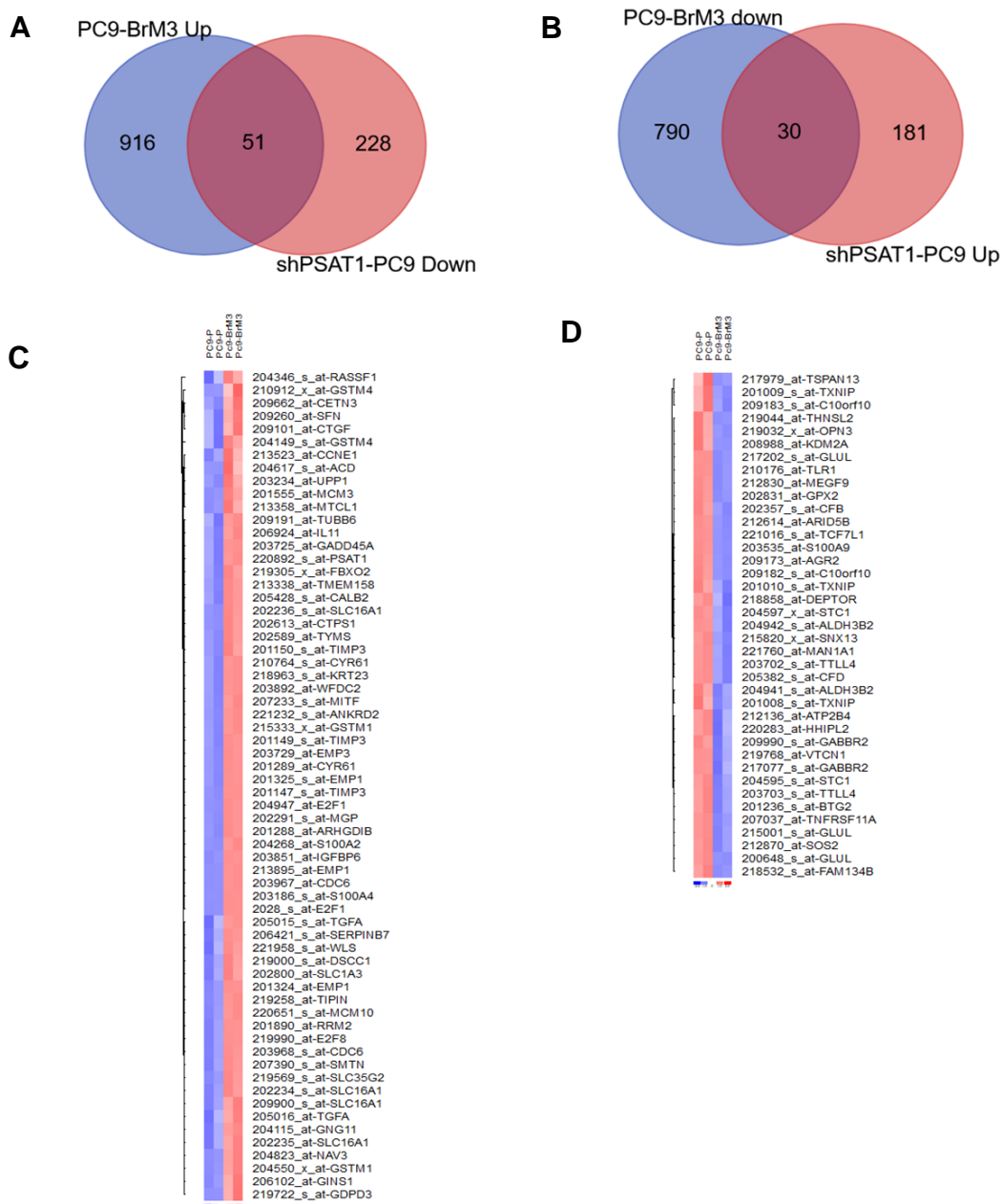
Figure 50. Potential PSAT1-associated metastatic genes are obtained from the differentially expressed genes between PC9-parental and PC9-BrM3 sublines. **(A-B)** Venn diagram displaying the number common genes in **A)** shPSAT1-down-regulated list and **B)** shPSAT1-up-regulated list**. (C-D)** Heatmaps displaying the expression profile of the common genes identified from **C)** Venn diagram in A and **D)** Venn diagram in B. Color key (Blue, Red)→(-2,2).

Discussion

PSAT1 expression is elevated in many types of cancer, including NSCLC and associated with poor patient outcomes (1, 2, 44). While its metabolic function within SSP activity contributes to cell proliferation and tumor growth, oncogenic signals may promote alternative functions that may promote tumor progression; particularly as nuclear localization of PSAT1 in EGFR-activated lung cancer cells was observed in our study. To gain better insight into the role of PSAT1 in tumorigenesis and identify potential alternative activities, genome-wide expression profiling by RNA-seq technology was performed. Differentially expressed genes were intensely interrogated using bioinformatics tools for comparisons with other gene expression datasets.

Inhibition of serine biosynthetic pathway impacts several metabolic pathways, including folate, glutathione, and nucleotide biosynthesis (Fig. 2) (15, 20, 40, 45). PSAT1 silencing led to down-regulation of genes involved in these pathways and reduced anchorage-independent growth, which was partially restored by downstream metabolites supplementation. These findings support a metabolic function for PSAT1 within the serine biosynthetic pathway. PSAT1 is also implicated in the inhibition of GSK3β dependent phosphorylation and proteasomal degradation of target proteins (Fig. 5)(1, 43, 69).   In addition, PSAT1-mediated stabilization of cyclin D1 promotes E2F transactivation in NSCLC cells and consistent with this finding, loss of PSAT1 was found to reduce the expression of E2F target genes (1). β-catenin was another potential target for PSAT1/GSK3β pathway and implicated in EGFR-mutant lung tumorigenesis (43, 176, 178). Although our gene expression analysis was unable to demonstrate how PSAT1 loss alters β-catenin transactivation, reduction in the total and nuclear β-catenin level and luciferase activity corroborates these previous findings that PSAT1 may be involved in the regulation of β-catenin stability. Taken together, these suggest that PSAT1 loss mediated gene expression changes support known tumorigenic functions of PSAT1.

Loss of PSAT1 severely affects the cell motility of EGFR-activated cells, as shown in Chapter 2. Through exploring gene expression alterations involved in cell migration, we observed down-regulation of genes involved in actin cytoskeleton arrangement in PSAT1 silenced cells. Among these genes, expressions of FHOD1, TMSBX4, and S100A4, which are well-known actin-

134

associated proteins involved in actin fiber formation and cell migration, were assessed and validated as the downstream targets of PSAT1. However, their role in PSAT1-mediated cell migration requires further investigation.

Nuclear localized metabolic enzymes, including PDC, ACLY, α-KGDH, are involved in epigenetic regulation via providing substrate for histone modifications (122, 124, 127). Accordingly, finding nuclear PSAT1 in EGFR activated lung cancer cells and previous reports showing the involvement of PSAT1 in epigenetic regulation prompted us to explore the differentially regulated genes located within certain chromosomal regions (46, 136). Twenty-nine genes located in Chr18p11 were found to be down-regulated upon PSAT1 silencing. Real-time PCR analysis of seven out of eight genes verified as PSAT1 down-stream targets, implying a putative long-range gene expression regulation by PSAT1 within this genetic locus. Further investigation is also required to elucidate any involvement of PSAT1-mediated epigenetic regulation in this region.

Availability of gene expression datasets from EGFR mutant lung cancer and the use of publicly available bioinformatics software for expression analysis provided us the opportunity to examine the clinical significance of a PSAT1-associated gene signature. We found twenty-five PSAT1 associated genes linked to EGFR-mutant lung cancer from the analysis of six different patient-derived datasets. Survival prediction analysis found that a subset of genes within this list significantly predicts overall and relapse-free survival in EGFR-mutant NSCLC patients. Consistent with this, the expression pattern of these genes in the stage I high-risk group is similar to that observed in the stage II high-risk group. On the other hand, this signature fails to predict other NSCLC types of tumors' patient outcomes. However, at this time, the limited number of KRAS mutant tumors analyzed precludes us from making a definitive conclusion that this signature is specific to EGFR mutant tumors.

As early-stage cancers dominate the gene signature obtained from human EGFR mutant lung tumors, analysis of genes involved in late-stage tumor progression and metastasis is limited. Therefore, differentially expressed genes between parental PC9-P and brain metastatic PC9-BrM3 were extracted from the Nguyen *et al.* study (172). Comparative analysis with RNA-seq data found

that 18.2 % of shPSAT1-down-regulated and 14.2% of shPSAT1-upregulated genes displayed the same pattern between metastatic versus parental PC9 cells and were defined as a potential PSAT1-associated metastatic gene signature. PSAT1 and PSAT1-mediated actin-related proteins, including S100A4, SMTN, and CALB2, were found within this list, supporting the notion that PSAT1 contributes to cell motility via regulating the actin cytoskeleton. Thus, these findings suggest the putative involvement of PSAT1 in the metastasis of EGFR mutant lung cancer.

In summary, these studies examined genome-wide expression changes upon PSAT1 silencing using gene profiling and bioinformatics approaches. Our analysis corroborated previous findings on the role of PSAT1 within the serine biosynthetic pathway in regulating E2F activity and β-catenin protein expression/transcription activity. We also validated PSAT1's impact on actin-related genes as F-actin stress fiber formation was restored by re-expression of PSAT1. Comparative analysis of our genomic profiling against public gene expression data yielded a PSAT1-associated gene signature with prognostic value in EGFR-mutant NSCLC patient outcomes.

CHAPTER 4

CONCLUSION & FUTURE STUDIES

Investigation into the oncogenic function of PSAT1 has been relatively limited to general phenotype analysis in response to silencing or ectopic expression in tumor cells. Therefore, the complete mechanism(s) for the tumor-promoting activity of PSAT1 remains elusive. Through biochemical and genomic approaches, this work highlights a novel function for PSAT1 in EGFR-mediated lung tumorigenesis.

Results supportive of a non-canonical function of PSAT1

In this study, we initially assessed PSAT1's metabolic contribution to cell migration through metabolite rescue upon PSAT1 loss. Separately, we also compared PSAT1's cell motility effects to those caused by PHGDH silencing. We found that metabolite supplementation failed to rescue the migration defect due to PSAT1 suppression and loss of PHGDH significantly impacted cell motility to a lesser extent than PSAT1 depletion (Chapter 5, Fig. 55). More notably, unlike PSAT1 silencing, depletion of PHGDH did not affect nuclear PKM2 translocation (Chapter 5, Fig. 54). Taken together, we postulate that PSAT1 differentially contributes to EGFR-mutant lung cancer cell motility through a non-canonical function, potentially facilitating nuclear PKM2 localization and activity.

EGFR mutant lung cancer preferentially metastasizes to the brain and bone (204-207). Due to the blood-brain barrier, serine biosynthesis in neuronal cells is crucial and targeting SSP activity could have detrimental side effects (15). Our bioinformatic analysis indicated elevated PSAT1 expression in a brain-metastatic subline (PC9-BrM3) of EGFR-mutant NSCLC. Further, our findings suggest that other activities beyond PSAT1's metabolic activity may be required for cell migration. Therefore, it is crucial to elucidate any non-canonical function(s) of PSAT1 in cell migration and the metastatic potential of PC-BrM3 cells. Targeting these PSAT1 functions may

prove to be a therapeutic option to suppress brain metastasis in EGFR-mutant lung cancer patients.

Potential mechanisms by which nuclear PSAT1 may mediate gene regulation

This study has demonstrated that the EGFR signaling facilitates the nuclear localization of PSAT1. Nuclear localization of PSAT1 appears independent of PKM2 function (Chapter 2, Fig. 15) and elucidating the mechanism(s) which facilitate PSAT1 translocation is currently ongoing. Yet, we propose a model by which PSAT1 may exert its nuclear activity (Fig. 51).

Catalytic-dependent pathway

Similar to PSAT1, we also observed activated EGFR-dependent nuclear localization of PHGDH (Chapter 5, Fig.54). As both SSP enzymes are driven to the same cellular compartment, we speculate that nuclear PHGHD and PSAT1 catalytic activity may influence the cellular epigenetic landscape by producing key metabolites required for epigenetic modifiers (Fig. 51A). Specifically, α-KG serves as a substrate for both the Jumonji C domain containing lysine demethylases (KDM2-7) and ten-eleven translocation hydroxylases (TET1-3) that mediate histone and DNA demethylation, respectively (204). In support of this, epigenetic regulation by PSAT1-derived α-KG is required for the pluripotency of mouse embryonic stem cells (136). Thus, we postulate that nuclear α-KG production through concerted PHGDH and PSAT1 activity leads to hypomethylation of DNA and histones. While less likely, alternatively, nuclear PHGDH could metabolize α-KG for the production of the oncometabolite 2-HG. As 2-HG competitively inhibits the KDM and TET enzymes, this would lead to histone and DNA hypermethylation. Although PHGDH derived 2-HG has been reported in breast cancer cells, it is still unclear whether the level of 2-HG produced is sufficient to impact the epigenetic landscape in these cells (135). As described in chapter 1, there are several examples of metabolic enzymes contributing to histone modifications due to nuclear localization and local substrate production (122, 126, 127); therefore, it is plausible that nuclear-localized PHGDH and PSAT1 may act to produce metabolites that impact the epigenetic landscape in these lung cancer cells. This potentially would lead to differential gene

expression across a large chromosomal area, similar to what we observed for the 18p11 cytogenetic locus.
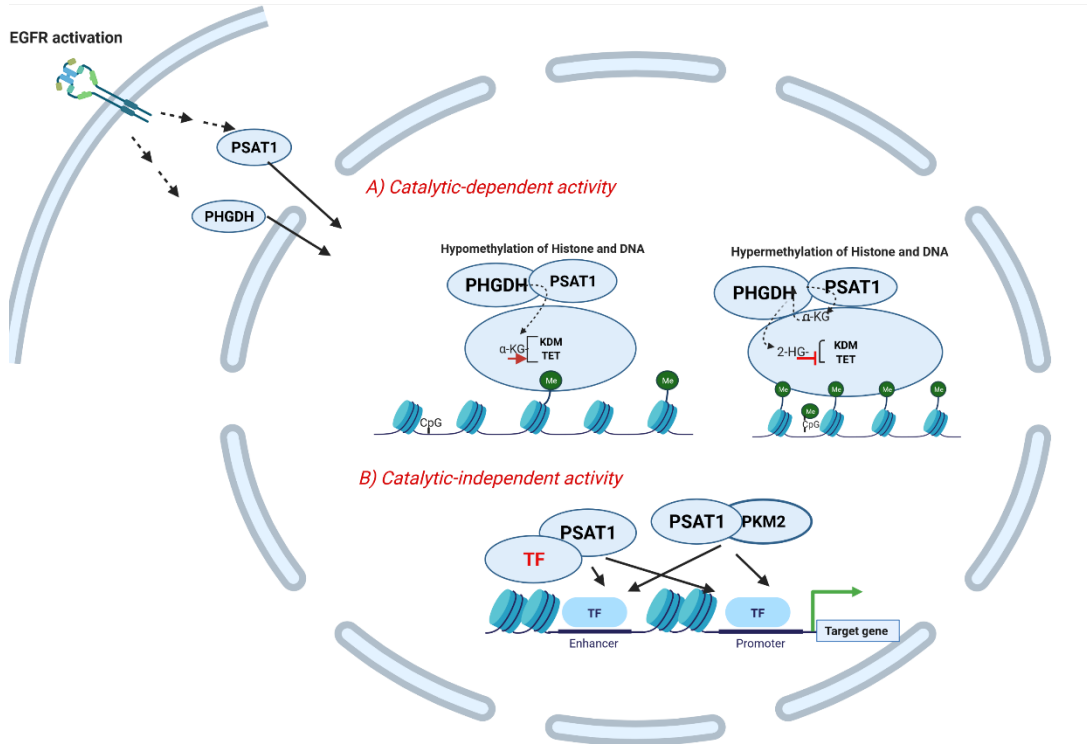
Figure 51. Schematic representation of putative nuclear PSAT1 function(s) in EGFR-activated cells. A) Catalytic-dependent nuclear PSAT1 function. Increased α-KG production may lead to both histone and DNA hypomethylation via activation of enzymes: KDM and TET. Conversely, PHGDH-mediated 2-HG production that would inhibit these α-KG-dependent enzymes and result in hypermethylation **B)** Catalytic-independent nuclear PSAT1 function. PSAT1 contributes to gene regulation through interaction with other transcription factors (TF) or nuclear PKM2. KDM: Lysine demethylase; TET: ten–eleven translocation hydroxylases.

PSAT1 may also exert a nuclear function as part of a transcriptional complex, similar to that reported with PKM2 and β-catenin (Fig. 51B)(113). As both PSAT1 and PKM2 localize to the nucleus in EGFR-activated cells, we can question whether nuclear PSAT1 may influence gene expression via interacting with PKM2.

In short, our findings demonstrate the nuclear localization of PSAT1 in both EGF-stimulated EGFR-WT A549 and EGFR-mutant PC9 NSCLC cell lines, but elucidation of its nuclear function as it relates to tumor progression requires further investigation. Our initial future plans are to generate cells expressing PSAT1 catalytically inactive and/or nuclear localization deficient mutants to explore effects on nuclear metabolism, histone modifications, and interacting proteins within the nucleus. The differentially expressed genes from the RNA-seq data (Chapter 3) can serve as read-outs to delineate the metabolic vs. non-metabolic and cytosolic vs. nuclear function of PSAT1 in gene regulation. For example, UHRF1 (Ubiquitin-like, with PHD And Ring finger domains 1) is one of the EGFR linked PSAT1 associated genes, which is down-regulated upon PSAT1 silencing. UHRF1 functions as an epigenome adaptor protein that can recognize hemi-methylated DNA and methylated histones to recruit DNA methyltransferase 1 and histone methyltransferase (205, 206). Several reports demonstrated the involvement of UHRF1 in silencing tumor suppressor genes by DNA hypermethylation. FILIP1L (Filamin A interacting protein 1 like) and BTG2 within the shPSAT1-upregulated gene list act as tumor suppressors and are decreased in lung tumors by promoter hypermethylation (3, 35, 36). Thus, we can ask whether UHFR1 plays a role in PSAT1-mediated epigenetic regulation and whether the upregulation of these tumor suppressor genes is a result of DNA hypomethylation through using DNA immunoprecipitation (DIP)-PCR or DIP-seq analysis.

A potential role for PSAT1 in immune modulation through regulating the protein secretory pathway

We have so far focused on the intrinsic oncogenic function(s) of PSAT1 in EGFR-activated NSCLC and demonstrated its effects on anchorage-independent growth, cell migration, and actin

cytoskeleton rearrangements. However, GO analysis of the transcriptomic data in Chapter 3 also suggest a potential extrinsic function for PSAT1.

According to GO_BP analysis, genes involved in immune response and leukocyte migration/chemotaxis were upregulated upon PSAT1 silencing (Chapter 3, Table 5). In addition, exocytosis, endocytosis, and secretion are other biological processes observed to be regulated by PSAT1 and tumor cells routinely utilize these mechanisms to modulate the tumor microenvironment (207, 208). The cellular component analysis found up-regulated genes whose protein products are localized in the Golgi, within the membrane and lumen of vesicles, and within secretory membranes, suggesting a change in vesicle-mediated transport and secretion. While it is hard to determine the extrinsic activity of PSAT1 by analyzing intrinsic transcriptomic profiles, these studies suggest, at the least, that loss of PSAT1 may alter the secretory pathway in tumor cells.

Immunotherapy yields promising results if it is applicable to the patients. Immune checkpoint inhibitors (ICI) have become the part of the therapy for NSCLC patients, but EGFR mutant lung cancer patients are excluded from this treatment since EGFR mutant patients have limited responses to ICI treatment (209). Thus, it is intriguing to investigate how tumoral PSAT1 may modulate the tumor microenvironment and whether targeting PSAT1 activity may sensitize EGFR mutant lung tumors to ICI treatment.

Potential role in resistance to EGFR-TKI therapies

Although patients with EGFR-activating mutations exhibit clinical responses to EGFR-TKI treatments, the development of resistance typically occurs within a year (98). A secondary mutation at T750M accounts for 50% of these cases. Mutations in genes involved in downstream pathways or activation of other RTKs represent other potential mechanisms that cause recurrence. Therefore, targeting resistance mechanisms within EGFR signaling underscores the rationale for current combination therapy research.

Recently, targeting metabolic pathways has become a strategy in combination therapies. Dong *et al.* demonstrated that PHGDH was upregulated in erlotinib resistance cells and inhibition

of activity via either inhibitor or silencing induces sensitivity (47). Another study supports this via ectopic expression of PSAT1 in EGFR mutant HCC827 NSCLC cells, which induced resistance to EGFR-TKI treatment (210). A xenograft study with EGFR mutant lung cancer cells demonstrated that combination therapy with a glutaminase (GLS) inhibitor enhances the anti-tumor activity of erlotinib (102). Therefore, it is intriguing whether targeting PSAT1 function together with EGFR-TKI improves patients' outcomes as PSAT1 is the connection between both serine synthesis and glutaminolysis.

Findings that yield new questions

- PKM2 was identified as a PSAT1-associating protein in NSCLC cells and required PSAT1 expression for translocation into the nucleus upon EGFR activation. Interestingly, it is still unclear whether this interaction is completely responsible for the nuclear localization of PKM2. Separately, loss of PSAT1 could impact EGFR signaling, including ERK, that is involved in mediating PKM2 nuclear localization. GPRCA5 is upregulated upon PSAT1 loss and is associated with a better overall and relapse-free survival rate of EGFR mutant lung cancer. A previous study reported that loss of GPRCA5 expression was associated with poor patient outcomes in NSCLC, as it functions as a tumor suppressor in lung tumorigenesis (32). Loss of GPRCA5 expression promotes EGFR signaling activation, which is lost by GPRCA5 restoration (34). Therefore, we speculate that PSAT1 may promote EGFR signaling via suppressing GPRC5A expression.

- Nuclear PKM2 is required for EGFR-induced β-catenin transactivation of target genes involved in cell proliferation, the Warburg effect, and cell invasion in various tumor cell types (113, 158). In our experimental settings, loss of PSAT1 led to decreased β-catenin expression and nuclear PKM2 localization. Nuclear acetyl-mimetic PKM2 re-expression failed to restore β-catenin expression in PSAT1-depleted cells, indicating that regulation of β-catenin expression is independent of nuclear PKM2 function. As the restoration of nuclear PKM2 partially rescued the migration defect due to PSAT1 loss, it is intriguing whether reduced β-catenin expression separately impacts cell motility.

143

- Co-IP analysis with recombinant proteins demonstrated the direct interaction between PSAT1 and PKM2, but not PKM1 (Chapter 2). Furthermore, we found that the pyruvate kinase activity of recombinant PKM2, but not PKM1, increases in the presence of active PSAT1 (Chapter 5, Fig. 52). PSAT1 further induces recPKM2 activity in the presence of allosteric activators: fructose 1,6-bisphosphate (FBP) and serine (Chapter 5, Fig. 53). These results indicate that PSAT1 has a functional consequence on PKM2 activity, at least under these conditions. However, loss of PSAT1 did not lead to reduced cellular pyruvate kinase activity in two NSCLC cell types. This could be due to saturating conditions of PKM2 allosteric regulators and maybe context-dependent or environment-specific (*i.e.,* limiting nutrient conditions). It should also be noted that the activity of PSAT1 was not assessed in the presence of PKM2. It is possible that PSAT1 activity may also be affected by PKM2, as PSAT1 could be a protein substrate for PKM2's protein kinase activity.

Summary

In this dissertation, I investigated a pro-tumorigenic function for PSAT1 that may be beyond its activity within the serine biosynthetic pathway. For this, I employed two independent discovery methodologies: identification of PSAT1 interacting proteins by GST-pull down coupled MS analysis and RNA-seq profiling. PSAT1 interacts with PKM2 and induces recombinant PKM2 pyruvate kinase activity *in vitro*, but the disruption of this interaction by PSAT1 silencing does not impact the cellular pyruvate kinase activity in NSCLC cells. Yet, PSAT1 is required for the EGFR-mediated nuclear localization of PKM2.

PSAT1 loss impairs anchorage-independent growth and cell migration in EGFR-mutant NSCLC cells. Mechanistic studies using a variety of rescue experiments demonstrated that anchorage-independent growth requires the metabolic function of PSAT1 but not nuclear PKM2 activity. On the other hand, nuclear PKM2 contributes to PSAT1-mediated cell migration in EGFR-activated cells. Although my results suggest the involvement of a non-canonical function for PSAT1 in cell migration, rescue studies using a catalytically inactive, localization-dependent PSAT1 mutant are currently ongoing to unravel the full mechanism.

RNA-seq analysis corroborates the phenotypic analysis of PSAT1 loss and provides molecular insight about genomic changes that are regulated by PSAT1. For example, I found differential expression of genes involved in actin cytoskeleton rearrangement that have defined impacts on cell migration, which was confirmed by alterations in F-actin formation. Lastly, I identified a PSAT1-dependent gene signature that had prognostic value for patient outcomes in EGFR-mutant NSCLC.

In conclusion, I postulate that PSAT1 has a novel function that contributes to EGFR-mediated lung tumorigenesis beyond its metabolic activity in SSP. Our findings in this study will guide us as we continue to dissect the contribution of both the canonical and/or non-canonical functions of PSAT1 involved in promoting EGFR-mutant NSCLC.

CHAPTER 5

EXTENDED RESULTS DISCUSSED IN CHAPTER 4

Recombinant PSAT1 enhances pyruvate kinase activity of recombinant PKM2

Our proteomic study revealed an interaction between PSAT1 and PKM2 (Chapter 2); yet a functional role for this interaction on enzymatic activity was unknown. In this small study, we investigated the consequence of recombinant (rec-)PSAT1 on the pyruvate kinase activity of rec-PKM2. We also tested whether rec-PSAT1 would influence the known effects of rec-PKM2 allosteric activators. We modeled our study according to the protocol described in Chaneton *et al.* (57). We found that rec-PKM2 activity *in vitro* increased in a dose-dependent manner in response to rec-PSAT1 concentrations and that heat-inactivation abrogated this effect (Fig. 52). As we have demonstrated that rec-PSAT1 selectively associates with rec-PKM2, the presence of rec-PSAT1 had no effect on rec-PKM1 activity (Fig. 52). Therefore, this result indicates that PSAT1 can induce PKM2, at least in this *in vitro* cell-free system.

To further examine rec-PSAT1's influence on rec-PKM2, we determined the pyruvate kinase activity of rec-PKM2 in the presence of allosteric activators, such as fructose-1,6-bisphosphate (FBP) or serine, in response to different concentrations of rec-PSAT1. We found that the addition of rec-PSAT1 can further activate rec-PKM2 in the presence of the known activator FBP (Fig. 53A). In addition, rec-PSAT1 also stimulated rec-PKM2 in the presence of serine (Fig. 53B). In short, these results demonstrate that rec-PSAT1 induction is specific to rec-PKM2 *in vitro* and may differently regulate rec-PKM2 compared to other known allosteric activators.
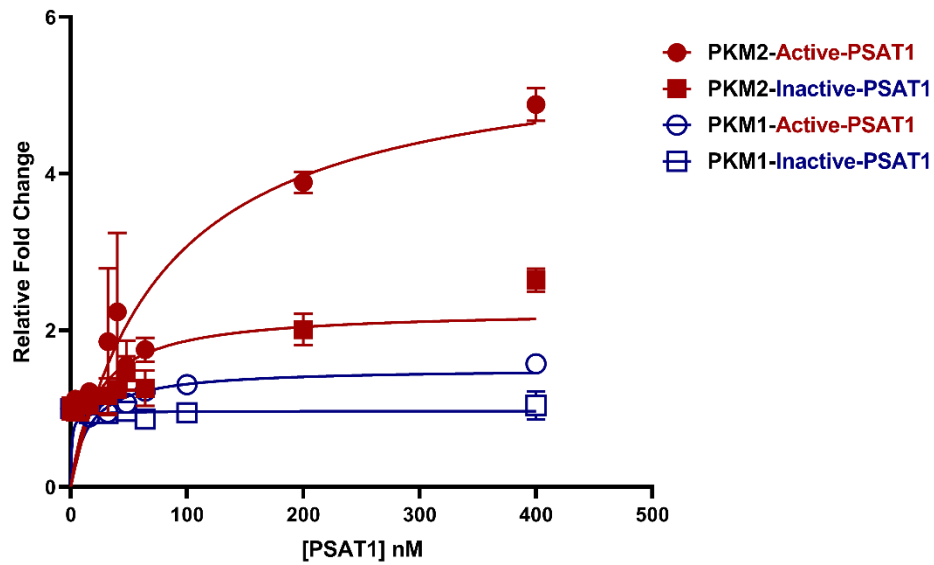
Figure 52. rec-PSAT1 induces the pyruvate kinase activity of rec-PKM2 but not rec-PKM1. Pyruvate kinase activity was assessed by quantifying levels of ATP using luminescent Kinase-Glo reagent (Promega) after addition of either rec-PKM2 or rec-PKM1 in the presence of increasing concentrations of rec-PSAT1. To verify requirement for active rec-PSAT1, the protein was inactivated via boiling for 10 minutes prior to addition to the *in vitro* reaction.
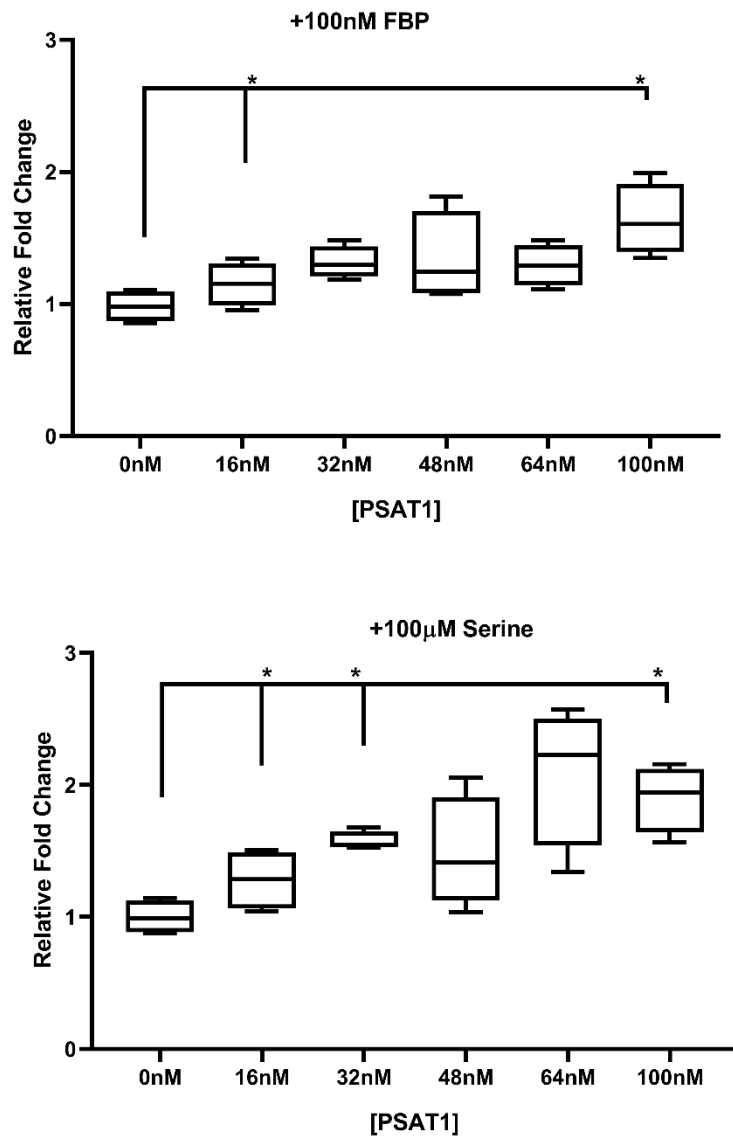
Figure 53. rec-PSAT1 further induces rec-PKM2 activity in the presence of allosteric activators. Rec-PKM2's pyruvate kinase activity was followed by quantifying levels of ATP using luminescent Kinase-Glo reagent (Promega) in the presence of **A)** FBP or **B)** serine and increasing concentrations of rec-PSAT1. Rec-PKM2 activity in the presence of the allosteric activator but in the absence of rec-PSAT1 was set to 1. * , p≤ 0.05

Loss of PHGDH does not impact the nuclear localization of PKM2

As shown in chapter 2, PSAT1 is required for EGFR-mediated PKM2 nuclear localization. We then questioned whether other SSP enzymes may also be involved in this regulation. PHGDH, the rate-limiting enzyme, was stably silenced in PC9 cells and cell fractionation was performed to examine protein localization. Unlike PSAT1, loss of PHGDH did not affect the nuclear localization of PKM2 (Fig. 54). However, we also observed the nuclear localization of PHGDH that is dependent on EGFR-signaling. This implies that there may be a nuclear requirement for SSP activity in EGFR activated NSCLC.

Next, we performed wound-healing assays to assess the effect of PHGDH loss in cell migration. We found that PHGDH depletion resulted in only a slight reduction in cell migration, which was considerably less than that observed with PSAT1 loss (Fig. 55). Taken together, these results suggest that inhibition of serine biosynthesis via PHGDH depletion may not fully recapitulate the loss of PSAT1 phenotype in EGFR-mediated PKM2 nuclear localization and cell migration, potentially due to PSAT1's selective requirement for PKM2 nuclear translocation.
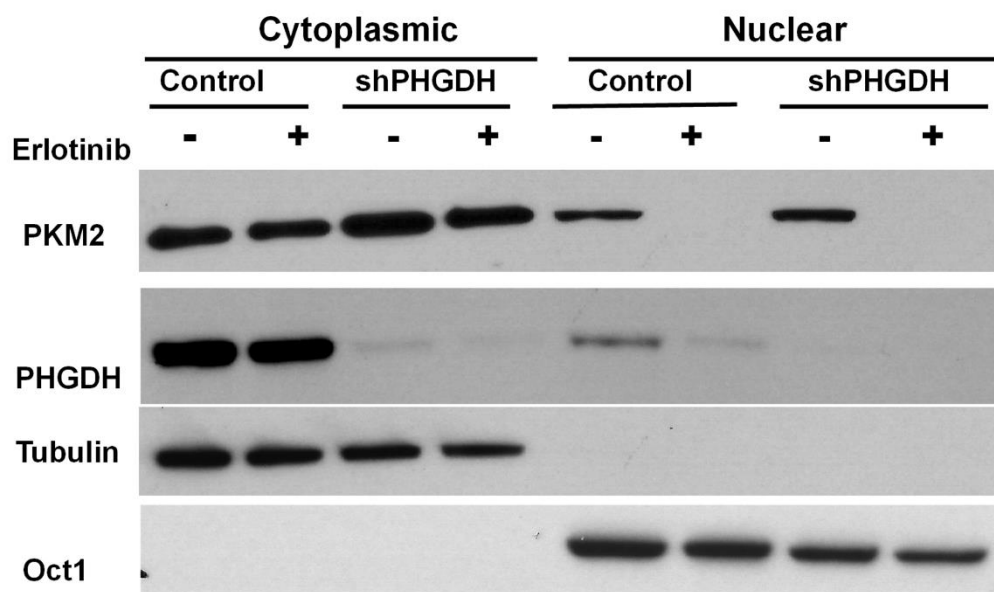
Figure 54. Loss of PHGDH does not affect the nuclear localization of PKM2 in PC9 cells. EGFR-mutant PC9 cells stably expressing Control or PHGDH shRNA were treated with 1 μM of erlotinib for 48 hrs. Cytoplasmic and nuclear fractions were examined by immunoblot analysis using anti-PKM2 and anti-PHGDH antibodies. OCT1 and α-tubulin served as loading controls for nuclear and cytoplasmic compartments, respectively. Shown are representative images from three separate experiments.
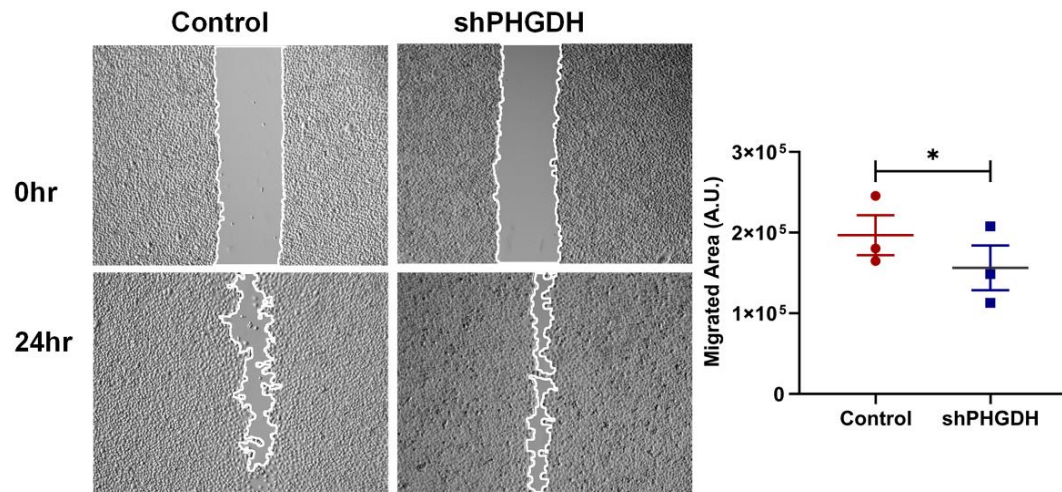
Figure 55. Cell migration is slightly affected upon PHGDH depletion in PC9 cells. Wound healing assay of serum-starved PC9 cells expressing Control or PHGDH-specific shRNA. Representative images at 0 hr and 24 hr with migrating cells demarcated by white continuous lines. Data is presented as migrated area after 24 hours and shown is mean ± SE from three independent experiments. * $p < 0.005$.

REFERENCES

1. Yang Y, Wu J, Cai J, He Z, Yuan J, Zhu X, et al. PSAT1 regulates cyclin D1 degradation and sustains proliferation of non-small cell lung cancer cells. Int J Cancer. 2015;136(4):E39-50.

2. Chan YC, Chang YC, Chuang HH, Yang YC, Lin YF, Huang MS, et al. Overexpression of PSAT1 promotes metastasis of lung adenocarcinoma by suppressing the IRF1-IFNgamma axis. Oncogene. 2020;39(12):2509-22.

3. Shen S, Zhang R, Guo Y, Loehrer E, Wei Y, Zhu Y, et al. A multi-omic study reveals BTG2 as a reliable prognostic marker for early-stage non-small cell lung cancer. Mol Oncol. 2018;12(6):913-24.

4. Director's Challenge Consortium for the Molecular Classification of Lung A, Shedden K, Taylor JM, Enkemann SA, Tsao MS, Yeatman TJ, et al. Gene expression-based survival prediction in lung adenocarcinoma: a multi-site, blinded validation study. Nat Med. 2008;14(8):822-7.

5. Vazquez A, Kamphorst JJ, Markert EK, Schug ZT, Tardito S, Gottlieb E. Cancer metabolism at a glance. J Cell Sci. 2016;129(18):3367-73.

6. Pavlova NN, Thompson CB. The Emerging Hallmarks of Cancer Metabolism. Cell Metab. 2016;23(1):27-47.

7. Hsieh CH, Chou YT, Kuo MH, Tsai HP, Chang JL, Wu CW. A targetable HB-EGF-CITED4 axis controls oncogenesis in lung cancer. Oncogene. 2017;36(21):2946-56.

8. Kaira K, Ohde Y, Nakagawa K, Okumura T, Murakami H, Takahashi T, et al. Thymidylate synthase expression is closely associated with outcome in patients with pulmonary adenocarcinoma. Med Oncol. 2012;29(3):1663-72.

9. Liberti MV, Locasale JW. The Warburg Effect: How Does it Benefit Cancer Cells? Trends Biochem Sci. 2016;41(3):211-8.

10. Shiba-Ishii A, Noguchi M. Aberrant stratifin overexpression is regulated by tumor-associated CpG demethylation in lung adenocarcinoma. Am J Pathol. 2012;180(4):1653-62.

11. Radhakrishnan VM, Jensen TJ, Cui H, Futscher BW, Martinez JD. Hypomethylation of the 14-3-3sigma promoter leads to increased expression in non-small cell lung cancer. Genes Chromosomes Cancer. 2011;50(10):830-6.

12. Shiba-Ishii A, Kano J, Morishita Y, Sato Y, Minami Y, Noguchi M. High expression of stratifin is a universal abnormality during the course of malignant progression of early-stage lung adenocarcinoma. Int J Cancer. 2011;129(10):2445-53.

13. Shiba-Ishii A, Hong J, Hirokawa T, Kim Y, Nakagawa T, Sakashita S, et al. Stratifin Inhibits SCF(FBW7) Formation and Blocks Ubiquitination of Oncoproteins during the Course of Lung Adenocarcinogenesis. Clin Cancer Res. 2019;25(9):2809-20.

14. Wu DM, Liu T, Deng SH, Han R, Xu Y. SLC39A4 expression is associated with enhanced cell migration, cisplatin resistance, and poor survival in non-small cell lung cancer. Sci Rep. 2017;7(1):7211.

15. Mattaini KR, Sullivan MR, Vander Heiden MG. The importance of serine metabolism in cancer. J Cell Biol. 2016;214(3):249-57.

16. Locasale JW. Serine, glycine and one-carbon units: cancer metabolism in full circle. Nat Rev Cancer. 2013;13(8):572-83.

17. Labuschagne CF, van den Broek NJ, Mackay GM, Vousden KH, Maddocks OD. Serine, but not glycine, supports one-carbon metabolism and proliferation of cancer cells. Cell Rep. 2014;7(4):1248-58.

18. Maddocks OD, Berkers CR, Mason SM, Zheng L, Blyth K, Gottlieb E, et al. Serine starvation induces stress and p53-dependent metabolic remodelling in cancer cells. Nature. 2013;493(7433):542-6.

19. Locasale JW, Grassian AR, Melman T, Lyssiotis CA, Mattaini KR, Bass AJ, et al. Phosphoglycerate dehydrogenase diverts glycolytic flux and contributes to oncogenesis. Nat Genet. 2011;43(9):869-74.

20. Pacold ME, Brimacombe KR, Chan SH, Rohde JM, Lewis CA, Swier LJ, et al. A PHGDH inhibitor reveals coordination of serine synthesis and one-carbon unit fate. Nat Chem Biol. 2016;12(6):452-8.

21. Romero-Ventosa EY, Blanco-Prieto S, Gonzalez-Pineiro AL, Rodriguez-Berrocal FJ, Pineiro-Corrales G, Paez de la Cadena M. Pretreatment levels of the serum biomarkers CEA, CYFRA 21-1, SCC and the soluble EGFR and its ligands EGF, TGF-alpha, HB-EGF in the prediction of outcome in erlotinib treated non-small-cell lung cancer patients. Springerplus. 2015;4:171.

22. Liu ZY, Wu T, Li Q, Wang MC, Jing L, Ruan ZP, et al. Notch Signaling Components: Diverging Prognostic Indicators in Lung Adenocarcinoma. Medicine (Baltimore). 2016;95(20):e3715.

23. Tu Z, Deng X, Hou S, Feng A, Zhang Q. UHRF1 predicts poor prognosis by triggering cell cycle in lung adenocarcinoma. J Cell Mol Med. 2020;24(14):8069-77.

24. Chen L, Zhou Q, Xu B, Liu J, Shi L, Zhu D, et al. MT2-MMP expression associates with tumor progression and angiogenesis in human lung cancer. Int J Clin Exp Pathol. 2014;7(6):3469-77.

25. Liu Y, Sun X, Feng J, Deng LL, Liu Y, Li B, et al. MT2-MMP induces proteolysis and leads to EMT in carcinomas. Oncotarget. 2016;7(30):48193-205.

26. Sanada H, Seki N, Mizuno K, Misono S, Uchida A, Yamada Y, et al. Involvement of Dual Strands of miR-143 (miR-143-5p and miR-143-3p) and Their Target Oncogenes in the Molecular Pathogenesis of Lung Adenocarcinoma. Int J Mol Sci. 2019;20(18).

27. Yin J, Fu W, Dai L, Jiang Z, Liao H, Chen W, et al. ANKRD22 promotes progression of non-small cell lung cancer through transcriptional up-regulation of E2F1. Sci Rep. 2017;7(1):4430.

28. Yang M, Vousden KH. Serine and one-carbon metabolism in cancer. Nat Rev Cancer. 2016;16(10):650-62.

29. Li S, Jiang Z, Li Y, Xu Y. Prognostic significance of minichromosome maintenance mRNA expression in human lung adenocarcinoma. Oncol Rep. 2019;42(6):2279-92.

30. Cheung CHY, Hsu CL, Chen KP, Chong ST, Wu CH, Huang HC, et al. MCM2-regulated functional networks in lung cancer by multi-dimensional proteomic approach. Sci Rep. 2017;7(1):13302.

31. Goswami MT, Chen G, Chakravarthi BV, Pathi SS, Anand SK, Carskadon SL, et al. Role and regulation of coordinately expressed de novo purine biosynthetic enzymes PPAT and PAICS in lung cancer. Oncotarget. 2015;6(27):23445-61.

32.   Jin E, Wang W, Fang M, Wang W, Xie R, Zhou H, et al. Clinical significance of reduced GPRC5A expression in surgically resected non-small cell lung cancer. Oncol Lett. 2019;17(1):502-7.

33.   Lin X, Zhong S, Ye X, Liao Y, Yao F, Yang X, et al. EGFR phosphorylates and inhibits lung tumor suppressor GPRC5A in lung cancer. Mol Cancer. 2014;13:233.

34.   Zhong S, Yin H, Liao Y, Yao F, Li Q, Zhang J, et al. Lung Tumor Suppressor GPRC5A Binds EGFR and Restrains Its Effector Signaling. Cancer Res. 2015;75(9):1801-14.

35.   Kwon M, Lee SJ, Reddy S, Rybak Y, Adem A, Libutti SK. Down-regulation of Filamin A interacting protein 1-like Is associated with promoter methylation and an invasive phenotype in breast, colon, lung and pancreatic cancers [corrected]. PLoS One. 2013;8(12):e82620.

36.   Kwon M, Lee SJ, Wang Y, Rybak Y, Luna A, Reddy S, et al. Filamin A interacting protein 1-like inhibits WNT signaling and MMP expression to suppress cancer cell invasion and metastasis. Int J Cancer. 2014;135(1):48-60.

37.   Yang CYW, L.; Mu, D. C.; Li, F. F.; Shen, H.; Yang, X. R.; Zheng, S., Y. High Expression of CDCA7 Promotes Cell Proliferation, Migration, Invasion and Apoptosis in Non-Small-Cell Lung Cancer. Journal of Nutritional Oncology. 2020;5(2).

38.   Maddocks OD, Labuschagne CF, Adams PD, Vousden KH. Serine Metabolism Supports the Methionine Cycle and DNA/RNA Methylation through De Novo ATP Synthesis in Cancer Cells. Mol Cell. 2016;61(2):210-21.

39.   Kim H, Park YJ. Links between Serine Biosynthesis Pathway and Epigenetics in Cancer Metabolism. Clin Nutr Res. 2018;7(3):153-60.

40.   Possemato R, Marks KM, Shaul YD, Pacold ME, Kim D, Birsoy K, et al. Functional genomics reveal that the serine synthesis pathway is essential in breast cancer. Nature. 2011;476(7360):346-50.

41.   Mullarky E, Lucki NC, Beheshti Zavareh R, Anglin JL, Gomes AP, Nicolay BN, et al. Identification of a small molecule inhibitor of 3-phosphoglycerate dehydrogenase to target serine biosynthesis in cancers. Proc Natl Acad Sci U S A. 2016;113(7):1778-83.

42.   Zhang B, Zheng A, Hydbring P, Ambroise G, Ouchida AT, Goiny M, et al. PHGDH Defines a Metabolic Subtype in Lung Adenocarcinomas with Poor Prognosis. Cell Rep. 2017;19(11):2289-303.

43.   Gao S, Ge A, Xu S, You Z, Ning S, Zhao Y, et al. PSAT1 is regulated by ATF4 and enhances cell proliferation via the GSK3beta/beta-catenin/cyclin D1 signaling pathway in ER-negative breast cancer. J Exp Clin Cancer Res. 2017;36(1):179.

44.   Amelio I, Markert EK, Rufini A, Antonov AV, Sayan BS, Tucci P, et al. p73 regulates serine biosynthesis in cancer. Oncogene. 2014;33(42):5039-46.

45.   DeNicola GM, Chen PH, Mullarky E, Sudderth JA, Hu Z, Wu D, et al. NRF2 regulates serine biosynthesis in non-small cell lung cancer. Nat Genet. 2015;47(12):1475-81.

46.   Kottakis F, Nicolay BN, Roumane A, Karnik R, Gu H, Nagle JM, et al. LKB1 loss links serine metabolism to DNA methylation and tumorigenesis. Nature. 2016;539(7629):390-5.

47.   Dong JK, Lei HM, Liang Q, Tang YB, Zhou Y, Wang Y, et al. Overcoming erlotinib resistance in EGFR mutation-positive lung adenocarcinomas through repression of phosphoglycerate dehydrogenase. Theranostics. 2018;8(7):1808-23.

48.   Zhao E, Ding J, Xia Y, Liu M, Ye B, Choi JH, et al. KDM4C and ATF4 Cooperate in Transcriptional Control of Amino Acid Metabolism. Cell Rep. 2016;14(3):506-19.

49.   Ding J, Li T, Wang X, Zhao E, Choi JH, Yang L, et al. The histone H3 methyltransferase G9A epigenetically activates the serine-glycine synthesis pathway to sustain cancer cell survival and proliferation. Cell Metab. 2013;18(6):896-907.

50. Jin N, Bi A, Lan X, Xu J, Wang X, Liu Y, et al. Identification of metabolic vulnerabilities of receptor tyrosine kinases-driven cancer. Nat Commun. 2019;10(1):2701.

51. Xia Y, Ye B, Ding J, Yu Y, Alptekin A, Thangaraju M, et al. Metabolic Reprogramming by MYCN Confers Dependence on the Serine-Glycine-One-Carbon Biosynthetic Pathway. Cancer Res. 2019;79(15):3837-50.

52. Ye J, Mancuso A, Tong X, Ward PS, Fan J, Rabinowitz JD, et al. Pyruvate kinase M2 promotes de novo serine synthesis to sustain mTORC1 activity and cell proliferation. Proc Natl Acad Sci U S A. 2012;109(18):6904-9.

53. Riscal R, Schrepfer E, Arena G, Cisse MY, Bellvert F, Heuillet M, et al. Chromatin-Bound MDM2 Regulates Serine Metabolism and Redox Homeostasis Independently of p53. Mol Cell. 2016;62(6):890-902.

54. Sun L, Song L, Wan Q, Wu G, Li X, Wang Y, et al. cMyc-mediated activation of serine biosynthesis pathway is critical for cancer progression under nutrient deprivation conditions. Cell Res. 2015;25(4):429-44.

55. Wu S, Le H. Dual roles of PKM2 in cancer metabolism. Acta Biochim Biophys Sin (Shanghai). 2013;45(1):27-35.

56. Prakasam G, Iqbal MA, Bamezai RNK, Mazurek S. Posttranslational Modifications of Pyruvate Kinase M2: Tweaks that Benefit Cancer. Front Oncol. 2018;8:22.

57. Chaneton B, Hillmann P, Zheng L, Martin ACL, Maddocks ODK, Chokkathukalam A, et al. Serine is a natural ligand and allosteric activator of pyruvate kinase M2. Nature. 2012;491(7424):458-62.

58. Wiese EK, Hitosugi T. Tyrosine Kinase Signaling in Cancer Metabolism: PKM2 Paradox in the Warburg Effect. Front Cell Dev Biol. 2018;6:79.

59. Abeywardana T, Oh M, Jiang L, Yang Y, Kong M, Song J, et al. CARM1 suppresses de novo serine synthesis by promoting PKM2 activity. J Biol Chem. 2018;293(39):15290-303.

60. Anastasiou D, Yu Y, Israelsen WJ, Jiang JK, Boxer MB, Hong BS, et al. Pyruvate kinase M2 activators promote tetramer formation and suppress tumorigenesis. Nat Chem Biol. 2012;8(10):839-47.

61. Kung C, Hixon J, Choe S, Marks K, Gross S, Murphy E, et al. Small molecule activation of PKM2 in cancer cells induces serine auxotrophy. Chem Biol. 2012;19(9):1187-98.

62. Parnell KM, Foulks JM, Nix RN, Clifford A, Bullough J, Luo B, et al. Pharmacologic activation of PKM2 slows lung tumor xenograft growth. Mol Cancer Ther. 2013;12(8):1453-60.

63. Abdelfattah F, Kariminejad A, Kahlert AK, Morrison PJ, Gumus E, Mathews KD, et al. Expanding the genotypic and phenotypic spectrum of severe serine biosynthesis disorders. Hum Mutat. 2020;41(9):1615-28.

64. Acuna-Hidalgo R, Schanze D, Kariminejad A, Nordgren A, Kariminejad MH, Conner P, et al. Neu-Laxova syndrome is a heterogeneous metabolic disorder caused by defects in enzymes of the L-serine biosynthesis pathway. Am J Hum Genet. 2014;95(3):285-93.

65. Sirr A, Lo RS, Cromie GA, Scott AC, Ashmead J, Heyesus M, et al. A yeast-based complementation assay elucidates the functional impact of 200 missense variants in human PSAT1. J Inherit Metab Dis. 2020;43(4):758-69.

66. Qian C, Xia Y, Ren Y, Yin Y, Deng A. Identification and validation of PSAT1 as a potential prognostic factor for predicting clinical outcomes in patients with colorectal carcinoma. Oncol Lett. 2017;14(6):8014-20.

67. Liao KM, Chao TB, Tian YF, Lin CY, Lee SW, Chuang HY, et al. Overexpression of the PSAT1 Gene in Nasopharyngeal Carcinoma Is an Indicator of Poor Prognosis. Journal of Cancer. 2016;7(9):1088-94.

68. Wang X, Min S, Liu H, Wu N, Liu X, Wang T, et al. Nf1 loss promotes Kras-driven lung adenocarcinoma and results in Psat1-mediated glutamate dependence. EMBO Mol Med. 2019;11(6).

69. Liu B, Jia Y, Cao Y, Wu S, Jiang H, Sun X, et al. Overexpression of Phosphoserine Aminotransferase 1 (PSAT1) Predicts Poor Prognosis and Associates with Tumor Progression in Human Esophageal Squamous Cell Carcinoma. Cell Physiol Biochem. 2016;39(1):395-406.

70. Zheng MJ, Li X, Hu YX, Dong H, Gou R, Nie X, et al. Identification of molecular marker associated with ovarian cancer prognosis using bioinformatics analysis and experiments. J Cell Physiol. 2019;234(7):11023-36.

71. Metcalf S, Dougherty S, Kruer T, Hasan N, Biyik-Sit R, Reynolds L, et al. Selective loss of phosphoserine aminotransferase 1 (PSAT1) suppresses migration, invasion, and experimental metastasis in triple negative breast cancer. Clin Exp Metastasis. 2019.

72. Zhou YY, Chen LP, Zhang Y, Hu SK, Dong ZJ, Wu M, et al. Integrated transcriptomic analysis reveals hub genes involved in diagnosis and prognosis of pancreatic cancer. Mol Med. 2019;25(1):47.

73. Zhang Y, Li J, Dong X, Meng D, Zhi X, Yuan L, et al. PSAT1 Regulated Oxidation-Reduction Balance Affects the Growth and Prognosis of Epithelial Ovarian Cancer. Onco Targets Ther. 2020;13:5443-53.

74. Vie N, Copois V, Bascoul-Mollevi C, Denis V, Bec N, Robert B, et al. Overexpression of phosphoserine aminotransferase PSAT1 stimulates cell growth and increases chemoresistance of colon cancer cells. Mol Cancer. 2008;7:14.

75. Martens JW, Nimmrich I, Koenig T, Look MP, Harbeck N, Model F, et al. Association of DNA methylation of phosphoserine aminotransferase with response to endocrine therapy in patients with recurrent breast cancer. Cancer Res. 2005;65(10):4101-17.

76. Metcalf S, Petri BJ, Kruer T, Green B, Dougherty S, Wittliff JL, et al. Serine synthesis influences tamoxifen response in ER+ human breast carcinoma. Endocr Relat Cancer. 2021;28(1):27-37.

77. Yan S, Jiang H, Fang S, Yin F, Wang Z, Jia Y, et al. MicroRNA-340 Inhibits Esophageal Cancer Cell Growth and Invasion by Targeting Phosphoserine Aminotransferase 1. Cell Physiol Biochem. 2015;37(1):375-86.

78. Sun C, Zhang X, Chen Y, Jia Q, Yang J, Shu Y. MicroRNA-365 suppresses cell growth and invasion in esophageal squamous cell carcinoma by modulating phosphoserine aminotransferase 1. Cancer Manag Res. 2018;10:4581-90.

79. Dai J, Wei R, Zhang P, Kong B. Overexpression of microRNA-195-5p reduces cisplatin resistance and angiogenesis in ovarian cancer by inhibiting the PSAT1-dependent GSK3beta/beta-catenin signaling pathway. J Transl Med. 2019;17(1):190.

80. Wang H, Cui L, Li D, Fan M, Liu Z, Liu C, et al. Overexpression of PSAT1 regulated by G9A sustains cell proliferation in colorectal cancer. Signal Transduct Target Ther. 2020;5(1):47.

81. Fang Y, Liang X, Xu J, Cai X. miR-424 targets AKT3 and PSAT1 and has a tumor-suppressive role in human colorectal cancer. Cancer Manag Res. 2018;10:6537-47.

82. Coloff JL, Murphy JP, Braun CR, Harris IS, Shelton LM, Kami K, et al. Differential Glutamate Metabolism in Proliferating and Quiescent Mammary Epithelial Cells. Cell Metab. 2016;23(5):867-80.

83. Robertson H, Hayes JD, Sutherland C. A partnership with the proteasome; the destructive nature of GSK3. Biochem Pharmacol. 2018;147:77-92.

84. Beurel E, Grieco SF, Jope RS. Glycogen synthase kinase-3 (GSK3): regulation, actions, and diseases. Pharmacol Ther. 2015;148:114-31.

85. Li L, Wei Y, To C, Zhu CQ, Tong J, Pham NA, et al. Integrated omic analysis of lung cancer reveals metabolism proteome signatures with prognostic impact. Nat Commun. 2014;5:5469.

86. Zhang WC, Shyh-Chang N, Yang H, Rai A, Umashankar S, Ma S, et al. Glycine decarboxylase activity drives non-small cell lung cancer tumor-initiating cells and tumorigenesis. Cell. 2012;148(1-2):259-72.

87. Chu YW, Yang PC, Yang SC, Shyu YC, Hendrix MJ, Wu R, et al. Selection of invasive and metastatic subpopulations from a human lung adenocarcinoma cell line. Am J Respir Cell Mol Biol. 1997;17(3):353-60.

88. ACS. Cancer Facts and Statistics. Atlanta: American Cancer Society; 2020.

89. NAMN Howlader A-MN, Martin Krapcho, Jessica Garshell, D Miller, SF Altekruse, CL Kosary, M Yu, J Ruhl, Z Tatalovich, A Mariotto, DR Lewis, HS Chen, EJ Feuer, KA Cronin. SEER cancer statistics review, 1975–2011. Bethesda, MD: National Cancer Institute. 2014;19.

90. Tsao AS, Scagliotti GV, Bunn PA, Jr., Carbone DP, Warren GW, Bai C, et al. Scientific Advances in Lung Cancer 2015. J Thorac Oncol. 2016;11(5):613-38.

91. Cheng L, Zhang S, Alexander R, Yao Y, MacLennan GT, Pan CX, et al. The landscape of EGFR pathways and personalized management of non-small-cell lung cancer. Future Oncol. 2011;7(4):519-41.

92. Siegelin MD, Borczuk AC. Epidermal growth factor receptor mutations in lung adenocarcinoma. Lab Invest. 2014;94(2):129-37.

93. Paz-Ares L, Soulieres D, Melezinek I, Moecks J, Keil L, Mok T, et al. Clinical outcomes in non-small-cell lung cancer patients with EGFR mutations: pooled analysis. J Cell Mol Med. 2010;14(1-2):51-69.

94. Bethune G, Bethune D, Ridgway N, Xu Z. Epidermal growth factor receptor (EGFR) in lung cancer: an overview and update. J Thorac Dis. 2010;2(1):48-51.

95. Jurisic V, Obradovic J, Pavlovic S, Djordjevic N. Epidermal Growth Factor Receptor Gene in Non-Small-Cell Lung Cancer: The Importance of Promoter Polymorphism Investigation. Anal Cell Pathol (Amst). 2018;2018:6192187.

96. Mitsudomi T, Yatabe Y. Epidermal growth factor receptor in relation to tumor development: EGFR gene and cancer. FEBS J. 2010;277(2):301-8.

97. Brambilla E, Gazdar A. Pathogenesis of lung cancer signalling pathways: roadmap for therapies. Eur Respir J. 2009;33(6):1485-97.

98. Grigoriu B, Berghmans T, Meert AP. Management of EGFR mutated nonsmall cell lung carcinoma patients. Eur Respir J. 2015;45(4):1132-41.

99. Makinoshima H, Takita M, Matsumoto S, Yagishita A, Owada S, Esumi H, et al. Epidermal growth factor receptor (EGFR) signaling regulates global metabolic pathways in EGFR-mutated lung adenocarcinoma. J Biol Chem. 2014;289(30):20813-23.

100. De Rosa V, Iommelli F, Monti M, Fonti R, Votta G, Stoppelli MP, et al. Reversal of Warburg Effect and Reactivation of Oxidative Phosphorylation by Differential Inhibition of EGFR Signaling Pathways in Non-Small Cell Lung Cancer. Clin Cancer Res. 2015;21(22):5110-20.

101. Kim JH, Nam B, Choi YJ, Kim SY, Lee JE, Sung KJ, et al. Enhanced Glycolysis Supports Cell Survival in EGFR-Mutant Lung Adenocarcinoma by Inhibiting Autophagy-Mediated EGFR Degradation. Cancer Res. 2018;78(16):4482-96.

102. Momcilovic M, Bailey ST, Lee JT, Fishbein MC, Magyar C, Braas D, et al. Targeted Inhibition of EGFR and Glutaminase Induces Metabolic Crisis in EGFR Mutant Lung Cancer. Cell Rep. 2017;18(3):601-10.

103. Zhang J, Song F, Zhao X, Jiang H, Wu X, Wang B, et al. EGFR modulates monounsaturated fatty acid synthesis through phosphorylation of SCD1 in lung cancer. Mol Cancer. 2017;16(1):127.

104. Huangyang P, Simon MC. Hidden features: exploring the non-canonical functions of metabolic enzymes. Dis Model Mech. 2018;11(8).

105. Park SM, Seo EH, Bae DH, Kim SS, Kim J, Lin W, et al. Phosphoserine Phosphatase Promotes Lung Cancer Progression through the Dephosphorylation of IRS-1 and a Noncanonical L-Serine-Independent Pathway. Mol Cells. 2019;42(8):604-16.

106. Lee SM, Kim JH, Cho EJ, Youn HD. A nucleocytoplasmic malate dehydrogenase regulates p53 transcriptional activity in response to metabolic stress. Cell Death Differ. 2009;16(5):738-48.

107. Zhang D, Jin N, Sun W, Li X, Liu B, Xie Z, et al. Phosphoglycerate mutase 1 promotes cancer cell migration independent of its metabolic activity. Oncogene. 2017;36(20):2900-9.

108. Lu S, Wang Y. Nonmetabolic functions of metabolic enzymes in cancer development. Cancer Commun (Lond). 2018;38(1):63.

109. Snaebjornsson MT, Schulze A. Non-canonical functions of enzymes facilitate cross-talk between cell metabolic and regulatory pathways. Exp Mol Med. 2018;50(4):34.

110. Lv L, Xu YP, Zhao D, Li FL, Wang W, Sasaki N, et al. Mitogenic and oncogenic stimulation of K433 acetylation promotes PKM2 protein kinase activity and nuclear localization. Mol Cell. 2013;52(3):340-52.

111. Yang W, Xia Y, Hawke D, Li X, Liang J, Xing D, et al. PKM2 phosphorylates histone H3 and promotes gene transcription and tumorigenesis. Cell. 2012;150(4):685-96.

112. Li Q, Zhang D, Chen X, He L, Li T, Xu X, et al. Nuclear PKM2 contributes to gefitinib resistance via upregulation of STAT3 activation in colorectal cancer. Scientific reports. 2015;5:16082.

113. Yang W, Xia Y, Ji H, Zheng Y, Liang J, Huang W, et al. Nuclear PKM2 regulates beta-catenin transactivation upon EGFR activation. Nature. 2011;480(7375):118-22.

114. Gao X, Wang H, Yang JJ, Liu X, Liu ZR. Pyruvate kinase M2 regulates gene transcription by acting as a protein kinase. Mol Cell. 2012;45(5):598-609.

115. Jiang Y, Li X, Yang W, Hawke DH, Zheng Y, Xia Y, et al. PKM2 regulates chromosome segregation and mitosis progression of tumor cells. Mol Cell. 2014;53(1):75-87.

116. Jiang Y, Wang Y, Wang T, Hawke DH, Zheng Y, Li X, et al. PKM2 phosphorylates MLC2 and regulates cytokinesis of tumour cells. Nat Commun. 2014;5:5566.

117. Liang J, Cao R, Wang X, Zhang Y, Wang P, Gao H, et al. Mitochondrial PKM2 regulates oxidative stress-induced apoptosis by stabilizing Bcl2. Cell Res. 2017;27(3):329-51.

118. Li X, Jiang Y, Meisenhelder J, Yang W, Hawke DH, Zheng Y, et al. Mitochondria-Translocated PGK1 Functions as a Protein Kinase to Coordinate Glycolysis and the TCA Cycle in Tumorigenesis. Mol Cell. 2016;61(5):705-19.

119. Qian X, Li X, Cai Q, Zhang C, Yu Q, Jiang Y, et al. Phosphoglycerate Kinase 1 Phosphorylates Beclin1 to Induce Autophagy. Mol Cell. 2017;65(5):917-31 e6.

120. Yu X, Ma R, Wu Y, Zhai Y, Li S. Reciprocal Regulation of Metabolic Reprogramming and Epigenetic Modifications in Cancer. Front Genet. 2018;9:394.

121. Lee JV, Carrer A, Shah S, Snyder NW, Wei S, Venneti S, et al. Akt-dependent metabolic reprogramming regulates tumor cell histone acetylation. Cell Metab. 2014;20(2):306-19.

122. Sutendra G, Kinnaird A, Dromparis P, Paulin R, Stenson TH, Haromy A, et al. A nuclear pyruvate dehydrogenase complex is important for the generation of acetyl-CoA and histone acetylation. Cell. 2014;158(1):84-97.

123. Campbell SL, Wellen KE. Metabolic Signaling to the Nucleus in Cancer. Mol Cell. 2018;71(3):398-408.

124. Sivanand S, Rhoades S, Jiang Q, Lee JV, Benci J, Zhang J, et al. Nuclear Acetyl-CoA Production by ACLY Promotes Homologous Recombination. Mol Cell. 2017;67(2):252-65 e6.

125. Jiang Y, Qian X, Shen J, Wang Y, Li X, Liu R, et al. Local generation of fumarate promotes DNA repair through inhibition of histone H3 demethylation. Nat Cell Biol. 2015;17(9):1158-68.

126. Li X, Qian X, Lu Z. Local histone acetylation by ACSS2 promotes gene transcription for lysosomal biogenesis and autophagy. Autophagy. 2017;13(10):1790-1.

127. Wang Y, Guo YR, Liu K, Yin Z, Liu R, Xia Y, et al. KAT2A coupled with the alpha-KGDH complex acts as a histone H3 succinyltransferase. Nature. 2017;552(7684):273-7.

128. Katoh Y, Ikura T, Hoshikawa Y, Tashiro S, Ito T, Ohta M, et al. Methionine adenosyltransferase II serves as a transcriptional corepressor of Maf oncoprotein. Mol Cell. 2011;41(5):554-66.

129. Christofk HR, Vander Heiden MG, Wu N, Asara JM, Cantley LC. Pyruvate kinase M2 is a phosphotyrosine-binding protein. Nature. 2008;452(7184):181-6.

130. Yang YC, Cheng TY, Huang SM, Su CY, Yang PW, Lee JM, et al. Cytosolic PKM2 stabilizes mutant EGFR protein expression through regulating HSP90-EGFR association. Oncogene. 2016;35(26):3387-98.

131. Mukherjee J, Ohba S, See WL, Phillips JJ, Molinaro AM, Pieper RO. PKM2 uses control of HuR localization to regulate p27 and cell cycle progression in human glioblastoma cells. Int J Cancer. 2016;139(1):99-111.

132. Li B, Qiu B, Lee DS, Walton ZE, Ochocki JD, Mathew LK, et al. Fructose-1,6-bisphosphatase opposes renal carcinoma progression. Nature. 2014;513(7517):251-5.

133. Liu J, Guo S, Li Q, Yang L, Xia Z, Zhang L, et al. Phosphoglycerate dehydrogenase induces glioma cells proliferation and invasion by stabilizing forkhead box M1. J Neurooncol. 2013;111(3):245-55.

134. Ma X, Li B, Liu J, Fu Y, Luo Y. Phosphoglycerate dehydrogenase promotes pancreatic cancer development by interacting with eIF4A1 and eIF4E. J Exp Clin Cancer Res. 2019;38(1):66.

135. Fan J, Teng X, Liu L, Mattaini KR, Looper RE, Vander Heiden MG, et al. Human phosphoglycerate dehydrogenase produces the oncometabolite D-2-hydroxyglutarate. ACS Chem Biol. 2015;10(2):510-6.

136. Hwang IY, Kwak S, Lee S, Kim H, Lee SE, Kim JH, et al. Psat1-Dependent Fluctuations in alpha-Ketoglutarate Affect the Timing of ESC Differentiation. Cell Metab. 2016;24(3):494-501.

137. Hanahan D, Weinberg RA. Hallmarks of cancer: the next generation. Cell. 2011;144(5):646-74.

138. Choi YK, Park KG. Targeting Glutamine Metabolism for Cancer Treatment. Biomol Ther (Seoul). 2018;26(1):19-28.

139. Ruiz-Perez MV, Sanchez-Jimenez F, Alonso FJ, Segura JA, Marquez J, Medina MA. Glutamine, glucose and other fuels for cancer. Curr Pharm Des. 2014;20(15):2557-79.

140. Lunt SY, Vander Heiden MG. Aerobic glycolysis: meeting the metabolic requirements of cell proliferation. Annu Rev Cell Dev Biol. 2011;27:441-64.

141. Yu X, Li S. Non-metabolic functions of glycolytic enzymes in tumorigenesis. Oncogene. 2017;36(19):2629-36.

142. Yang YC, Chien MH, Liu HY, Chang YC, Chen CK, Lee WJ, et al. Nuclear translocation of PKM2/AMPK complex sustains cancer stem cell populations under glucose restriction stress. Cancer Lett. 2018;421:28-40.

143. De Marchi T, Timmermans MA, Sieuwerts AM, Smid M, Look MP, Grebenchtchikov N, et al. Phosphoserine aminotransferase 1 is associated to poor outcome on tamoxifen therapy in recurrent breast cancer. Sci Rep. 2017;7(1):2099.

144. Pollari S, Kakonen SM, Edgren H, Wolf M, Kohonen P, Sara H, et al. Enhanced serine production by bone metastatic breast cancer cells stimulates osteoclastogenesis. Breast Cancer Res Treat. 2011;125(2):421-30.

145. Larsen CP, Trivin-Avillach C, Coles P, Collins AB, Merchant M, Ma H, et al. LDL Receptor-Related Protein 2 (Megalin) as a Target Antigen in Human Kidney Anti-Brush Border Antibody Disease. J Am Soc Nephrol. 2018;29(2):644-53.

146. Villafuerte BC, Barati MT, Rane MJ, Isaacs S, Li M, Wilkey DW, et al. Over-expression of insulin-response element binding protein-1 (IRE-BP1) in mouse pancreatic islets increases expression of RACK1 and TCTP: Beta cell markers of high glucose sensitivity. Biochim Biophys Acta Proteins Proteom. 2017;1865(2):186-94.

147. Grada A, Otero-Vinas M, Prieto-Castrillo F, Obagi Z, Falanga V. Research Techniques Made Simple: Analysis of Collective Cell Migration Using the Wound Healing Assay. J Invest Dermatol. 2017;137(2):e11-e6.

148. Baecker V. ImageJ Macro Tool Sets for Biological Image Analysis. ImageJ User and Developer Conference 2012; Luxembourg: Centre de Recherche Public Henri Tudor2012.

149. Gallo-Oller G, Rey JA, Dotor J, Castresana JS. Quantitative method for in vitro matrigel invasiveness measurement through image analysis software. Mol Biol Rep. 2014;41(10):6335-41.

150. Lumachi F, Luisetto G, Basso SM, Basso U, Brunello A, Camozzi V. Endocrine therapy of breast cancer. Current medicinal chemistry. 2011;18(4):513-22.

151. Simon R, Lam A, Li MC, Ngan M, Menenzes S, Zhao Y. Analysis of gene expression data using BRB-ArrayTools. Cancer Inform. 2007;3:11-7.

152. Lu Z, Hunter T. Metabolic Kinases Moonlighting as Protein Kinases. Trends Biochem Sci. 2018;43(4):301-10.

153. Israelsen WJ, Vander Heiden MG. Pyruvate kinase: Function, regulation and role in cancer. Semin Cell Dev Biol. 2015;43:43-51.

154. Li N, Feng L, Liu H, Wang J, Kasembeli M, Tran MK, et al. PARP Inhibition Suppresses Growth of EGFR-Mutant Cancers by Targeting Nuclear PKM2. Cell Rep. 2016;15(4):843-56.

155. Yamadori T, Ishii Y, Homma S, Morishima Y, Kurishima K, Itoh K, et al. Molecular mechanisms for the regulation of Nrf2-mediated cell proliferation in non-small-cell lung cancers. Oncogene. 2012;31(45):4768-77.

156. Lauand C, Rezende-Teixeira P, Cortez BA, Niero EL, Machado-Santelli GM. Independent of ErbB1 gene copy number, EGF stimulates migration but is not associated with cell proliferation in non-small cell lung cancer. Cancer Cell Int. 2013;13(1):38.

157. Bhardwaj A, Das S. SIRT6 deacetylates PKM2 to suppress its nuclear localization and oncogenic functions. Proc Natl Acad Sci U S A. 2016;113(5):E538-47.

158. Fan FT, Shen CS, Tao L, Tian C, Liu ZG, Zhu ZJ, et al. PKM2 regulates hepatocellular carcinoma cell epithelial-mesenchymal transition and migration upon EGFR activation. Asian Pac J Cancer Prev. 2014;15(5):1961-70.

159. Liang J, Cao R, Zhang Y, Xia Y, Zheng Y, Li X, et al. PKM2 dephosphorylation by Cdc25A promotes the Warburg effect and tumorigenesis. Nat Commun. 2016;7:12431.

160. Chen S, Youhong T, Tan Y, He Y, Ban Y, Cai J, et al. EGFR-PKM2 signaling promotes the metastatic potential of nasopharyngeal carcinoma through induction of FOSL1 and ANTXR2. Carcinogenesis. 2019.

161. Chen YJ, Wang YN, Chang WC. ERK2-mediated C-terminal serine phosphorylation of p300 is vital to the regulation of epidermal growth factor-induced keratin 16 gene expression. J Biol Chem. 2007;282(37):27215-28.

162. Hamabe A, Konno M, Tanuma N, Shima H, Tsunekuni K, Kawamoto K, et al. Role of pyruvate kinase M2 in transcriptional regulation leading to epithelial-mesenchymal transition. Proc Natl Acad Sci U S A. 2014;111(43):15526-31.

163. Tanaka F, Yoshimoto S, Okamura K, Ikebe T, Hashimoto S. Nuclear PKM2 promotes the progression of oral squamous cell carcinoma by inducing EMT and post-translationally repressing TGIF2. Oncotarget. 2018;9(73):33745-61.

164. Govindarajan R, Duraiyan J, Kaliyappan K, Palanisamy M. Microarray and its applications. J Pharm Bioallied Sci. 2012;4(Suppl 2):S310-2.

165. Quackenbush J. Microarray analysis and tumor classification. N Engl J Med. 2006;354(23):2463-72.

166. Hong M, Tao S, Zhang L, Diao LT, Huang X, Huang S, et al. RNA sequencing: new technologies and applications in cancer research. J Hematol Oncol. 2020;13(1):166.

167. Liberzon A, Subramanian A, Pinchback R, Thorvaldsdottir H, Tamayo P, Mesirov JP. Molecular signatures database (MSigDB) 3.0. Bioinformatics. 2011;27(12):1739-40.

168. Wang J, Duncan D, Shi Z, Zhang B. WEB-based GEne SeT AnaLysis Toolkit (WebGestalt): update 2013. Nucleic Acids Res. 2013;41(Web Server issue):W77-83.

169. Clough E, Barrett T. The Gene Expression Omnibus Database. Methods Mol Biol. 2016;1418:93-110.

170. Simon RM, Subramanian J, Li MC, Menezes S. Using cross-validation to evaluate predictive accuracy of survival risk classifiers based on high-dimensional data. Brief Bioinform. 2011;12(3):203-14.

171. Li C. WWH. DNA-Chip Analyzer (dChip). In: Parmigiani G. GES, Irizarry R.A., Zeger S.L., editor. The Analysis of Gene Expression Data Statistics for Biology and Health: Springer, New York, NY; 2003.

172. Nguyen DX, Chiang AC, Zhang XH, Kim JY, Kris MG, Ladanyi M, et al. WNT/TCF signaling through LEF1 and HOXB9 mediates lung adenocarcinoma metastasis. Cell. 2009;138(1):51-62.

173. Aktary Z, Bertrand JU, Larue L. The WNT-less wonder: WNT-independent beta-catenin signaling. Pigment Cell Melanoma Res. 2016;29(5):524-40.

174. Stewart DJ. Wnt signaling pathway in non-small cell lung cancer. J Natl Cancer Inst. 2014;106(1):djt356.

175. Valenta T, Hausmann G, Basler K. The many faces and functions of beta-catenin. EMBO J. 2012;31(12):2714-36.

176. Nakayama S, Sng N, Carretero J, Welner R, Hayashi Y, Yamamoto M, et al. beta-catenin contributes to lung tumor development induced by EGFR mutations. Cancer Res. 2014;74(20):5891-902.

177. Yang F, Xu J, Li H, Tan M, Xiong X, Sun Y. FBXW2 suppresses migration and invasion of lung cancer cells via promoting beta-catenin ubiquitylation and degradation. Nat Commun. 2019;10(1):1382.

178. Nakata A, Yoshida R, Yamaguchi R, Yamauchi M, Tamada Y, Fujita A, et al. Elevated beta-catenin pathway as a novel target for patients with resistance to EGF receptor targeting drugs. Sci Rep. 2015;5:13076.

179. Togashi Y, Hayashi H, Terashima M, de Velasco MA, Sakai K, Fujita Y, et al. Inhibition of beta-Catenin enhances the anticancer effect of irreversible EGFR-TKI in EGFR-mutated non-small-cell lung cancer with a T790M mutation. J Thorac Oncol. 2015;10(1):93-101.

180. Zhang Y, Zhang X, Huang J, Dong Q. Wnt signaling regulation of stem-like properties in human lung adenocarcinoma cell lines. Med Oncol. 2015;32(5):157.

181. Yang F, Li Y, Liu B, You J, Zhou Q. Cancer stem cell-like population is preferentially suppressed by EGFR-TKIs in EGFR-mutated PC-9 tumor models. Exp Cell Res. 2018;362(1):195-202.

182. Arasada RR, Shilo K, Yamada T, Zhang J, Yano S, Ghanem R, et al. Notch3-dependent beta-catenin signaling mediates EGFR TKI drug persistence in EGFR mutant NSCLC. Nat Commun. 2018;9(1):3198.

183. Wang J, Zhou P, Wang X, Yu Y, Zhu G, Zheng L, et al. Rab25 promotes erlotinib resistance by activating the beta1 integrin/AKT/beta-catenin pathway in NSCLC. Cell Prolif. 2019;52(3):e12592.

184. Gross SR. Actin binding proteins: their ups and downs in metastatic life. Cell Adh Migr. 2013;7(2):199-213.

185. Melak M, Plessner M, Grosse R. Actin visualization at a glance. J Cell Sci. 2017;130(3):525-30.

186. Schonichen A, Mannherz HG, Behrmann E, Mazur AJ, Kuhn S, Silvan U, et al. FHOD1 is a combined actin filament capping and bundling factor that selectively associates with actin arcs and stress fibers. J Cell Sci. 2013;126(Pt 8):1891-901.

187. Shi X, Zhao S, Cai J, Wong G, Jiu Y. Active FHOD1 promotes the formation of functional actin stress fibers. Biochem J. 2019;476(20):2953-63.

188. Koka S, Neudauer CL, Li X, Lewis RE, McCarthy JB, Westendorf JJ. The formin-homology-domain-containing protein FHOD1 enhances cell migration. J Cell Sci. 2003;116(Pt 9):1745-55.

189. Heuser VD, Mansuri N, Mogg J, Kurki S, Repo H, Kronqvist P, et al. Formin Proteins FHOD1 and INF2 in Triple-Negative Breast Cancer: Association With Basal Markers and Functional Activities. Breast Cancer (Auckl). 2018;12:1178223418792247.

190. Gardberg M, Kaipio K, Lehtinen L, Mikkonen P, Heuser VD, Talvinen K, et al. FHOD1, a formin upregulated in epithelial-mesenchymal transition, participates in cancer cell migration and invasion. PLoS One. 2013;8(9):e74923.

191. Cha HJ, Jeong MJ, Kleinman HK. Role of thymosin beta4 in tumor metastasis and angiogenesis. J Natl Cancer Inst. 2003;95(22):1674-80.

192. Rottner K, Faix J, Bogdan S, Linder S, Kerkhoff E. Actin assembly mechanisms at a glance. J Cell Sci. 2017;130(20):3427-35.

193. Lee CW, Vitriol EA, Shim S, Wise AL, Velayutham RP, Zheng JQ. Dynamic localization of G-actin during membrane protrusion in neuronal motility. Curr Biol. 2013;23(12):1046-56.

194. Ji P, Diederichs S, Wang W, Boing S, Metzger R, Schneider PM, et al. MALAT-1, a novel noncoding RNA, and thymosin beta4 predict metastasis and survival in early-stage non-small cell lung cancer. Oncogene. 2003;22(39):8031-41.

195. Huang D, Wang S, Wang A, Chen X, Zhang H. Thymosin beta 4 silencing suppresses proliferation and invasion of non-small cell lung cancer cells by repressing Notch1 activation. Acta Biochim Biophys Sin (Shanghai). 2016;48(9):788-94.

196. Helfman DM, Kim EJ, Lukanidin E, Grigorian M. The metastasis associated protein S100A4: role in tumour progression and metastasis. Br J Cancer. 2005;92(11):1955-8.

197. Fei F, Qu J, Zhang M, Li Y, Zhang S. S100A4 in cancer progression and metastasis: A systematic review. Oncotarget. 2017;8(42):73219-39.

198. Ahn MJ, Won HH, Lee J, Lee ST, Sun JM, Park YH, et al. The 18p11.22 locus is associated with never smoker non-small cell lung cancer susceptibility in Korean populations. Hum Genet. 2012;131(3):365-72.

199. Arao T, Fukumoto H, Takeda M, Tamura T, Saijo N, Nishio K. Small in-frame deletion in the epidermal growth factor receptor as a target for ZD6474. Cancer Res. 2004;64(24):9101-4.

200. Zhou W, Han L, Altman RB. Imputing gene expression to maximize platform compatibility. Bioinformatics. 2017;33(4):522-8.

201. Gillet JP, Calcagno AM, Varma S, Davidson B, Bunkholt Elstrand M, Ganapathi R, et al. Multidrug resistance-linked gene signature predicts overall survival of patients with primary ovarian serous carcinoma. Clin Cancer Res. 2012;18(11):3197-206.

202. Chen R, Zhang G, Zhou Y, Li N, Lin J. A time course-dependent metastatic gene expression signature predicts outcome in human metastatic melanomas. Diagn Pathol. 2014;9:155.

203. Mandrekar JN. Receiver operating characteristic curve in diagnostic test assessment. J Thorac Oncol. 2010;5(9):1315-6.

204. Zdzisinska B, Zurek A, Kandefer-Szerszen M. Alpha-Ketoglutarate as a Molecule with Pleiotropic Activity: Well-Known and Novel Possibilities of Therapeutic Use. Arch Immunol Ther Exp (Warsz). 2017;65(1):21-36.

205. Bronner C, Krifa M, Mousli M. Increasing role of UHRF1 in the reading and inheritance of the epigenetic code as well as in tumorogenesis. Biochem Pharmacol. 2013;86(12):1643-9.

206. Sidhu H, Capalash N. UHRF1: The key regulator of epigenetics and molecular target for cancer therapeutics. Tumour Biol. 2017;39(2):1010428317692205.

207. Karagiannis GS, Pavlou MP, Diamandis EP. Cancer secretomics reveal pathophysiological pathways in cancer molecular oncology. Mol Oncol. 2010;4(6):496-510.

208. da Cunha BR, Domingos C, Stefanini ACB, Henrique T, Polachini GM, Castelo-Branco P, et al. Cellular Interactions in the Tumor Microenvironment: The Role of Secretome. J Cancer. 2019;10(19):4574-87.

209. Lin A, Wei T, Meng H, Luo P, Zhang J. Role of the dynamic tumor microenvironment in controversies regarding immune checkpoint inhibitors for the treatment of non-small cell lung cancer (NSCLC) with EGFR mutations. Mol Cancer. 2019;18(1):139.

210. Zeng H, Castillo-Cabrera J, Manser M, Lu B, Yang Z, Strande V, et al. Genome-wide CRISPR screening reveals genetic modifiers of mutant EGFR dependence in human NSCLC. Elife. 2019;8.

CURRICULUM VITAE

Rumeysa Biyik-Sit

Clinical and Translational Research Building, #433C, University of Louisville

505 S Hancock St., Louisville, KY 40202, USA

r0biyi01@louisville.edu

EDUCATION

May 2021	University of Louisville, Louisville, KY
	Ph.D. in Biochemistry and Molecular Genetics
August 2017	University of Louisville, Louisville, KY
	M.S. in Biochemistry and Molecular Genetic**s**
August 2012	The Ohio State University, Columbus, OH
	M.S. in Molecular, Cellular, and Developmental Biology
August 2009	Bilkent University, Ankara, Turkey
	M.S. in Molecular Biology and Genetics
May 2007	Bilkent University, Ankara, Turkey
	B.S. in Molecular Biology and Genetics

RESEARCH POSITIONS

2015-Present:	University of Louisville, Louisville, KY
	Graduate Research Assistant
	Investigating a novel function for PSAT1 in EGFR-activated lung
	tumorigenesis
	PI: Associate Professor Brian F. Clem

2009-2012	The Ohio State University, Columbus, OH
	Graduate Research Associate
	Understanding the role of stromal PTEN regulated miR-101 and miR-130b
	in tumor microenvironment.
	PI: Professor Michael C. Ostrowski
2007-2009	Bilkent University, Ankara, Turkey
	Graduate Research Assistant
	Nicotine-modulated gene expression profiles in MCF7 breast cancer cell
	line and involvement of estrogen in CHRNA5 mRNA expression
	PI: Associate Professor Ozlen Konu
Fall-Spring	Bilkent University, Ankara, Turkey
2006-07	Senior Project: Analyzing the NIS(Na/I symporter) expression in placenta
	PI: Associate Professor Uygar H Tazebay
Summer 2006	Northwestern Ontario Regional Cancer Center,
	Thunder Bay, ON, Canada
	Research Assistant
	Investigating the anti-tumorigenic compound extracted from S.Lateriflora
	PI: Associate Professor John Th'ng and co-PI: Professor Lada Malek
Summer 2005	University of Duisburg-Essen, Essen, Germany
	Research Assistant
	Examining the role of sphingolipids and membrane rafts in fibroblast cells
	from the CFTR-/- mouse during bacterial and viral infections
	PI: Professor Erich Gulbins

ABSTRACTS & PRESENTATIONS

Poster Presentations

- Rumeysa Biyik-Sit, Traci Kruer, Susan M. Dougherty, James Bradley, Mike Merchant, John O. Trent, and Brian F. Clem (2020). Nuclear Pyruvate Kinase M2 (PKM2) contributes to Phosphoserine Aminotransferase 1 (PSAT1)-mediated cell migration in EGFR-activated lung cancer cells. AACR Virtual Annual Meeting II 2020 June 22-24, 2020. (Presenter)

- Rumeysa Biyik-Sit, Traci Kruer, Susan M. Dougherty, James Bradley, Mike Merchant, John O. Trent, and Brian F. Clem (2019). Nuclear Pyruvate Kinase M2 (PKM2) contributes to Phosphoserine Aminotransferase 1 (PSAT1)-mediated cell migration in EGFR-activated lung cancer cells. Research!Louisville 2019, University of Louisville, Louisville, KY. (Presenter)

- Bhavana Pavuluri, Rumeysa Biyik-Sit, Brian Clem (2019). Understanding the Impact of PSAT1 on the β-catenin Transactivation in EGFR-mutant PC9 Lung Cancer Cells. Research!Louisville 2019, University of Louisville, Louisville, KY. (Author) (1ST place poster award, Prodigy Award for High School Translational Research)

- Rumeysa Biyik-Sit, Traci Kruer, Susan M. Dougherty, James Bradley, Mike Merchant, John O. Trent, and Brian F. Clem (2019). Delineating the Requirement for Phosphoserine Aminotransferase 1 (PSAT1) in Lung Cancer Progression. Biochemistry and Molecular Genetics Retreat, 2019, Louisville Zoo, Louisville, KY. (Presenter)

- Rumeysa Biyik-Sit, Traci Kruer, Susan M. Dougherty, James Bradley, Mike Merchant, John O. Trent, and Brian F. Clem (2018). Delineating the Requirement for Phosphoserine Aminotransferase 1 (PSAT1) in Lung Cancer Progression. Research!Louisville 2018, University of Louisville, Louisville, KY. (Presenter)

- Stephanie Metcalf, Traci Kruer, Susan Dougherty, Rumeysa Biyik Sit, Carolyn Klinge, Brian Clem (2018). The Role of PSAT1 in Triple Negative Breast Cancer Metastasis. Research!Louisville 2018, University of Louisville, Louisville, KY. (Author)

- Philip Burns, Rumeysa Biyik-Sit, Brian Clem (2018). Determining the role of phosphoserine aminotransferase 1 (PSAT1) in glioblastoma cell progression. Research!Louisville 2018, University of Louisville, Louisville, KY. (Author)

- Rumeysa Biyik-Sit, Traci Kruer, Susan M. Dougherty, James Bradley, Mike Merchant, John O. Trent, and Brian F. Clem (2018). Delineating the Requirement for Phosphoserine Aminotransferase 1 (PSAT1) in Lung Cancer Progression. 59th Annual National Student Research Forum (NSRF), University of Texas Medical Branch in Galveston; April 25-27, 2018; Galveston, Texas. (Presenter)

- Rumeysa Biyik-Sit, Traci Kruer, Susan M. Dougherty, James Bradley, Mike Merchant, John O. Trent, and Brian F. Clem (2018). Delineating the Metabolic and Non-Metabolic Requirements for Phosphoserine Aminotransferase (PSAT1) in Lung Cancer Progression. Graduate Student Regional Research Conference (GSRRC) March 2-3, 2018; University of Louisville, KY (Presenter)

- Rumeysa Biyik-Sit, Traci Kruer, Susan M. Dougherty, James Bradley, Mike Merchant, John O. Trent, and Brian F. Clem (2017). Potential role for a phosphoserine aminotransferase 1 and pyruvate kinase M2 (PSAT1:PKM2) functional interaction in lung cancer cells. Research!Louisville 2017, University of Louisville, Louisville, KY. (Presenter)

- Rumeysa Biyik Sit, Traci Kruer, James Bradley, Michael Merchant, John O. Trent, Brian F. Clem (2017). Potential role for a phosphoserine aminotransferase 1 and pyruvate kinase M2 (PSAT1:PKM2) functional interaction in lung cancer cells. Biochemistry and Molecular Genetics Retreat, 2017, KingFish Restaurant, Louisville, KY. (Presenter)

- Rumeysa B. Sit, Traci Kruer, James Bradley, Michael Merchant, John O. Trent, Brian F. Clem (2017). Potential role for a phosphoserine aminotransferase 1 and pyruvate kinase M2 (PSAT1:PKM2) functional interaction in lung cancer cells. AACR Annual Meeting 2017 Apr 1-5; Washington, DC. (Presenter)

- Rumeysa Biyik Sit, Traci Kruer, James Bradley, Charles K Castaneda, Mike Merchant, John Trent, and Brian F. Clem (2016). Understanding the Functional Role of PSAT1-PKM2 Interaction in Lung Cancer Cells. Research!Louisville 2016, University of Louisville, Louisville, KY. (Presenter)

- Rumeysa Biyik, Agnieszka Bronisz, Anisha Mathur, Michael C Ostrowski (2012). Stromal PTEN Regulated miRNAs Affect PDGF Signaling in the Breast Tumor Microenvironment. OSUCCC - James 14th Annual Scientific Meeting, The Ohio State University, Columbus, OH. (Presenter)

Oral Presentations

- Delineating the Metabolic and Non-Metabolic Requirements for Phosphoserine Aminotransferase (PSAT1) in Lung Cancer Progression, Graduate Student Regional Research Conference (GSRRC), University of Louisville, KY. 2018

- Potential role for a phosphoserine aminotransferase 1 and pyruvate kinase M2 (PSAT1:PKM2) functional interaction in lung cancer cells, Biochemistry and Molecular Genetics Retreat, Louisville, KY. 2017

PUBLICATIONS

Peer-reviewed Publications

- Shehwana H, Keskus AG, Ozdemir SE, Acikgöz AA, Biyik-Sit R, Cagnan I, Gunes D, Jahja E, Cingir-Koker S, Olmezer G, Sucularli C, Konu O. CHRNA5 belongs to the secondary estrogen signaling network exhibiting prognostic significance in breast cancer. Cell Oncol (Dordr). (2021).

- Metcalf, S., Dougherty, S., Kruer, T., Hasan N, Biyik-Sit, R, Reynolds, and Clem, B.F. Selective loss of phosphoserine aminotransferase 1 (PSAT1) suppresses migration, invasion, and experimental metastasis in triple negative breast cancer. Clin Exp Metastasis 37, 187–197 (2020).

Publications in Revision

- Biyik-Sit, R., Kruer, T., Dougherty, S.M., Bradley, J.A., Wilkey, D.W., Merchant, M.L., Trent, J.O., and Clem, B.F. Nuclear Pyruvate Kinase M2 (PKM2) contributes to Phosphoserine Aminotransferase 1 (PSAT1) mediated cell migration in EGFR-activated lung cancer cells. Submitted to Cancer Letters(3/15/2021)

AWARDS & HONORS

- Dissertation Completion Award, Fall 2020, University of Louisville, Louisville, KY.

- Second Place poster award, Doctoral Basic Science Graduate Student, Research!Louisville 2017, University of Louisville, Louisville, KY.

- Full scholarship awarded by National Scholarship Program for M.S. Students   from The Scientific and Technological Council of Turkey (TUBITAK) (2007-2009)

- Full scholarship awarded by Bilkent University (2002-2007) (including tuition waiver, housing, and stipends).

- Ranked top 0.01^{th} percentile among approximately 1.5 million candidates in the National University Entrance Examination (OSS) in Turkey (2002)

- Ranked first among the graduating students in Kayseri Science High School (one of the highest-ranked high schools in science education in Turkey) (2002)

TEACHING & MENTORING EXPERIENCE

Summer 2019: University of Louisville, Department of Biochemistry and Molecular Genetics

- Mentoring summer student
  - **Project:** Understanding the Impact of PSAT1 on the ß-catenin Transactivation in EGFR-mutant PC9 Lung Cancer Cells.

Summer 2018: University of Louisville, Department of Biochemistry and Molecular Genetics

- Mentoring summer student

- **Project:** Determining the role of phosphoserine aminotransferase 1 (PSAT1) in glioblastoma cell progression.

Spring 2017: University of Louisville, Department of Biochemistry and Molecular Genetics

- **Graduate Teaching Assistant:** BMG 547/647- Biochemistry II /Adv. Biochemistry II
  - Reviewed weekly lectures during recitations and graded homework

Fall 2016: University of Louisville, Department of Biochemistry and Molecular Genetics

- **Graduate Teaching Assistant:** BMG 611 Advanced Tech. in Biochem. and Mol. Biology
  - Laboratory works on basic biochemistry and molecular biology: RNASeq analysis, co-IP, and enzyme assays.

Spring 2008: Bilkent University, Department of Molecular Biology and Genetics

- **Graduate Teaching Assistant:** MBG 418 Genomics
  - Prepared handouts about web tools used for genomics application
  - Prepared and graded homework
- **Mentoring two senior students**
  - Analyzed microarray data on colon and breast cancer from the GEO database and performed expression profiling and class prediction.

Fall 2008: Bilkent University, Department of Molecular Biology and Genetics

- **Graduate Teaching Assistant:** MBG 418 Genomics
  - Laboratory works on fundamental genetic analysis of *C. elegans* and *D. melanogaster*

AFFILIATIONS

2016 - Present Member, Golden Key International Honour Society

2017 - Present Member, American Association for Cancer Research (AACR)

2020 - Present   Member, The Society for Collegiate Leadership & Achievement (SCLA)